STUDYING INTERACTIONS OF GAS MOLECULES WITH NANOMATERIALS LOADED IN A MICROWAVE RESONANT CAVITY

Aman Anand, B.A.

Dissertation Prepared for the Degree of

DOCTOR OF PHILOSOPHY

UNIVERSITY OF NORTH TEXAS

August 2007

APPROVED:

J. A. Roberts, Major Professor
Floyd McDaniel, Major Professor and Chair of the Department of Physics
W. D. Deering, Committee Member
Paolo Grigolini, Committee Member
Arkadii Krokhin, Committee Member
J.N. Dahiya, Committee Member
Sandra L. Terrell, Dean of the Robert B. Toulouse School of Graduate Studies

Anand, Aman. Studying Interactions of Gas Molecules with Nanomaterials Loaded in a Microwave Resonant Cavity, Doctor of Philosophy (Physics), August 2007, 137 pages, 27 tables, 60 figures, references, 81 titles.

A resonant cavity operating in TE_{011} mode was used to study the adsorption response of single walled carbon nanotubes (SWCNTs) and other nanomaterials for different types of gas molecules. The range of the frequency signal as a probe was chosen as geometry dependent range between 9.1 -9.8 GHz. A highly specific range can be studied for further experiments dependent on the type of molecule being investigated. It was found that for different pressures of gases and for different types of nanomaterials, there was a different response in the shifts of the probe signal for each cycle of gassing and degassing of the cavity. This dissertation suggests that microwave spectroscopy of a complex medium of gases and carbon nanotubes can be used as a highly sensitive technique to determine the complex dielectric response of different polar as well as non-polar gases when subjected to intense electromagnetic fields within the cavity. Also, as part of the experimental work, a range of other micro-porous materials was tested using the residual gas analysis (RGA) technique to determine their intrinsic absorption/adsorption characteristics when under an ultra-high vacuum environment. The scientific results obtained from this investigation, led to the development of a chemical biological sensor prototype. The method proposed is to develop operational sensors to detect toxin gases for homeland security applications and also develop sniffers to detect toxin drugs for law enforcement agency personnel.

ACKNOWLEDGEMENTS

My doctoral research work performed at the University of North Texas (UNT) turns out to have produced an extremely successful dissertation. This document takes a moment to sincerely appreciate the constant involvement of many persons from a very diverse background, who played their own very critical role in getting this experimental investigation to accomplish its target.

My major professor, Dr. James A. Roberts, has not only been my mentor but my bank of intellectual wisdom. His tireless enthusiasm and his selfless interests in this experiment, as well as his tremendous expertise in the field of microwave electronics and instrumentation, never let me slow down even a bit. His decades of experience in doing extraordinary research (that produced 40 dissertations) can also be read in almost this entire document. His attitude and his support to me have always helped me remain focused and challenged. I appreciate to the utmost his professional companionship that has trained me to become an independent researcher.

The preparation of this dissertation involved equal contributions from my other committee members, and Dr. Floyd McDaniel is acknowledged for his kind support and routine discussions over the progress of this work. Drs. William Deering, Arkady Krokhin, Paolo Grigolini, and J.N. Dahiya have also played a very critical role in this work. Through their constant discussions, suggestions, and positive critiques, I have been able to maintain the lead in my experimental research.

I sincerely thank the Office of the Provost at the university and Dr. Don Henley from the Office of Research and Technology Transfer for their benevolent support in partially funding my research assistantship, and for their swift office work in filing the patent on the part of the results reported in this research.

I am grateful to Dr. Neal Lane from Rice University, and I consider it an honor to have him demonstrate some of the applied results of this dissertation work. I thank him sincerely for sparing his precious time and visiting our facility with an open mind and encouraging views.

I also thank Dr. Zeke Insepov, computational scientist from the Mathematics and Computer Science Division at Argonne National Laboratory for his constant interest and encouraging responses. The scientific communications with him have assisted me in creative thinking, and have always helped me think big!

I thank Mr. Dennis Roedemeier from Missouri Research Corporation (MRC), Mr. Ron Selfors from Missouri Enterprise organization, Mr. Mike True from Fort Leonard Wood, Dr. John Kramer, and the regional crime laboratory for assisting me by providing wonderful opportunities of presenting and demonstrating my doctoral research work to Boeing Corporation's Integrated Defense Systems, Drug Enforcement Agencies, and to their regional crime laboratories. My acknowledgements to MRC would be incomplete without thanking Ms. Christy Legrand, who has been very instrumental and upbeat in getting many presentations and grant proposals organized for potential future funding for part of the project originating from this work. Mr. Rob Simon from Boeing Corporation is also thanked for his frequent visits, and his informational support on part of this project.

I thank Norit® corporation in Texas for providing us with activated carbon material supply, SWeNT™ technology of Oklahoma for providing us with top-quality samples of single-walled carbon nanotubes, Linde® gas corporation for top-grade lecture bottles of various gas samples, and Swagelok® Corporation for providing us with Swagelok® connectors and other vacuum supplies in a very timely manner. Without their valuable support, this project would have failed in achieving its scientific purposes.

The Office of Naval Research and the Robert A. Welch Foundation of Texas are thanked for funding this project in part through providing me with an instrumental and a scholarship grant, respectively.

The UNT Department of Physics, its staff, and its members are thanked cordially for providing me with a very congenial environment and for their patience in keeping up with my constant demands for support.

Toulouse School of Graduate Studies at the University of North Texas is specially thanked for providing me with this wonderful opportunity to obtain this prestigious degree.

My heart is grateful to my parents for their countless sacrifices, support, and their blind faith behind my endeavors. I shall always remain indebted to them throughout my life. My sister is thanked equally for her timely advice, and for her numerous contributions to my pocket change, on which a graduate student depends heavily.

Last, the most significant contribution toward the successful accomplishment of my work has been made by my beloved wife Vandana. She has stood by me at all times and under all circumstances. Her sacrifices, her support, and her immense cooperation are what kept me focused into my research work. I simply call her a “half-physicist” to whom I shall always remain grateful.

TABLE OF CONTENTS

Page

LIST OF TABLES

Page

LIST OF FIGURES

Page

CHAPTER 1

INTRODUCTION

General Overview

Carbon nanotubes have been shown to exhibit a number of unusual properties in their electrical conductivity and their complex dielectric response. Due to some of their unusual properties such as large surface-to-mass ratio they have also found numerous applications.[1] Since their discovery by Ijima,[2] many researchers worldwide have shown interest in these materials. Various studies are being done on these materials to characterize their electrical, optical, and mechanical as well as thermal properties. So far, there are many different ways of synthesizing these nanomaterials.[3] Depending upon the nature of their synthesis and the impurities in these materials, carbon nanotubes can be classified as possessing either metallic properties or semiconducting properties.[4] These properties play an important role in our experiment, as the nanotubes with metallic properties will have a different dielectric response to a microwave signal than the non-metallic nanotubes.

There are two basic structures that occur for these nanotubes: armchair structures, which are metallic in nature, and zigzag structures, which are generally narrow-gap semiconductors. The rule governing these characteristics is the relation between the Miller indices of their symmetry as given by Eq. (1.1).

For given indices (a,b) the nanotubes behave as expressed below: [5]

$$\begin{aligned} &\text{Metallic if:} && 2a + b = 3N \\ &\text{Semiconductor if:} && 2a + b \neq 3N \ \ (N \text{ positive integer}) \end{aligned} \qquad (1.1)$$

A computer simulated model of both of these structures was used to generate the patterns shown in Fig. 1.[6] The figure on the left shows the armchair nanotubes that were generated with a

(6,6) symmetry and which have a diameter of ~ 8.42 $\overset{o}{A}$. The figure on the right shows the zigzag nanotubes with an outer diameter of 9.52 $\overset{o}{A}$.

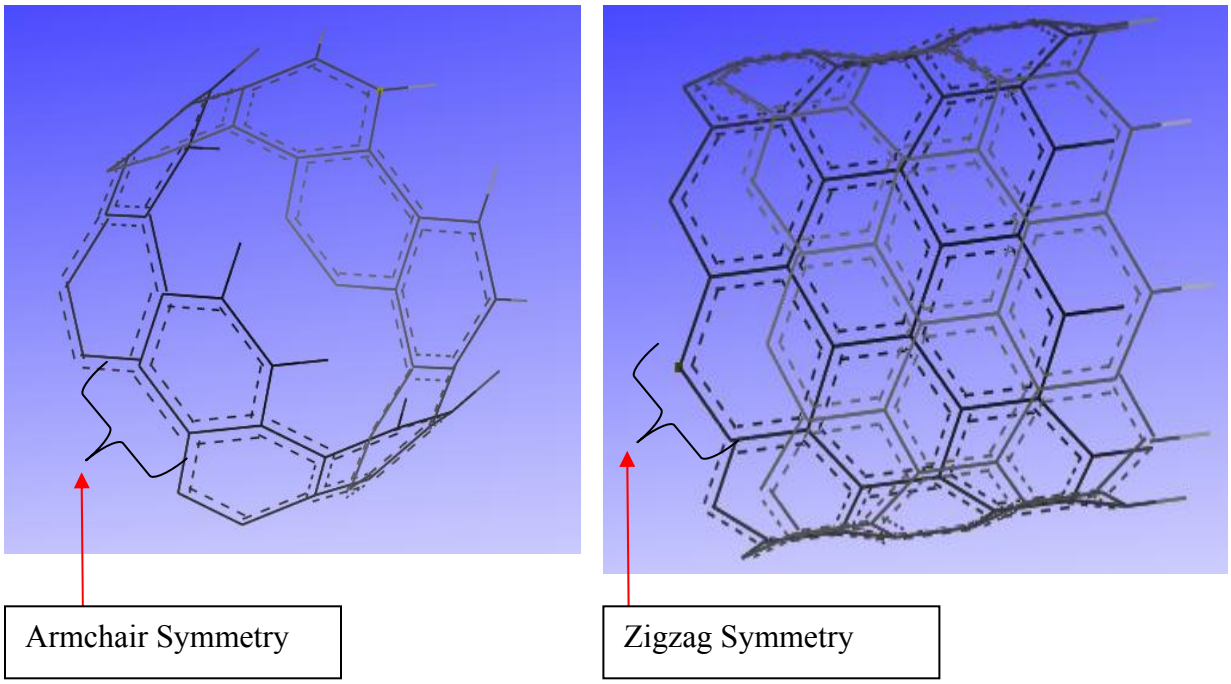

FIG. 1. Computer generated images of armchair as well as zigzag symmetries observed in the single wall nanotube.

Resonant cavities are well-known, highly sensitive devices that have been used to make measurements of fundamental properties of matter in all its phases.[7] A resonant cavity can be considered to be multiple Inductor Capacitor Resistance (LCR) circuits connected in parallel. These resonant cavities have widely been studied in determining shifts in the resonant profiles because of their high quality factor (around 5000 +). In this experimental work, these cavities were used to study the interactions of various gas molecules with carbon nanotubes and other porous materials loaded within the cavity. The microwave spectral response of these cavities containing different gases possessing different indices of refraction served as the signature of

interactions of these gases in a complex dielectric medium. Fig. 2 shows a typical setup of the resonant cavity that was used in carrying out this study of gas interactions with nanomaterials.

FIG. 2. A picture of the typical resonant cavity with the gas connector cables and the waveguide coupling through the iris hole.

These cavities were loaded with different types of materials (carbon based, silica gel, and cotton fibers). Upon energizing these cavities in their fundamental modes a non-destructive study was performed to investigate the perturbation response of the load with several different gases. The frequency range of 9.1 – 9.8 GHz was used in our experiment to study their perturbation response. Upon perturbing the cavity with a small load (30 mg of single-walled carbon nanotubes), there was a shift in the center frequency of the apparatus as shown in Fig. 3.

The spectral parameters as shown in the above figure have been plotted to characterize the dielectric responses of the various gases with and without loads present in the resonant cavities. It is seen in this experimental investigation that different materials interact differently with different gases. In this scientific study, investigation is made to determine the effect of various forces such as Van der Waals (VdW), as well as other exchange forces that have significant contributions in the interaction behavior of gaseous molecules with the substrates. An

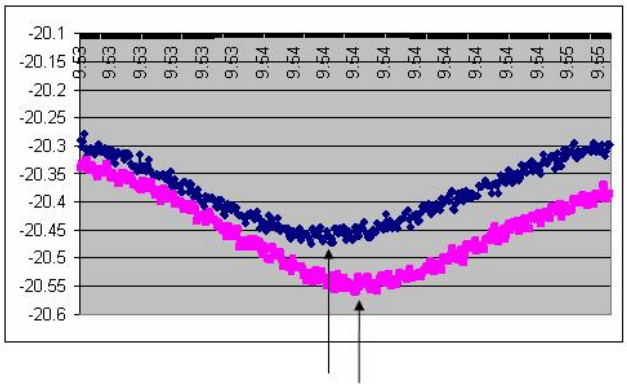

FIG. 3. A typical scan of shift in the resonance frequency due to the perturbation of an external load.

empirical study of this experiment will also be discussed to address the dielectric responses of solid-gas mixture under a time dependent field.

What are Carbon Nanotubes?

It is well known that carbon belongs to the group IV family of the periodic table and exhibits unique properties distinct from other members in the same family. It exists in many forms in nature such as graphite, diamonds, peat, coal, graphite whiskers, glassy carbon, carbon black, amorphous carbon, catalytic coated carbon particles, liquid carbon graphite intercalation compounds, charcoal, and metal-coated fullerenes. Depending upon the geometry of the primary lattice structure of this element, there are different associated types of bonding (sp^3, sp^2).[8] With recent discoveries of zero- and one-dimensional forms of carbon, fullerenes, and carbon nanotubes, respectively, the whole scientific community is experiencing an elevated interest in investigating these materials for advanced applications. With major breakthroughs in the field of superconductivity, these materials have stimulated a frenzy of activity in researching such materials. The discovery of fullerenes led to the discovery of carbon nanotubes. An in-depth systematic study has been performed on graphite and diamond materials and now researchers

have concentrated their efforts in analyzing and characterizing carbon nanotubes based on their lattice constants, atomic densities, specific gravity, specific heat, binding energies, bulk modulus, band gaps, resistivities, electrical conductivities, and magnetic permeability.[9] The name carbon nanotube is given to a specific geometrical structure of graphene sheets. As investigated by many electron microscope specialists and solid state physicists, these structures can be defined as single-layered graphene sheets rolled up into a hollow cylinder, whose ends are chopped off and replaced with half-closed fullerene molecules. Dresselhaus *et al.*[10] have offered a theoretical model of these tubule-like structures in their chapter "Introduction to Carbon Materials." As a result of different stacking of the lattice sheets, these materials exhibit different band gap properties. Based upon the band gap differences in these tubules, nanotubes tend to exhibit metallic or semiconducting properties as given in Eq. (1.1).

This timeline study in tabular format (Fig. 4[11]) provides an overview of major breakthroughs in application-based study related to SWCNTs. The list is a comprehensive view of the field of applied nanotube technology, which in my opinion forms the backbone or the fundamental principle for other advanced applications of this material. The list mentions only selected work that is relevant to this document and does not imply either limited scope or stalled progress in the field of nanotechnology research.

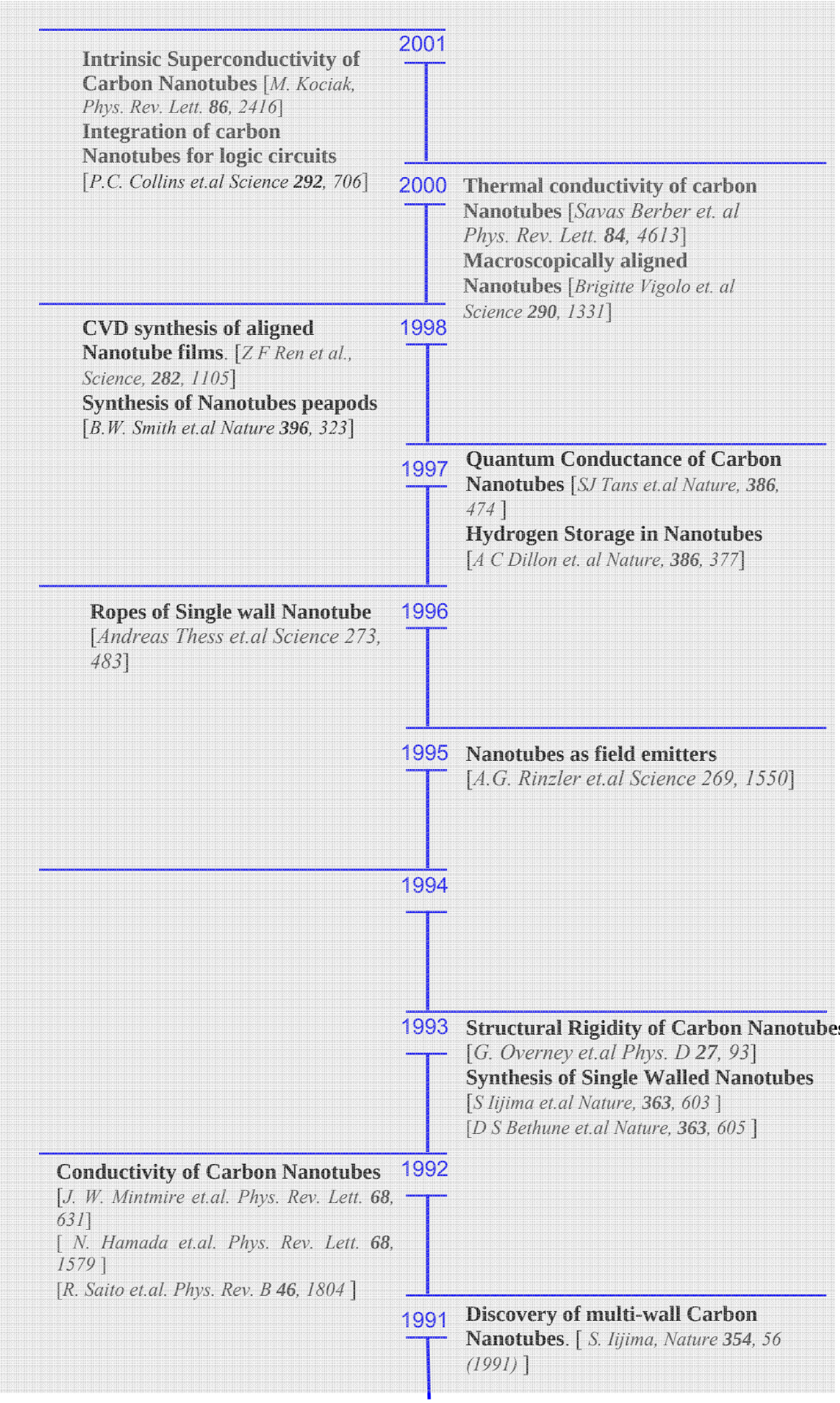

FIG. 4 Carbon nanotubes – a time line.

Various Structures and Their Morphologies Explored by Others

Several researchers have studied the structure and anatomy of carbon nanotubes and have classified them into three broad categories: single-walled, double-walled and multi-walled carbon nanotubes (SWCNT, DWCNT, and MWCNT, respectively). These classifications of carbon nanotubes originate from respective diameter of the tubules. Since I have carried out experiments with SWCNTs, my theory and results will be applicable to these particular structures. SWCNTs are cylindrical sheets of graphite with their diameters in the range of ~0.7-10.0 nm. Any higher value of the radii of the tubes will then fall under the category of either double or multi-walled structures. An essential description of the structures of these nanotubes follows from the process of their growth. Depending upon the orientations of the benzene rings along the cylindrical axis and their lattice alignments, these structures are labeled as: a) arm-chair type, b) zigzag types, or c) chiral nanotubes. Various critical locations on the lengths of these tubular structures are defined by the chirality of these tubes.[12] These tubes can be understood as honeycomb lattices which, when unfolded, give us a clear measure of the alignments between the hexagonal benzene-shaped rings. These structures have been explained in much greater detail in the work of Saito, Dresselhaus and Dresselhaus.[13] The spiral structure observed in these tubes is due to different conformations of this chirality. For the purpose of understanding our experiments performed on these nanostructures, it is necessary to have a brief discussion of the geometry of these nanoparticles. Dependent properties such as the capillarity of these tubes and their surface tensions are related to their ratio of length to diameter (aspect ratio). This paper assumes that the readers are familiar with the basics of symmetries and their properties, i.e. lattice constants, unit cells, cis-trans symmetries, and Brillouin zones. These concepts are all necessary in theoretically defining the parameters of the nanotubes. In my

experiments, I am dealing with the bulk properties of nanotubes instead of one single strand of this nanostructure. The contents of our discussion will be limited to such theoretical details. It is obvious that the bulk properties of these nanotubes will superimpose the minute details associated with their lengths and their alignments within our setup.

Even though the structural details of these nanotubes play a vital part in the results of our experiment of gas absorption, there are two other very necessary details that need to be addressed in relation to our experiments of the interactions of gases in an electromagnetic field environment: 1) the type of impurities that lie embedded inside the tubes as well as outside the tubes in the bulk medium and 2) the overall conductive properties of the tubes due to the nature of such impurities.

As a part of their growth process, as mentioned in some details of section B2 of this chapter, the resultant carbon nanotubes remain doped with certain metallic impurities (Fe, Co, polymers, etc;). Due to these impurities present in these nanomaterials, the study sample is expected to predict different types of responses. Higher concentration of metals in carbon based materials will produce metallic properties in the bulk material, contrary to the more insulating polymers. The more dielectric the material, the larger is its response towards the downshift in resonances as demonstrated later in this document. One aim of the experiment is to study the response of pure gases with semi-pure carbon based materials and to characterize their electrical properties in the medium. Hence, sections B2 and B3 are aimed at providing the readers with an understanding of the synthesis process, as well as the electronic and other properties of these nanomaterials, in order to be able to relate to the response presented in the experimental section of this paper.

Various Methods of Synthesis of Carbon Nanotubes and Their Catalysts

Various growth procedures as described below play a very critical role in determining the amount and type of residual particles present in the nanotubes. Particles such as cobalt, iron, molybdenum etc; also termed as impurities affect the electro-chemical properties of these samples. As mentioned earlier, the presence of such impurities in the bundles of nanotubes plays a significant role in our experiments. The nature of the nanotube band gaps and the conductivity of the ensemble due to these impurities determine the spectral response of these nanomaterials to the electromagnetic fields driving our resonant cavities. Hence, I will summarize a few of the methods that have to this date been developed in synthesis of these nanotubes. Since the discovery of nanotubes by Ijima,[14] researchers have been extensively studying the various methods of synthesis of nanotubes. Some of the most popular and widespread methods are listed by Yumura; Saito Dresselhaus and Dresselhaus; Ebbesson; Gamaly; and Harris:[15]

a) By-product in an electric arc discharge

b) Laser ablation

c) Catalytic decomposition of hydrocarbon

d) Electrolysis

e) Solar energy to produce fullerenes

f) Pyrolytic methods

g) Condensation of carbon vapor in the absence of an electric field.

Elaboration of these methods will simply be redundant information and is not the major objective of this paper. What is important in any of these methods is the classification of many impurities that remain in these tubes as a result of the use of various metallic catalysts as well as other organometallics. These impurities, even though present at the nanogram level, affect the

microscopic properties of the electromagnetic waves which, with the use of resonant cavities, can be detected at macroscopic levels. Also, if in the future any new method is invented or discovered which is free from use of the catalysts, the entire model of calculating the effective dielectric response will have to be developed again. In the current methods of synthesizing these carbon nanotubes (CNTs), it is found that the most common types of catalysts, which remain present as impurities within the nanotube ropes and bundles, are the elements Fe, Ni, Co, some rare earth metals such as Y, and Gd. Also found are some mixed elements such as Fe/Ni, Co/Ni, and Co/Pt, all dependent upon the type of synthesis process used in the manufacturing. The presence of such elements at different concentrations produces some interesting features in nanomaterials. The electronic band gaps of these bundles are affected, the intercalated interaction properties are different, and, for that matter, the conductivity of the material on the whole changes as the mean free path for electron propagation changes. As of this date from the experimental stand-point, it is very difficult to compare the results from one batch of nanotubes to another due to the inhomogeneous distribution of these impurities within the nanotubes. In experimentally performed particle induced X-ray emission (PIXE) runs, it was observed that the readings performed on two sets of batches of the nanotubes purchased from the same vendor produced different mass spectrometry data. It was observed in 2003, when this processing of nanotubes was still new, that some manufacturers such as Carbon Nanotechnologies Inc.®, CNT Technologies® and many more were experiencing problems with their quality control process in the mass production of these materials. This resulted in variations in dielectric response similar to those I observed in my setup from one batch of the sample to another for a fixed amount or volume of nanotubes that were loaded within the cavity. As the processing techniques improved with time, certain manufacturers have been able to render quality-controlled batches of

nanotubes. Hence the results reported in this study have been performed on the samples that were procured from SWeNT® Corporation of Oklahoma, and are considered to be of superior quality, the best available on the market as of this date.

At this point, it is interesting to mention some of the fundamental electrical, magnetic, optical, and other rigid properties of the nanotubes for the basis of our discussion in future chapters. These properties are discussed briefly in the next section.

Interesting Properties of Carbon Nanotubes Related to Their Structures

These materials were discovered by electron microscopy and researchers worldwide are deeply involved in microscopic studies of these materials to explore their electronic, magnetic, and optical as well as thermal properties. In order to be able to characterize the geometries of these objects, which in turn tells us about their conduction and their heat radiation properties, researchers tend to combine electron diffraction studies with electron microscopy.[16] In many important studies the authors have developed models to study the stacking structure of graphene sheets and then compared them with many evolutionarily formed structures of carbon such as fullerenes, nanotubes, and nanopods[17]. These high resolution studies of nanomaterials reveal that they all exhibit extraordinary mechanical, electrical and optical properties. Their ability to bend into very small radii of curvature and their ability to return to their equilibrium state render them strong contenders for potential fiber applications such as the reinforcing materials being used in buildings, bridges, and bullet-proof vests.[18] Also, their ability to connect with other tubes in the bundle and their electronic conduction properties make them an ideal candidate for nanoelectronic-based applications.[19] The article mentioned by Amelinckx, Lucas, and Lambini[20] illustrates in detail the kinematical diffraction theory and their tilt angle as well as their chiral angles, which depend upon whether the tubes are helical or straight in nature. Some electrical

and electronic properties of these nanotubes are illustrated in section B3a. In order to be able to address these issues of electrical properties, I have investigated these properties using the tight binding calculation of solids and molecules.

Electronic structure of single-walled nanotubes. In determining the electronic structures of these one-dimensional graphene sheets, it is important to recognize the band structures of amorphous carbon and its allotropes, especially graphite. In the neutral state of existence, plain amorphous carbon has an electronic configuration of $1s^2$, $2s^2$, $2p^2$, thereby having four electrons in its outermost state. From Pauli's exclusion principles and principles of the valence bond theory or, for that matter, valence shell electron repulsion theory, one can easily find that these elements engage themselves in covalent bonding, in which two or subsequently more carbon atoms will share their outermost electrons in order to have a stable configuration of eight electrons in their outermost shell. In this process of bonding with another carbon atom, the valence electrons in their S state will share bonds through mutual exclusion as well as valence shell electron repulsion theory. In the computer simulated image (Fig. 5), the electronic band structure of typical (9,0) metallic type nanotubes is shown.

The electronic state of local density electrons is also shown in Fig. 5 on the right. This shows that the metallic type nanotubes are more conductive and have more free electrons in their valence shell, which will eventually reduce the effective volume of the cavity and thereby result in a shift of the resonant frequency towards higher values. Further details and discussions about the electrical forces and their response to the electromagnetic fields are discussed in the following chapters.

As shown in Fig. 5 these nanotubes have characteristic equilibrium energies measured in hartrees with respect to their Fermi energies where one hartree is a physical constant equal to

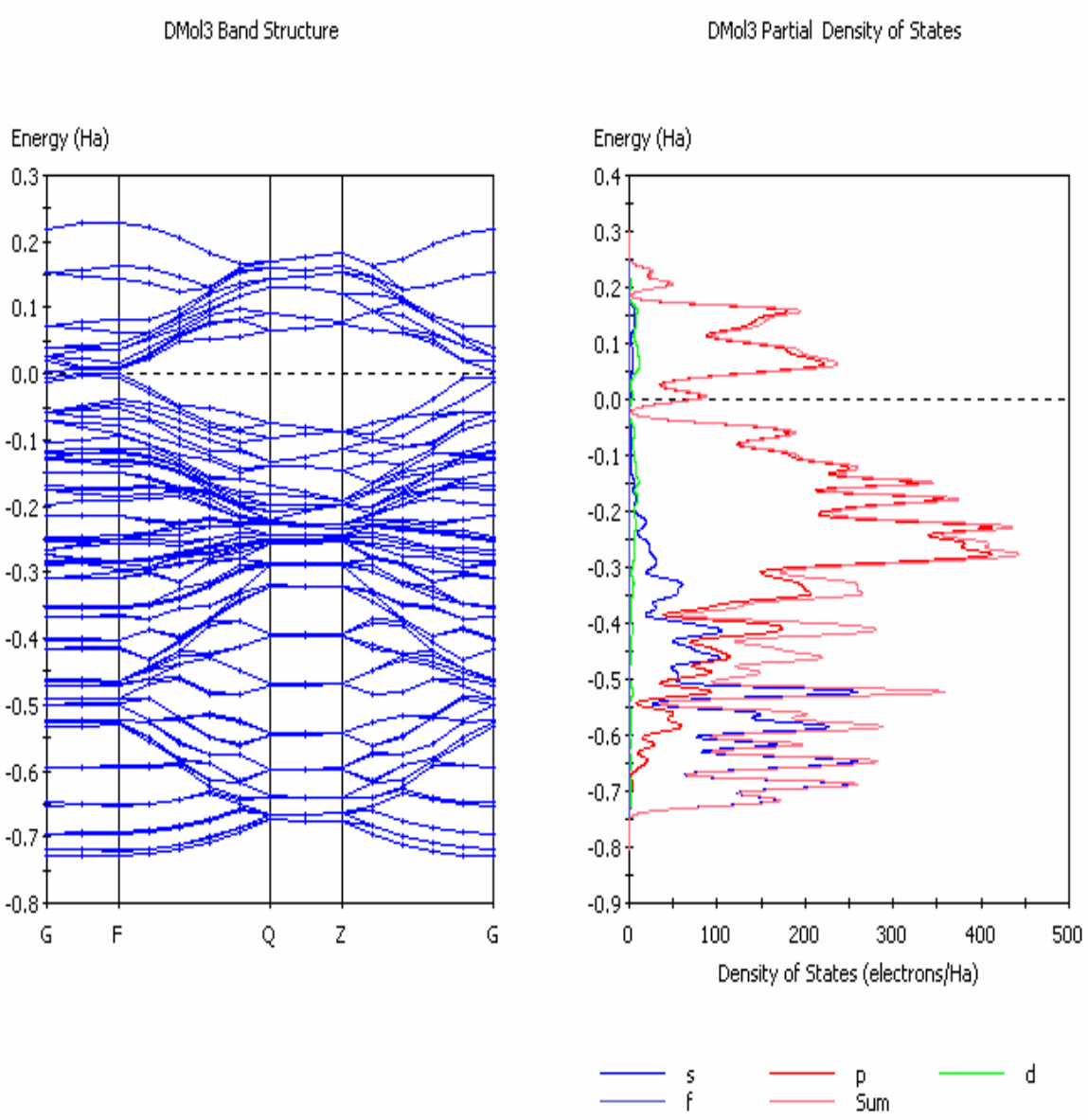

FIG. 5. Band structures showing the local optical as well as local acoustic modes of (9,0) type nanotubes

twice the binding energy of the electron in the ground state (the lowest-energy state) of the hydrogen atom. When a hydrogen atom is in this state, an amount of energy equal to 0.5 hartree is necessary to free the electron and thereby cause the atom to become an ion. The value of the Hartree energy is approximately 4.36 x 10^{-18} joule (J), or 27.2 electron volts (eV). The constant gets its name from the 20th-century physicist Douglas Hartree. It is sometimes used as an energy

unit in theoretical physics. These binding energies of the neighboring atoms shown in the band structure above indicate the polarizable capabilities of nanotubes in both static as well as time dependent harmonic fields which, in turn, will assist in developing theoretical models to indicate possible dipole-dipole as well as dipole induced dipole types of exchange forces with the perturbing molecules.

Overview of This Scientific Investigation

In this scientific investigation, the interactions of gas molecules (mildly polar as well as non-polar) with various substrates such as SWCNT powders, activated charcoal, silica gels and cotton fibers have been studied using microwave resonant circuitry to detect frequency shifts and quality factor changes (*Q*-changes) caused by adsorption of these molecules. The experiment involved measuring the interactions between the applied electric and magnetic fields, and the complex sample using a standard perturbation technique with a resonant cavity.[21] Resonant cavities are well-known, highly sensitive devices that have been used in investigating fundamental properties of matter in all its phases.[22] The interactions of the microwave field and the sample can be generically summarized by the relation expressed in Eq. (1.2):

$$Z = f_1(\mu_e, E) - f_2(\mu_m, H) \tag{1.2}$$

where $f_1(\mu_e, E)$ is a measure of electrical interaction and $f_2(\mu_m, H)$ is the measure of magnetic interaction. More details about the resonant cavities and their interactions with the load will be addressed in later chapters but, in general, these resonant cavities were tuned to resonate in their fundamental TE_{011} mode where electric field perturbations were dominant and hence the magnetic term in Eq. (1.2) is negligible. Two identical cylindrical resonant cavities were tuned in their TE_{011} mode, with one cavity used as the reference cavity. The nature of interactions of different gas loading with different substrates was studied through resonant shifts in the test

cavities. Progressive studies were done for each cycle of gassing and degassing of the test cavity that was loaded with different materials. Frequency shift results and the effective dielectric responses for several different runs have been summarized in Chapter 4. It was found that different substrates have shown different affinities for the gas molecules. The differences among these affinities are primarily attributed to the effective surface areas as well as the polarizabilities of different substrates and gases.

Carbon nanotubes have been shown to behave as ideal candidates for gas adsorption due to their high outer surface area for one single tube (1300-1500 m^2/g), and (285 m^2/g) in amorphous bulk powder form.[23] Due to such high surface area per mass properties of these carbon based nanomaterials and their electronic band structures,[24] many researchers have been investigating these nanomaterials for use in ultrahigh capacitor applications. Due to such interesting properties of carbon nanomaterials discussed earlier, I have macroscopically tried to study the microscopic properties of these materials, using microwave spectral response spectroscopy to analyze these materials interacting with different molecules.

CHAPTER 2

ELECTROMAGNETIC THEORY OF MICROWAVE RESONANT CAVITIES AND ITS APPLICATIONS

Inductance-Capacitance-Resistance (LCR) Circuits and Introduction to Resonant Cavities

The history of microwave resonant cavities goes as far back in time as the inductance-capacitance-resistor (LCR) circuits. From the principles of LCR circuits one is aware of the fact that the LCR circuits, whether connected in series or parallel, have characteristic qualities that define either their charge storage or charge delivery capabilities. Associated with these circuits are critical parameters such as impedance (Z) of the circuit, inductive reactance (X_l), capacitive reactance (X_c), and resonant frequency (f_r), where each quantity is expressed as

$$(X_l) = 2\pi f L \tag{2.1}$$

$$(X_c) = \frac{1}{2\pi f C} \tag{2.2}$$

$$(Z) = \sqrt{X_l^{\,2} + X_c^{\,2}} \tag{2.3}$$

where f is the frequency in cycles per second, L is the inductance measured in henrys and C is the capacitance of the circuit measured in farads. Resonance is the condition under which

$$| X_l | = | X_c | . \tag{2.4}$$

In any circuitry these components can be arranged either in series or parallel (as shown in Fig. 6), depending upon the nature or quality of the circuit desired. Besides the one shown in Fig. 6, there can be several different ways in which these circuits can be branched in order to make the entire circuit either purely capacitive, inductive, or resistive depending upon the application intended.

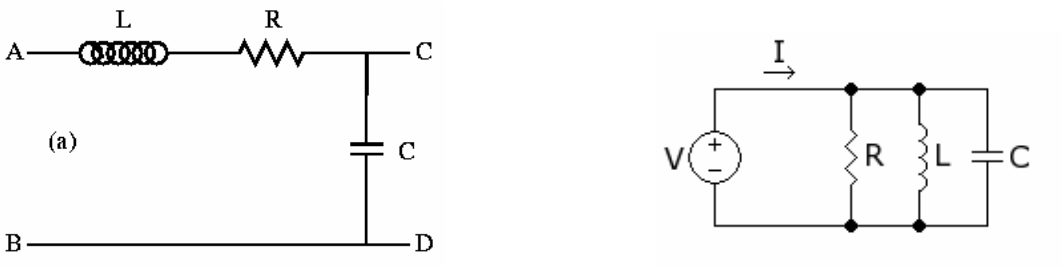

FIG. 6. On the left is an LCR network circuit in series. On the right is the circuit in parallel.

The prime difference between series and parallel LCR circuits is in their bandwidths. The design criteria depend upon whether the circuit has to be used as a band-pass or a band-stop filter. These circuits are called tuned circuits because their elements can be adjusted or tuned to resonate. In order for the circuits to be in resonance, impedance in the inductive branch should equal that of the capacitive branch. The condition then implies

$$(X_l) = (Xc) \Rightarrow f_r = \frac{1}{2\pi\sqrt{LC}} \quad . \tag{2.5}$$

Eq. (2.5) is the expression for the resonant frequency (f_r) of the circuit.

For details or the derivation, one can refer to any standard freshman level electronic textbook. A summary of these series and parallel resonant circuits is given in Table 1.

TABLE 1. A summary of series and parallel resonant circuits.

Property	Series LCR	Parallel LCR
Resonant Frequency	$\frac{1}{2\pi\sqrt{LC}}$	$\frac{1}{2\pi\sqrt{LC}}$
Voltage Across R	maximum at f_R	constant = V_0
Current Through R	constant = V_0/R	minimum at f_R
Q	$\frac{2\pi f_r L}{R}$	$\frac{R}{2\pi f_r L}$
Bandwidth	$\frac{f_r}{Q}$	$\frac{f_r}{Q}$

In most general applications of these circuits, it is found that the parallel resonant circuits are the most widely used circuits in electronic receivers and transmitters, as well as other frequency measuring devices.[25] Their interesting properties such as their bandwidth, quality factors (Q), and ability to resonate makes them widely used devices in today's electronic circuits.

Parallel resonant circuits are characterized by high impedance factors due to contributing resistance approaching zero. It can be shown that the impedance of the circuit at resonance is given by Eq. (2.6).[26]

$$Z_{AB} = \frac{X_L^2 - jX_c R_L}{R_L} \approx \frac{X_L^2}{R_L} - jX_c \qquad (2.6)$$

where, $X_L = 2\pi f L \quad (Ohms)$ and $X_c = \frac{1}{2\pi f L}(Ohms)$.

As mentioned earlier, the two most interesting characteristics of these parallel LCR circuits are the bandwidth (shown in Fig.7), which defines the sharpness of the circuit and is a critical factor in discriminating between frequencies that are off resonances and the center frequency of the resonance profile. Selectivity of these circuits is basically the ratio of the bandwidth to the resonant frequencies and is given by $\Delta W / f_r$.

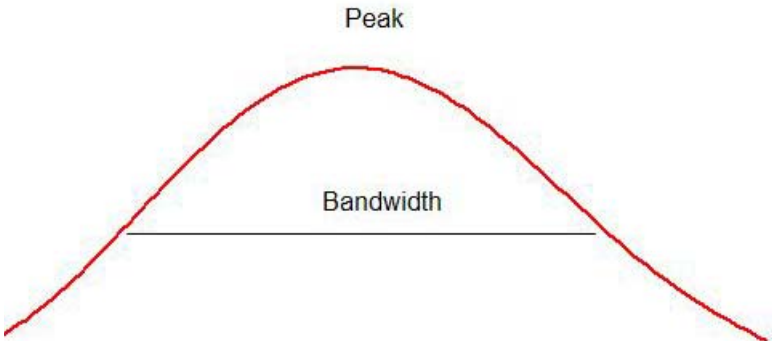

FIG. 7. Bandwidth profile, which depicts the frequency widths between half-power maxima.

These circuits operate both below and above resonances, depending upon whether the circuit impedance is inductive or capacitive, respectively, and when the two reactants are equal then the circuits are resonant. For the purpose of this experiment the interest is only in bandwidths, *Q* of those circuits, and the center frequency of the resonance.

Thus far in this document I have established primitive characteristics of a single LCR circuit in series as well as parallel and have demonstrated the inverse relationships between the bandwidth and *Q* factors of circuits in resonance. It is appropriate to establish the analogical relationship between the LCR circuits and the resonant cavities operating at microwave frequencies. Considering a circuit of *N* coupled oscillators such as described in Manolache and Sandu,[27] cylindrical cavities can be considered to be similarly branched oscillators where, depending upon the modes of couplings between R, C, and L of the individual branches of these resonators, we will have different field distributions. In this experiment the cylindrical cavity can be compared to *N* such resonators with all L's and C's of *N* branches considered in parallel. Now, depending upon the modes (explained in the next section) of energizing these cavities, we can have induced forced oscillations of either inductors (magnetic field) or capacitors (**E** field).

Unlike loop feeders, the antennas that deliver the generating fields into these cylinders are coupled such that the resulting network can be considered as the networked capacitors parallel to each other forming the top and bottom plates. *N* such inductors are networked along the walls of the cylinder and the medium of the cavity as well as the walls correspondingly acting as parallel resistors.

In order to understand the behavior of the electromagnetic fields, the solution to Maxwell's equations inside the cylindrical resonant cavity is used.[28] Microwaves have shorter wavelengths than radio waves and longer wavelengths than infrared waves. So in order to have a

sharp resonant profile with a very high *Q* factor, the LC coupling and resistances should be very low. In order to have low ohmic losses in the cavity there are two necessary steps:

1. Assuring a strong coupling between the wave-guides and the iris.
2. Plating the inner walls of the cavities with silver or gold, as good conductors will allow easy flow of electrical charges with less loss.

Electromagnetic Theory of Microwave Resonant Cavities

In the previous section, a method of storing electrical energy in a resonant circuit was presented. Such circuits suffer a drawback of leakage at reasonably high frequencies. Another efficient method of transferring electrical energy is by movement of electromagnetic fields either in space or in a contained environment such as waveguides and cavities. Extensive experimental, as well as theoretical, studies have been done in the past over various geometries and materials of electromagnetic devices.[29] Transmission lines, waveguides, and cylindrical and spherical resonators have found many applications in industries today.[30] These devices are highly efficient in storing energies with minimal losses, depending upon the materials used to construct them. Skin depth and ohmic losses are two major factors in considering the leakage of the fields.[31] In order to properly design electromagnetic devices, one should use the solutions of Maxwell's electromagnetic wave equations with appropriate boundary conditions within these devices. In this section, I will provide information about the a) principal modes, b) *Q* factors, and c) cut-off wavelengths which are associated with cylindrical cavities.

Waveguides, in general, are hollow metal pipes through which electromagnetic waves propagate. The general solutions to these equations can be found by solving Maxwell's equations under appropriate boundary conditions. The simplest case of understanding the propagation of

electromagnetic fields confined to the interior is by considering the geometry of the waveguides to be a rectangular parallelepiped as shown in Fig. 8.[32]

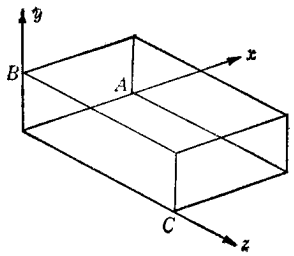

FIG. 8. A parallelepiped shown for rectangular geometry coordinates.

In order to understand how $\vec{E}$ and $\vec{B}$ fields of the electromagnetic waves propagate through these waveguides, we consider the waveguides to be perfect conductors with no closed end surfaces. From Maxwell's equations:

$$\left.\begin{array}{ll} \text{(i)} & \Delta \times \vec{E} = -\dfrac{d\vec{B}}{dt} \\ \text{(ii)} & \Delta \bullet \vec{B} = 0 \\ \text{(iii)} & \Delta \bullet \vec{E} = 0 \\ \text{(iv)} & \Delta \times \vec{B} = \dfrac{1}{c^2}\dfrac{d\vec{E}}{dt} \end{array}\right\} \qquad (2.7)$$

we can then study the propagation of fields and components along the *x, y* and *z* axis by simply solving the wave equations for the $\vec{E}$ and $\vec{B}$ fields that have sinusoidal time dependence of $e^{-i\omega t}$.

$$\text{This implies:} \quad \left.\begin{array}{ll} \text{(i)} & \vec{E}(x,y,z,t) = \vec{E}_o(x,y)e^{\pm i(kz-\omega t)} \\ \text{(ii)} & \vec{B}(x,y,z,t) = \vec{B}_o(x,y)e^{\pm i(kz-\omega t)} \end{array}\right\} \qquad (2.8)$$

where the electromagnetic waves are propagating along the $\pm z$ axis with angular frequency ω and have their directional components along *x,y,z* in order to fit the boundary conditions on the inner walls $E_{\|}$ to the walls and $B \perp = 0$ to the walls. We can show[33] that upon solving Maxwell's equations (2.7i) and (2.7iv) we get two uncoupled equations for the longitudinal components of $\vec{E}$ and $\vec{B}$ as given by Eq. (2.9).

$$\left.\begin{array}{ll} \text{(i)} & \left[\frac{\partial^2}{\partial x^2}+\frac{\partial^2}{\partial y^2}+\left(w/c\right)^2-k^2\right]E_z=0 \\ \text{(ii)} & \left[\frac{\partial^2}{\partial x^2}+\frac{\partial^2}{\partial y^2}+\left(w/c\right)^2-k^2\right]B_z=0 \end{array}\right\} \qquad (2.9)$$

Eq. (2.9) is an important equation that tells us about the dominant modes of the waveguide or cavity.

A detailed set of components of these fields can be found in any advanced electromagnetic textbook. But to summarize for waveguides, only one out of two major sets of predominant modes can exist, either transverse electric mode or transverse magnetic mode, implying that they are transverse with respect to the axis of reference. Mathematically, these can be expressed through Eq. (2.9) by setting, $E_z = 0$ for transverse electric or setting $B_z = 0$ for transverse magnetic modes.

Conventionally, from an engineering perspective, these modes are expressed as a set of integers *l, m* and *n*, depending upon the number of half-period variations of **E** and **B** fields which are along *x,y,z* axis. Hence, in order to specifically define the waveguide mode, the convention transverse electric (TE_{lmn}) or transverse magnetic (TM_{lmn}) will be used. These modes also play a critical role in calculating the cut-off wavelengths for propagating the E or B vectors through the waveguide of specified dimensions *A, B,* and *C* as shown in Fig. 8, where

l = number of half-period variations of $\vec{E}$ and $\vec{B}$ along x,

m = number of half-period variations of $\vec{E}$ and $\vec{B}$ along y,

n = number of half-period variations of $\vec{E}$ and $\vec{B}$ along z.

Using the knowledge of these *l,m,n*'s, which are basically eigenvalues of the wave equation, we can define the cut-off wavelengths to be

$$\lambda_c = \frac{2}{\sqrt{\left(\frac{l}{A}\right)^2 + \left(\frac{m}{B}\right)^2 + \left(\frac{n}{C}\right)^2}} \quad . \tag{2.10}$$

From Eq. (2.10) the cut-off frequency f_c can be computed simply using the identity $f_c = \frac{c}{\lambda_e}$.

These principle variations of the fields even define the impedance associated with the particular mode of these waveguides and can be expressed by Eq. (2.11):

$$\left.\begin{aligned} Z_o(TE_{\text{mode}}) &= \frac{\eta}{\sqrt{1-\left(\frac{f_c}{f}\right)^2}} \\ Z_o(TM_{\text{mode}}) &= \eta\sqrt{1-\left(\frac{f_c}{f}\right)^2} \end{aligned}\right\} \tag{2.11}$$

where, $\eta = \sqrt{\frac{\mu}{\varepsilon}}$, μ = permittivity of free space and ε = dielectric constant.

Eq. (2.10) states that either by varying *l,m,n* values or essentially the dimensions of the waveguide, we can generate an infinite combination of modes, thereby affecting the perturbation responses of the waveguides. In order to overcome this problem and to be able to discriminate other spurious frequency responses, the lowest mode TE_{010} and TE_{011} is used in most common applications.[34]

So far we have seen the most general solutions to the Maxwell's equations in rectangular coordinates. In our experiments, we used cylindrical resonant cavities to study the perturbation type responses of materials (solids/gases) to the electromagnetic fields present inside the hollow, cylindrical cavities. More about the experimental details is given in Chapter 3. In the next section, we present the fields inside cylindrical resonant cavities, their modes, cut-off frequencies, and *Q* values. Also, advanced applications of these cavities that have been studied by many other researchers in the past will be mentioned. A comprehensive list of selected readings is provided in the appendix.

Cylindrical Microwave Resonant Cavities

Even though electromagnetic resonators can assume any shape or geometry as long as they are low in nature and have defined boundaries for the electromagnetic propagation of waves, precise spectroscopic experiments can be designed from them. In this investigation I have chosen a cylindrical resonator, a cylindrical resonant cavity which is formed by closing the ends of a cylindrical waveguide by conducting plates on its ends as shown in Fig. 9.[35]

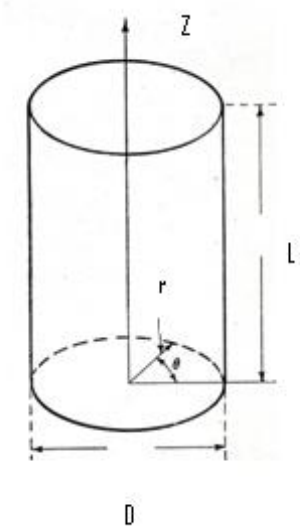

FIG. 9**.** Figure depicting cylindrical geometry coordinate system for a cylindrical resonant cavity

As discussed in previous sections, a cylindrical microwave resonant cavity can be considered to be *N* parallelly arranged LCR circuits where *N* tends to infinity and is constructed by λ/4 sections of such circuits as described in the Air Force manual *Radar Circuit Analysis*.[36]

In rectangular waveguides there exist two orthogonal fields **E** and **B.** Similarly, in the cylindrical resonant cavities these two fields are also orthogonal to each other and perpendicular to the direction of propagation of the wave vector (***k***). Eigenvalue solutions of the wave equation subjected to their boundary conditions are conventionally called the modes of resonance and are labeled as either transverse electric (TE_{lmn}) or transverse magnetic (TM_{lmn}). Subscripts *l,m,n* define the patterns of the fields along the circumference and the axis of the cylinder. Formally, these (*l,m,n*) values are the number of full period variations of E_r with respect to θ, number of half-period variations of E_θ with respect to *r*, and number of half-period variations of E_r with respect to the *z* axis, respectively.[37] In our investigation, the cylinder was tuned to oscillate in its fundamental TE_{011} mode, and will be used for all future references in this work for the purpose of our discussions. For a TE_{011} mode resonant cavity, the boundary conditions are

$E_z = 0$ for $\rho = r$ at the walls of the cavity (2.12)

and

$E\rho = E\phi = 0$ for $Z = 0,L$ at the end plates of the cavity (2.13)

The boundary conditions and the subscripts labeled with the electric field vector are with reference to Fig. 9. As seen from Eqs.(2.12) and (2.13) due to the boundary conditions the **E** field is confined between the cavity walls and the space between the end plates perpendicular to the axis of the cavity. Several parameters govern the resonant modes of these cavities and are to be discussed in a later section. For a complete description of the solution of the Maxwell's equations with the boundary conditions given above, one can refer to the appendix, but in

general these TE_{lmn} modes are the orders of the Bessel functions and their components can be expanded in terms of sine and cosine functions as given by Eq. (2.14).

$$\left.\begin{aligned} E_r &= -l\frac{J_l(k_1 r)}{k_1 r}\sin(l\theta)\sin(k_3 z) \\ E_\theta &= -J_l'(k_1 r)\cos(l\theta)\sin(k_3 z) \\ E_z &= 0 \end{aligned}\right\} for\ n,m>0$$

$$\left.\begin{aligned} B_r &= \frac{k_3}{k}J_l'(k_1 r)\cos(l\theta)\cos(k_3 z) \\ B_\theta &= -l\frac{k_3}{k}\frac{J_1(k_1 r)}{k_1 r}\sin(l\theta)\cos(k_3 z) \\ B_z &= \frac{k_1}{k}J_l(k_1 r)\cos(l\theta)\sin(k_3 z) \end{aligned}\right\} for\ n,m>0 \Bigg\}. \qquad (2.14)$$

where in the above equation $k_1 = x_{lm}/D,\ k_3 = n\pi/L,\ k^2 = k_1^2 + k_3^2,\ \lambda = 2\pi/k$
x_{lm} *are roots of* $J_1(x)$ *and* J_l'

D is the diameter of the cavity and L is the length of the cavity that is adjustable with the aid of a tuning plunger, and subscripts *l,m,n* are the usual eigen modes of resonance as discussed earlier.

Thus, in a TE_{011} mode, it can thus be concluded that the **E** field patterns are not repeated along the θ direction and are half-wavelengths along the ρ directions. Some of the field patterns for TE_{lmn} modes have been sketched in much detail, provided by Dahiya [30].

As Dahiya illustrates, the **E** field is most intense in the center of the cavity along the axis of the cavity and is in circular patterns. Just like the **E** fields, **B** fields have no θ dependence and are symmetric with θ. Derivations of the electrical and magnetic wave components and their relationships with resonant frequency have extensively been studied in the past.[38]

These cylindrical cavities have widely been studied in the past as resonant circuits in spectroscopy as absorption cells, and are used as wavemeters. The fact that their quality factor Q

can be made of the order of 20,000 makes them highly suitable for microwave spectroscopy as they can store a large amount of electromagnetic energies as seen by Eq. (2.14)[39]

$$Q = \frac{2\pi f \times Maximum\ stored\ energy}{Power\ loss\ per\ cycle} \tag{2.15}$$

where f is the frequency of oscillations in (rad/s) and the power loss is typically measured in decibels for low-powered electromagnetic circuits. The quantity Q is a unit-less quantity and primarily depends upon the geometry of the objects as well as the material used to construct the device. It has been shown in Slater's perturbation theory that the Q of a cavity can be expressed in terms of different parameters (skin depth and strength of the fields, etc.). In terms of laboratory measurements, the Q value of a circuit can be calculated by measuring the inflection points of a typical Lorentzian signal which tells us the width at half-power maxima and is simply a ratio expressed by Eq. (2.15)

$$\mathrm{Q} = \frac{f_o}{\Delta W} \tag{2.16}$$

where f_o is the resonant frequency and ΔW is the width at half-power maxima, which was shown previously. Samples placed in these devices will then be subjected to stray field strengths as compared with other resonant devices such as waveguides or disk resonators.

There are several different methods of determining the normal modes of resonance within these cavities. A good knowledge of cut-off wavelengths is required in order to be able to design a typical resonant cavity. Eqs. (2.17) and (2.18), along with Fig. 10, can be used to compute the cut-off wavelengths of the cylinder and be able to selectively tune the resonant cavity in TE_{011} mode by eliminating other spurious modes which exist in these cylinders.

$$\lambda = \frac{2}{\sqrt{\left(\left(\frac{2x_{lm}}{\pi D}\right)^2 + \left(\frac{n}{L}\right)^2\right)}} \tag{2.17}$$

and

$$(fD)^2 = \left(\frac{cx_{lm}}{\pi}\right)^2 + \left(\frac{cn}{2}\right)^2 + \left(\frac{D}{L}\right)^2 \tag{2.18}$$

where the *l,m,n* subscripts have their usual meanings, x_{lm} is the m^{th} root of the J_l's, D is the diameter, L is the length, c is the speed of light and f is the resonant frequency.

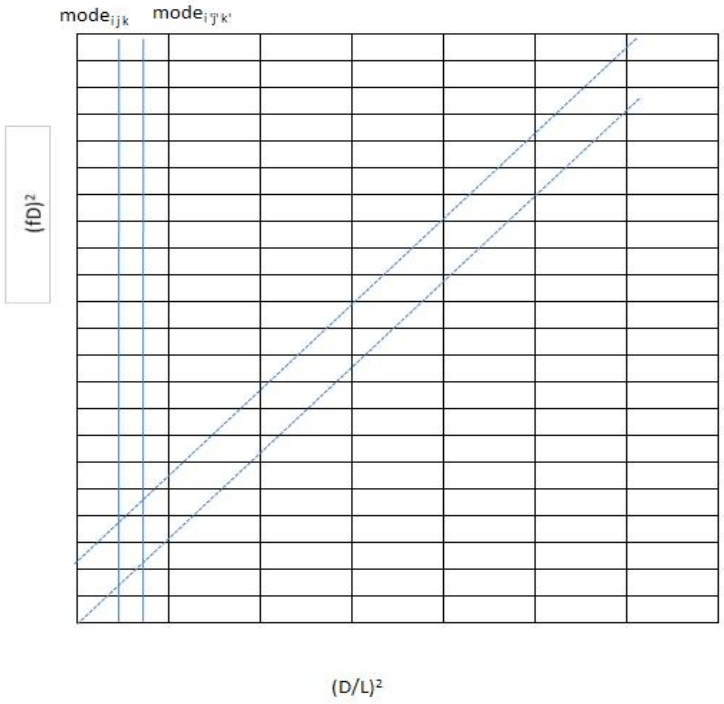

FIG. 10. Conceptualized mode chart from Technique of Microwave Measurements[40] in order to selectively tune the resonant cavity.

For experimental convenience, a spreadsheet software based procedure (as shown in Fig. 11), was designed to quickly tune the cavities to resonate in the TE_{011} mode for that particular frequency.

RESONANT FREQUENCY CALCULATIONS USING MODE-CHART

The Cavity's Diameter & Length is fixed

$$\lambda = \frac{2}{\sqrt{\left(\frac{2\chi_{lmn}}{\pi D}\right)^2 + \left(\frac{n}{L}\right)^2}} \quad cm$$

$$\nu = \frac{C}{\lambda} \quad GHz$$

Diameter in Cms:	5
C in cms/sec	3E+10
π =	3.14285714
n =	1

Length	D/L	(D/L)²	TE Mode	χ_{lm}	n	λ	ν	fD	fD²
2.4991503	2.00068	4.0027205	111	1.841	1	4.313214949	6.96E+09	3.48E+10	1.21E+21
			211	3.054		3.585234519	8.37E+09	4.18E+10	1.75E+21
			11	3.832		3.17033669	9.46E+09	4.73E+10	2.24E+21
			311	4.201		2.99481832	1.00E+10	5.01E+10	2.51E+21
			411	5.318		2.543664192	1.18E+10	5.90E+10	3.48E+21
			121	5.332		2.538710061	1.18E+10	5.91E+10	3.49E+21
			511	6.415		2.199653274	1.36E+10	6.82E+10	4.65E+21
			221	6.706		2.121718209	1.41E+10	7.07E+10	5.00E+21
			21	7.016		2.043946785	1.47E+10	7.34E+10	5.39E+21
			212	3.054	2	2.248020021	1.33E+10	6.67E+10	4.45E+21

FIG. 11. Spreadsheet designed to calculate the selective modes for a cavity.

A resonant cylindrical cavity equipped with a tuning rod as shown in Fig. 12 can be tuned with the help of the mode calculation and Eq. (2.17) and (2.18) in order to resonate in the fundamental mode at specific frequencies and discriminate against other neighboring modes that sometimes overlap for certain frequencies. For example, in our case for the given dimension of the cylinder, I tuned the cavity with the help of tuning rods and resonated it at ~9 GHz and was able to successfully isolate them from the neighboring modes TE_{311} and TE_{211} that otherwise could have led to spurious recording of the data.

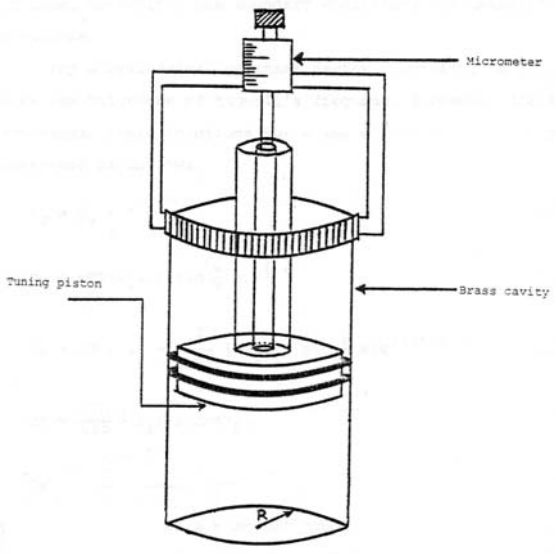

FIG. 12. Sketch of a tunable resonant cylindrical cavity with a plunger.

Experimental details are given in the following chapters. In my scientific investigation, I tuned the resonant cavities under vacuum in order to reduce losses to the neighboring atoms of air. The unloaded cavity was first studied to characterize its Q as well as its cut-off wavelength. For an unloaded cavity under vacuum and operating in TE_{lmn} mode,[41] the Q factor is given by Eq. (2.19).

$$\frac{Q\delta_s}{\lambda} = \frac{\left\{1-\left(\frac{l}{x_{lm}}\right)^2\right\}\left\{x_{lm}{}^2+\left(\frac{n\pi D}{2L}\right)^2\right\}^{3/2}}{2\pi\left\{x_{lm}{}^2+\left(\frac{n\pi D}{2L}\right)^2+\left(1-\frac{D}{L}\right)\left(\frac{n\pi Dl}{2Lx_{lm}}\right)^2\right\}} \tag{2.19}$$

where δ_s is the skin depth of the material used in the cavity for its construction and is primarily the main factor involved in the lossy part of the amplitude with respect to the depth of penetration of the electromagnetic waves; l,m,n have their usual meaning as defined previously; D is the diameter of the cavity; L is the length of the cavity; and x_{lm} is the m^{th} root of the Bessel function J_l'.

In this experimental set up, the resonant cylinder was coated with silver, which is a good conductor and whose skin depth at microwave frequencies is very low, being on the micron level. For TE_{011} mode Eq. (2.19) can be expressed by Eq. (2.20)

$$\frac{Q\delta_s}{\lambda} = \frac{1}{2\pi}\frac{\left\{(3.832)^2+\left(\frac{\pi D}{L}\right)^3\right\}}{\left\{(3.832)^2+\left(\frac{\pi D}{L}\right)^2\right\}}. \tag{2.20}$$

By using the skin depth of silver at ~ 9GHz, it can be shown that the Q value of these unloaded cavities under vacuum is of the order of 20,000. Due to such high quality factors, these resonant devices have a very sensitive perturbation response when loaded with any external medium.

Depending upon the permittivity as well as permeability of the sample, the response of these resonant cavities will have a shift in their resonant frequencies as well as changes in their quality factors. Whenever the samples are loaded in the intense electric field of the cavity, Slater's perturbation theory[42] states that the shift in the resonant frequencies and change in the Q values of the resonator can then be expressed by Eqs. (2.21) and (2.22) respectively as given below:

$$\frac{\delta f}{f_r} \approx -\frac{(\varepsilon' - 1)}{2} \frac{\int_{\Delta\upsilon} \vec{E} * \overrightarrow{E^*} d\upsilon}{\int_V \vec{E} * \overrightarrow{E^*} dV} \tag{2.21}$$

where δf is the shift from the resonant frequency, ε' is the real part of the dielectric constant, $d\upsilon$ is the volume of the sample perturbing the cavity, and V is the cavity volume, and

$$\Delta\left(\frac{1}{Q}\right) = \varepsilon'' \frac{\int_{\Delta\upsilon} \vec{E} * \overrightarrow{E^*} d\upsilon}{\int_V \vec{E} * \overrightarrow{E^*} dV}. \tag{2.22}$$

The above equation is an expression of the ratio of the energy dissipated into the sample to the total energy supplied to the resonator per cycle of resonance. The expressions above indicate how the dielectric loading or the now "pull-push" effect of the new material loaded in the resonant cavity depends upon its susceptibility. The above expression is true only in a case where there is perturbation of the electric field as in our study. When considering both magnetic as well as electric field perturbation, the expression for the Q change of the cavity can be expressed by Eq. (2.23) given below.

$$\Delta\left(\frac{1}{Q}\right) = \frac{\Delta w}{w_r} = \frac{1}{2w_s} \int_{\Delta v} \left(\mu_o H \bullet H^* - \varepsilon_o E \bullet E^*\right) dv \tag{2.23}$$

where in the above expression w_s is the total energy stored in the system and dv is the small volume element of the perturbing sample.

Depending upon the methods of coupling the cavities to the oscillator, the modes of excitation of these resonant devices can be determined. In practice, waveguides and directional couplers have been studied to energize these resonant cavities in their selective modes.[43] Proper coupling effectively reduces the losses in these resonant cavities and enhances the sensitivity of the equipment. Primarily losses in these resonant circuits arise due to the mechanical changes caused by joule heating. Such losses can be reduced significantly by polishing the interior wall surfaces of the cylinder with materials that have good conductivities.[44] In order to enhance the stored electromagnetic energies within the cylinder, efficient coupling of the waveguide is necessary.

For wavelengths below 3cm ($f \leq 10$ GHz), iris holes (which act as radiating dipoles) are used to couple the cylinders to the waveguides. The size of the hole and the thickness of the intervening walls determine the tightness of coupling. In cavities, this coupling is accomplished by one or two holes across the walls of the cavity. For our scientific investigation, the TE_{011} mode was excited through one single iris aperture with a waveguide coupler mounted on the sidewall of the cavity. The mode of attachment was such that the waveguide's long dimension was made parallel with the axis of the cavity in order to radiate the electric field between the two end plates. A schematic of our setup is provided in the following chapter.

Use of Cylindrical Cavities in the Experiment

The purpose of this scientific investigation was to study the interactions of various gas molecules (mildly polar to non-polar) with various dielectric loads introduced in them. The perturbation response of the cavities was studied by allowing the medium inside these vacuum

tight cylinders to progressively change through a set of controlled runs. It is seen through Eqs. (2.21) and (2.22) that by measuring the resonant frequency shifts as well as change in the Q values of these cavities, the nature of the dielectric response of the perturbing medium can be characterized. The complex dielectric response of various substrates such as single-walled carbon nanotubes (SWCNTs), silica gels, cotton fibers, and activated charcoal was studied with each cycle of gassing and degassing of various gas molecules onto them, mildly polar to non-polar. The responses were compared with several background runs made with cavities with only gas molecules perturbing them. Details about the experimental setup, as well as results, are discussed in the following chapters.

Using microwave perturbation techniques in this scientific investigation proves to be a very sensitive technique to measure the propensity of gases loading onto various substrates. This technique is a useful method to measure the difference in the propensity of the gas molecules on various substrates, and can selectively differentiate the response of various substrates for various gas molecules. This, in turn can be used as a highly specific, as well as sensitive, detector to "sniff" various pathogens and other chemical toxins.[45] The microwave resonant cavity technique is a well-studied technique for spectroscopy of materials. Researchers have used these cavities to calculate specific mass as well as moisture contents in the sample by measuring the relative shifts in the resonant frequencies and computing the relative dielectric constant of the medium being introduced inside these cavities.[46] Also many researchers have extensively researched dielectric responses of gaseous media,[47] investigating the polarization response of various gases by relating the dielectric response of the gases with their dielectric constant using the Claussius-Mossotti relationship [Eqs. (2.24) and (2.25) below] for both heavy as well as light gases.

$$\varepsilon = \frac{1 + 2\,A_\varepsilon \rho}{1 - A_\varepsilon \rho} \approx 1 + 3A_\varepsilon \rho \qquad (2.24)$$

where the density of gas is ρ, A_ε is the first dielectric virial coefficient and is given by Eq. (2.25).

$$A_\varepsilon = \frac{N_A}{3\varepsilon_o}\left(\alpha_o + \frac{\mu_o^{\,2}}{3KT}\right) \tag{2.25}$$

α_o is the polarizability tensor for a particular gas and μ_o is the permanent dipole moment, K being the Boltzmann constant and T is temperature of the system in kelvin.

From the above two equations one can now find the necessary details regarding the polarization and dielectric response of specific gas molecules by just measuring the shift in the frequency as stated in Eqs. (2.21) and (2.22). The complete operational details of this experiment are laid out in the next chapter. In this experiment, I will compare the dielectric responses of each gas in a fixed frequency at pressure intervals within an unloaded resonant cavity as well as in the cavity loaded with the chosen substrate to see how the polarization phenomenon for gas molecules deviates in a polarizable substrate medium., Thereby, will be able to conclude, in brief, the effect of these Coulomb forces in adsorption of select gases on select substrates.

CHAPTER 3

EXPERIMENTAL SETUP AND PROCEDURES

Experimental Setup

This part of the chapter is a discussion of the usage of scientific tools and instruments that were unique and necessary to carry out this scientific investigation. Some of the apparatus, such as the microwave resonant cavities, and the accompanying theory were discussed in the previous chapter. Since the investigation results were calibration- as well as mode-dependent, necessary steps have been laid out in this chapter to aid in fully understanding the instrumentation utilized to set up the electromagnetic fields and the gas manifolds to perform controlled runs.

Since this investigation was a study made to characterize the interactions of the gas molecules with various substrates, it was necessary to maintain a good vacuum. Also, due to the fact that the electromagnetic fields inside the waveguides and cavities are very sensitive to the boundary conditions as well as the nature of perturbants, it was necessary to maintain the space inside the cylinders free of any external atmospheric impurities. The customized manifold design shown in Fig. 13 was sketched and the assembly was machined at the students' machine shop facility.

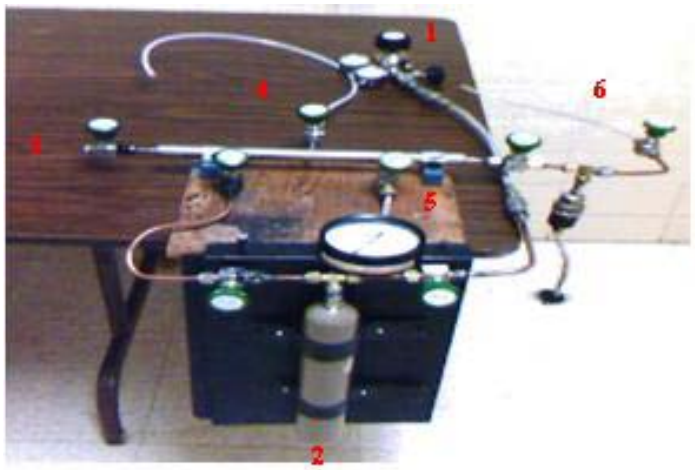

FIG. 13**.** Customized manifold assembly to regulate the flow of gas from high to low pressure.

As seen in this Swagelok® equipped valve assembly which has been numbered 1-6, each section of the manifold played its own role in channelizing the flow of the gas from the source cylinder of the gas to the resonant cavities. A high pressure miniature bottle source for cylinders of various gases was attached to the feed line through point 1. The gases used in the scientific study are listed in the appendix and their physical as well as chemical properties tabularized.[48] Research grade gases were obtained from Sigma-Aldrich® and Linde Gas® Corporation and were 99.9 % pure. The vacuum in the system was set up using a roughing pump that was attached to the system through point 6 shown in Fig. 13. A ring gauge as shown in Fig. 14(a) was attached at point 5 in Fig.13 and was used to read the relative pressure of the gas within the two resonant cavities [shown in Fig. 14(b)], which were attached at points 3 and 4 of the manifold assembly as shown in Fig.13. An extra reservoir cylinder attached at point 2 in Fig. 13 was used for a safety measure as it reduced the risk of significant pressure difference between a high-pressured source cylinder and the resonant cavities under high vacuum.

FIG.14a (left) and FIG.14b (right). Ring gauge and coupled resonant cavities.

The microwave source used in this study was a microwave network analyzer model IFR 6845[49] shown in Fig. 15. Integrated into this single instrument are a synthesized source, a three-input scalar analyzer, and a synthesized spectrum analyzer. Complete engineering details of this equipment are beyond the scope of this document, but the basic function of this instrument is to

generate a constant width (CW) output of microwaves capable of sweeping an oscillator with frequencies between 10 MHz to 47GHz. Depending upon the physical dimensions of the resonator and their coupling with the source, this spectrum analyzer can operate to detect the microwave absorption profile of the resonator either in the reflection or in the transmission mode, as shown on the liquid crystal display of the analyzer screen in Fig. 15.

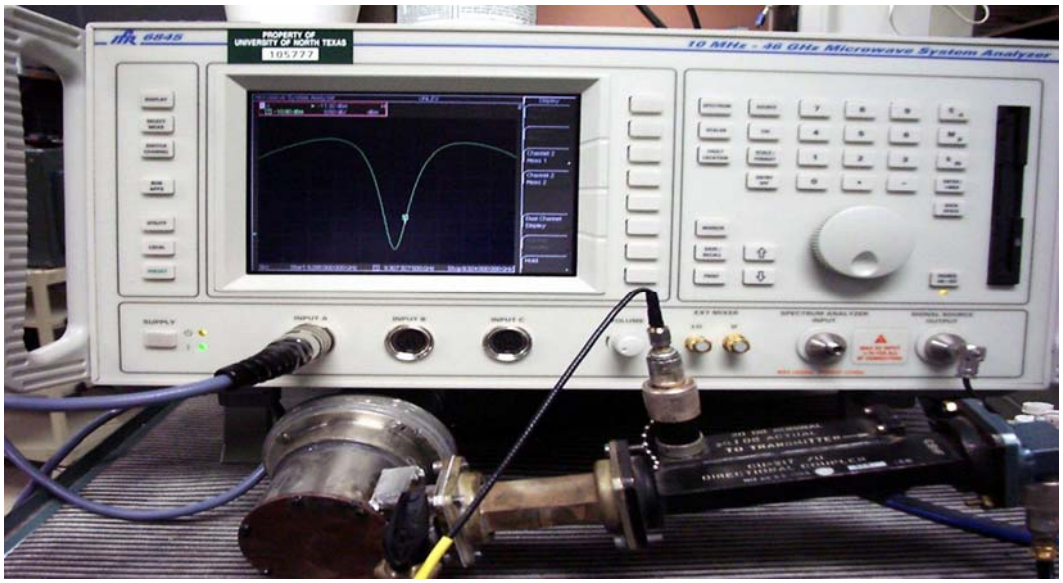

FIG.15**.** IFR6845 series microwave network analyzer used as the synthesized source to generate and feed the microwaves into the resonant cavities.

The synthesized source has low phase noise and 1Hz frequency resolution. The crystal detector used to detect the absorption profile usually produces an output current such that the current-voltage characteristic is represented by $I \propto V^2$. The output power can be approximately related to the square of the input power; hence, a small power that is input into the cavity containing some load will produce a relatively large change in the output signal. This engineering principle made it relatively simpler to study the effects of both low and high concentrations of gases absorbed onto the substrate. Equipped with a group delay, the electronics of the equipment provide us with an opportunity to study the distortion of the signal. This device

is internally capable to Fourier transform the signal from its time domain to its frequency domain as implied in Eq. (3.1)

$$\text{Time domain: } x(t)e^{i\omega_c t} \text{ to frequency domain: } X(\omega-\omega_c) \tag{3.1}$$

This signal, when fed into a device whose frequency response is $H(\omega)$, can be studied to reveal what effect the device had on the original signal. This is done internally by demodulating the original signal by multiplying it with a phasor of frequency ω_c and solving for the shift in the phase of the signal. The shift in the frequency and the phase shift of the signal can be related to the group delay of the detector by Eq. (3.2) below:

$$\delta\omega \approx \frac{\delta\phi}{T_g} \tag{3.2}$$

where T_g is the group delay and is a characteristic of the semiconductor crystal and, in our case, had a value ranging from $\pm 1\,\mu s \quad to \quad \pm 10\,\mu s$. So, for small value-changes in the phase of the signal, the crystal detector was able to detect the smallest shift in the frequency of the r-f waves. Female connectors (2.92 mm) made of gold for low impedance were used to connect the input and output from the source and the waveguide assembly, respectively, with the help of coaxial wires. The signals were fed into the main waveguide system that had a directional coupler on its side and a reflectometer on its end, as shown in Fig.16.

FIG. 16**.** Shown on the side wall of the waveguide is the feed in line on the opposite wall (not visible) and an output to measure the reflection profile of the signal.

For our scientific investigation, the TE_{011} mode was excited through one single iris aperture shown in Fig. 17, with a waveguide coupler mounted on the sidewall of the cavity. The iris in this experiment served dual purposes of both acting as radiating dipoles to transmit the electromagnetic radiations into the cavity as well as serves as the inlet hole for the gas molecules to flow in through copper tubing as shown in Fig. 17.

FIG. 17. An interior view of the bottom half of the cavity.

The mode of attachment was such that the waveguide's long dimension was made parallel to the axis of the cavity in order to radiate the electric field between the two end plates as shown in Fig.18.

FIG. 18. Coupling of the waveguide to the sidewall of the resonant cavity along its long dimensions parallel to the axis of the cavity.

Using the mode chart in Fig. 10 and Eqs. (2.16) and (2.17) the resonant cavity was tuned with the help of a tuning plunger as shown in Fig. 19 to resonate in the TE_{011} mode. The two cavities were coupled to each other with the help of waveguides and RF switches.

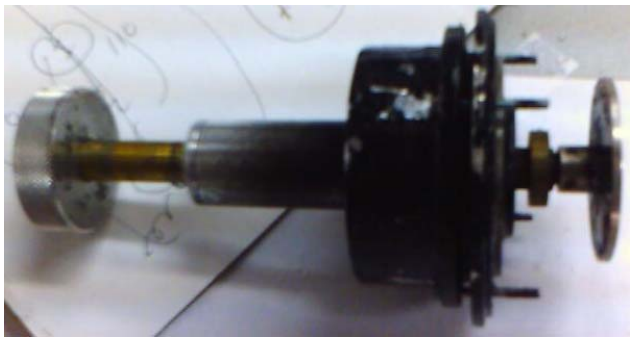

FIG. 19. A tuning rod for tuning the resonant cavity to a selective mode

The r-f switching along with an impedance coil tuner enabled us to use the two resonators in parallel in a differential form to conduct the reference studies as discussed in the following section.

Goal of This Scientific Investigation

This scientific investigation was an empirical study to observe and characterize the nature of interactions of various gases, both mildly polar as well as non-polar gases, with the various substrates listed in Table 2. The two resonant cavities served this purpose for doing comparative studies. A cavity containing no load was used as the reference cavity to characterize the nature of perturbation response of only the gas molecules, whereas, on the other hand, another similar resonator was loaded with different substrates (S1-S7) progressively and the same gases were cycled through them. On the whole, six different experiments were made to characterize the responses of the cavities when gases were cycled through them. Their responses in terms of their affinities to various substrates are listed in the table.

TABLE 2. Various substrates that were loaded in the test cavity extreme right as shown in Fig. 14b.

Labeled	Various substrates in amorphous as well as fibrous forms loaded for each experiment.	Form/Shape/Properties
S1	Untreated single walled carbon nanotubes (SWCNT)	Amorphous powder, chirality (7,5 and 6,5) semiconducting mixed with conducting
S2	Thermally treated nanotubes	Just as S1
S3	Activated charcoal	Granular crystals
S4	Silica gel	Amorphous granules
S5	Cotton fibers	Cotton medical grade

The experimental interest was to study how the dielectric response of the system changes when mixtures of gases as well as various loads perturb the free space of the system. In each experimental study with a specific substrate (S1-S5) the samples were placed in a rod-shaped Teflon® sample holder, which was then placed in the center of the bottom plate parallel to the axis of the cavity. (See Fig. 18.) From a knowledge of the E and B fields (p. 26, above) for the cavity in TE_{011} mode, it is clear that the center of the bottom plate of the cavity has the largest gradient of the E field and as such will be the most intense as well as sensitive portion of the field to do the perturbation studies. A Teflon® sample holder as a very low-loss material was chosen to assure minimal power loss in the holder itself and that most of the field will be absorbed/scattered by the samples loaded inside the holder.

The perturbation responses of the resonant cavities with and without the load were studied using the standard Slater's perturbation model. Studies have been made in the past[50] to study the response of various phases of matter; the experiment described in this investigation is a unique work done to characterize the nature of interactions of various gases with different nano- as well as micromaterial loads inside the resonant cavities. The dielectric responses, as well as

the deviation of the first dielectric coefficients for the gases, have been studied using this technique. The Claussius-Mossotti relation was used to find the polarizability of the gas molecules and the effect of nanomaterials on the effective polarizabilities on the gas molecules which aided in understanding the binding energies and selective adsorption of these gases onto the substrates. The next chapter provides a discussion of the results of varying adsorption properties of different substrates with different gases. Also, due to the high sensitivity of the device and selective adsorption of the materials, an innovative application resulted: a highly sensitive miniaturized sensor was developed to detect airborne chemical and biological toxins. Details have been provided in the conclusion of this dissertation.

Experimental Techniques Involved in Performing the Experiments

There were seven different types of experimental runs made on the whole. The purpose of the experiment was to differentiate between the responses of the microwave resonant cavities when subjected to different loads as well as different gases. Summarized below are the steps for the major types of runs that were performed:

1) Both unloaded (no substrate present) as well as loaded resonant cavities were vacuum sealed and maintained at a base pressure of 10^{-4} Torr below atmosphere.
2) The two cavities were tuned to their fundamental modes of resonance with the help of an impedance matching coil and were resonating in the frequency range of 8.4 – 9.4 GHz.
3) The test cavity for each experiment was loaded with an appropriate substrate (S1-S5) and was tuned back to its fundamental mode. The only change was in the fundamental frequency that is expressed by Eq. (3.3) below:

$$\frac{\Delta f}{f_o} = \frac{-\int_o^a \int_0^{\Delta l} \int_0^{2\pi} (\varepsilon^{'} - 1) E^2 r dr d\phi dz}{\int_0^{\rho} \int_0^{L} \int_0^{2\pi} E^2 r dr d\phi dz} \tag{3.3}$$

where the above equation implies that the shift in the resonance frequency will be towards a lower frequency when a dielectric sample changes the effective length of the cavity by Δl and the radius of the sample holder (*a)* is introduced into the cavity. As a result, whenever the samples were introduced into them, their fundamental resonant frequency was lowered due to the dielectric load.

4) On the other hand, the reference cavity that was void of any load was subjected to only the gas molecules that were cycled through the cavity, progressively incrementing the pressure by every inch. The gases were flushed in the cavity by incrementing the pressure of the gas from 0 inches of Hg through 15 inches of pressure and the frequency response of the cavity was recorded for each increment in the number of molecules introduced into the system. The frequency was also recorded for each decrement in the pressure/molecules from the cavity upon producing a vacuum.
5) Using a similar process, the test cavity loaded with different substrates was cycled progressively with different gases and the measurements of the frequency response of the cavity were logged. The complete experimental protocol is summarized by a thematic illustration, Fig. 20.
6) Finally, it is important to mention how the data from the microwave network analyzer was recorded for analysis of the frequency response. The microwave network analyzer described previously offers two options: automatic logging of the frequency absorption response of the system or manual recording of the data. Fig. 21 shows a typical

Lorentzian shaped shift in the absorption profile of the resonant cavity obtained automatically from the network analyzer when the cavity was perturbed when 1 inch of Hg pressure of the gas was introduced into the cavity.

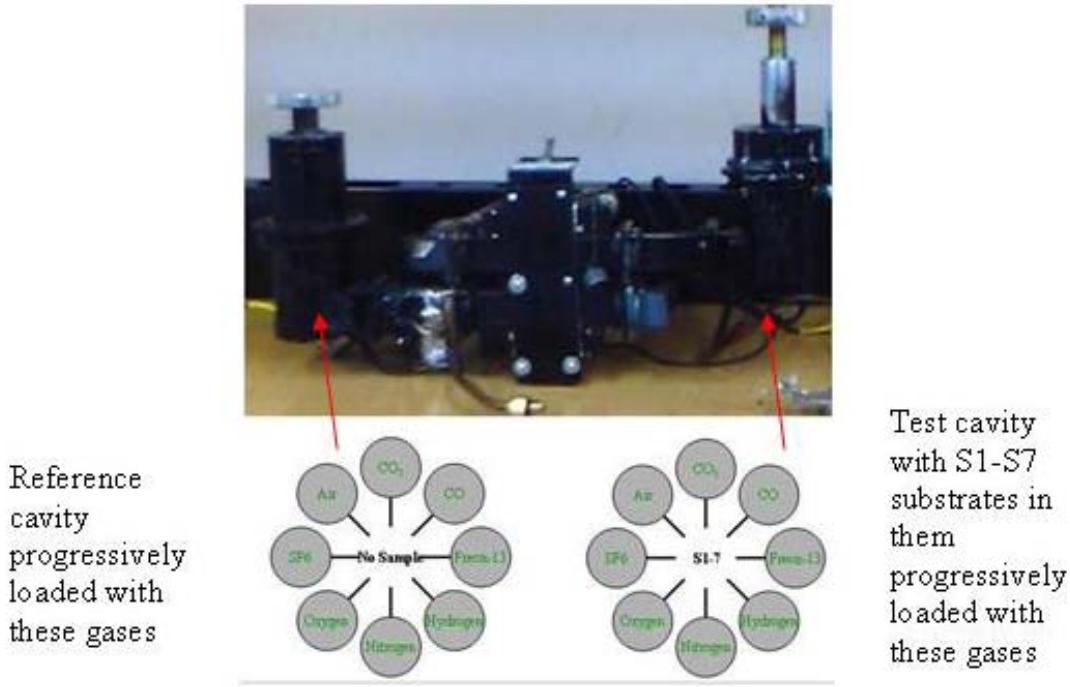

FIG. 20. Experimental protocol summed up in this figure about how the runs were made for different gases with two different resonant cavities.

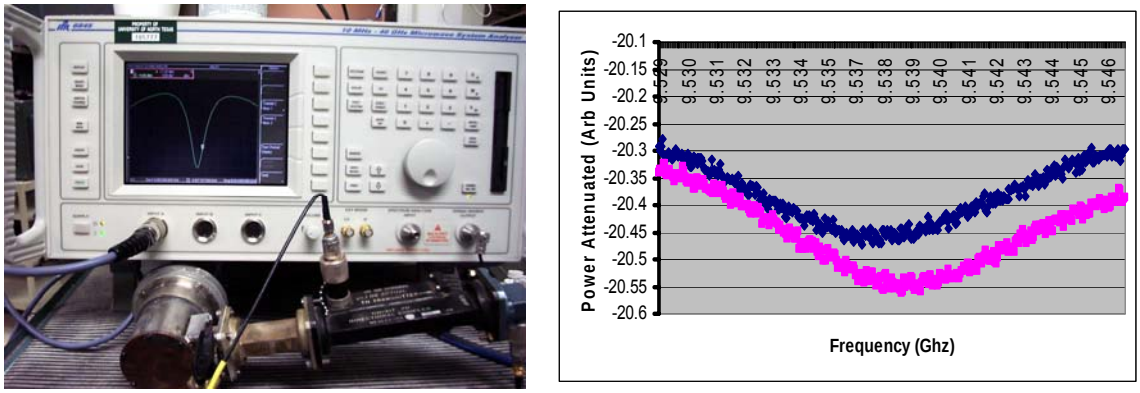

FIG. 21**.** A typical scan of the shift in the resonance frequency (pink and blue) spectral profile when one inch of atmospheric gas was introduced into the cavity, initially under vacuum. The spectral profile on the right is an Excel analysis of the network analyzer's marker profile as shown on the LCD display on the left.

7) Using this protocol, continuous runs were made, progressively increasing the gas pressure within the cavity. The plots were logged for various sweeps of frequency vs. pressure of the gas. Consecutive shifts in the marker of the analyzer were then plotted in Excel as shown in Fig 22.

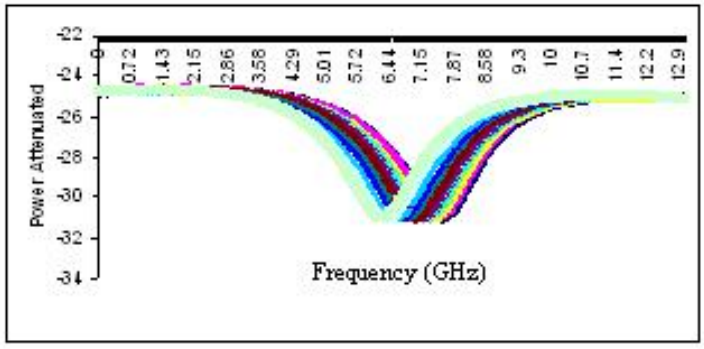

FIG. 22. As seen in the above figure, with every inch of increase in the gas pressure, the frequency of the cavity shifts to a lower value due to the increase in the dielectric material loading the cavity.

8) This procedure was found to be very time consuming as the data recording process onto the floppy diskettes was a lengthy process. In order to see the shifts in the frequency of the system, several Lorentzian fits were required. The Lorentzian method was involved in fitting the absorption profile using the standard Lorentzian fit method described by Eq. (3.4).

$$L = \frac{A}{\left[1+\left(\frac{x-x_o}{x_0}\right)^2\right]} \tag{3.4}$$

Using the above Lorentzian formula, the curves were plotted to make the "best fit" and the shift in the marker (x-x_o) points, in which x_o was the reference point of the marker and x was

the new position to which the marker was shifted due to the loading of gas. This value was calculated from the fit, which was then plotted against the pressure of the gas to see how the resonance frequency shifted upon cycling the gas through the system. Shown in Fig. 23 is the plot of the center marker position of each new shifted frequency vs. the pressure for complete cycling of the gas through the system.

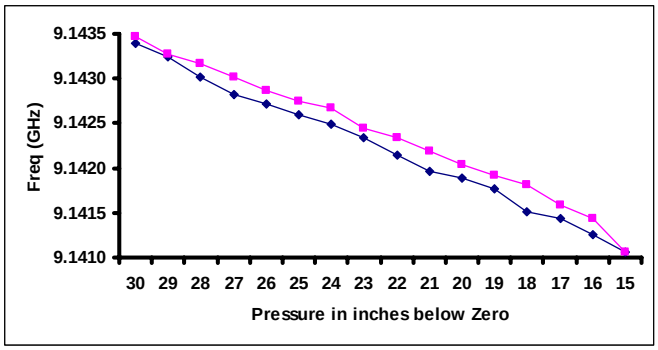

FIG. 23. A typical response of the frequency shifts vs. the pressure of the gas collected manually during a full cycle of gassing as well as degassing of the system.

Further, in order to quantify the area between the cycle of gassing and degassing, another best fit method was required. Hence, it is seen from this procedure that the process for carrying out a full experimental investigation was extremely long.

Modifying the setup and adding a data acquisition card that can link the network analyzer directly to the computer to do the scans as well as make the best-fit analysis can improve the efficiency for further data collection. Due to unavailability of such a setup at this time, an alternative approach was employed to efficiently carry out the experiments. Below is a brief discussion about how the data were collected manually and then plotted. A standard tabular Excel sheet shown in Table 3 below was used to record the data manually.

TABLE 3**.** Tabular sheet employed to record the data.

	A	B	C
1		Data Collection sheet	
2			
3	Press. (inch. of Hg)	Freq Response gassing	Freq Response degassing
4			
5	0	9.143537500	9.143500000
6	1	9.143412500	9.143425000
7	2	9.143262500	9.143350000
8	3	9.143137500	9.143237500
9	4	9.142962500	9.143162500
10	5	9.142862500	9.143087500
11	6	9.142750000	9.143012500
12	7	9.142650000	9.142962500
13	8	9.142600000	9.142862500
14	9	9.142512500	9.142762500
15	10	9.142450000	9.142650000
16	11	9.142387500	9.142512500
17	12	9.142300000	9.142387500
18	13	9.142225000	9.142237500
19	14	9.142125000	9.142100000
20	15	9.142025000	9.142025000

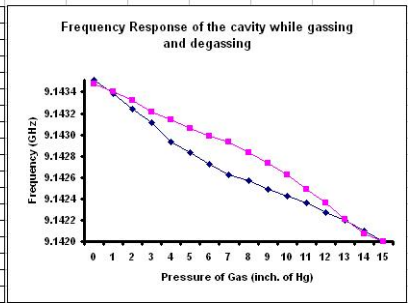

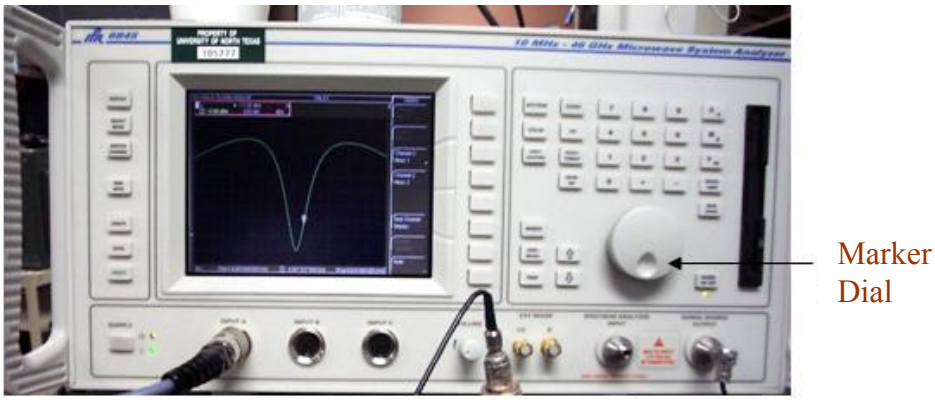

FIG. 24**.** The network analyzer showing a typical shift in the center frequency of the resonator as can be seen on the LCD by the shifted marker.

For every inch of increase/decrease in the gas pressure there is a shift in the resonant frequency profile of the cavity. Using the marker dial as shown in Fig 24, the marker is set to the center of the profile and the readings recorded as shown in Table 3. This approach used the visual technique. Careful measurements were made three or more times to preserve the integrity of the data. Once all the runs were made for each cycling of gas in both the cavities and the data were recorded, plots were made as shown in Table 3 to measure the amount of shift in the resonant frequencies as well as to compare the area between the curves for the complete cycle of gassing and degassing. Using similar procedures, the frequency response was collected for empty resonant cavities for various gases: carbon dioxide (CO_2), carbon monoxide (CO), oxygen (O_2),

hydrogen (H_2), Freon-13™, Freon-22™, argon, nitrogen, and air. The same gases for the same pressures were then tested with the cavity that was consecutively loaded with different substrates (S1-S5). The protocol of making the runs with various substrates was that, for each substrate, complete runs of all the gases were made, ensuring the integrity of the system was not compromised due to multiple openings and closings of the resonant cavities. Also, it is important to mention that before a new set of gas was tried with the same substrate, it was important to check the purity of the samples within the cavity. A residual gas analyzer system (RGA) as shown in Fig. 25 was engaged with the manifold to check for any impurity or contaminant within the sample-loaded resonant cavity. Baking and an ultra-high vacuum system technique was used to ensure that the residual gases were purged from the surface adsorbed nanomaterials.

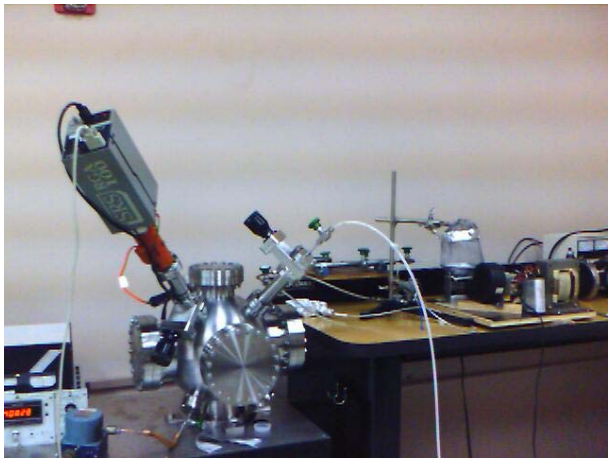

FIG. 25. A residual gas analyzer on the vacuum line to ensure there were no residual impurities present within the system

Using this process, several runs were made and the experiment was conducted with various gases and substrates to characterize the response of electromagnetic fields inside the cavity due to the complex medium of gases and substrates loaded within them. The next chapter deals with all the important results and the discussion that emerges from this experiment.

Tabulated in Table 4 (p. 54) is the summary of all the results that were obtained for four primary gases: CO_2, CO, O_2, and H_2.

CHAPTER 4

EXPERIMENTAL RESULTS AND DISCUSSION

This chapter is a discussion of the experimental results obtained from the gas exchange investigation with various substrates and different gases. For the purpose of simplicity, results for only four primary gases CO_2, CO, O_2, and H_2 are summarized. This range is sufficient to cover the aspects of polarity as well as other exchange forces playing their roles in the frequency response of the resonant cavity. With this set of gases it will be possible to present the response of mildly polar molecules to non-polar molecules such as carbon dioxide. Even though there can exist several models as well as theories that can entail the phenomenon of gas adsorption, this discussion will be limited to experimental-results-based physics of frequency response, dielectric response of the cavities with gases and no substrates, and dielectric response with gases and different substrates. In the conclusion of this chapter, other models are presented that support the experimental results obtained in this investigation. From the results shown below, it is apparent that the dielectric response of the medium present depends upon the polarizability of each medium (gases alone, and gases plus different substrates). The orientation of the substrates plays a critical role, along with the other parameters such as the diameters and the location of the molecules present on the substrate.

Due to the large amount of data collected in this experiment, it is reasonable to present a flowchart of how the data and scientific plots are presented. Summarized below is a comprehensive list of the types of experiments that were carried out. These are followed by a table that summarizes the various plots that are being presented.

Major Experiments Performed and Analyzed

1. Four different gases (CO_2, CO, O_2, and H_2) were introduced into the resonant cavities during each experimental investigation. Progressive scans were made for each cycle of gassing and degassing of these gases, and their frequency response was monitored for every inch of increment or decrement of gas pressure within the cavity.
2. Similarly, the cavity was then loaded with different substrates and the gases were introduced within them and the frequency response was recorded for each substrate with different gases progressively cycled through them.
3. Plots were then made for gases only, as well as for gases-substrates frequency response vs. the pressure of the gas.
4. Polynomial fits were made to compare the frequency response of the cavities to different gases only, as well as to the gases-substrates interactions.
5. Adsorption of gases among the various gases and substrates was then compared
6. Total frequency shifts Δf for various environments (different gases alone, as well as for different gases with different substrates) were then compared.
7. Dielectric constants were then computed and compared.
8. A measurable shift in the dielectric constant of nanotubes contaminated with different gases as compared to clean nanotubes is documented.

Response of adsorption is then quantitatively compared with the results of some theoretical papers published. The observed experimental results are discussed briefly to support the hypothesis that single walled carbon nanotubes (SWCNTs) are ideal candidates for gas adsorption devices. In addition, due to their selective polarization response to different gases,

they are ideal candidates that can be functionalized to act as toxin detectors. Summarized below, in Table 4, is a list of plots obtained from this investigation.

TABLE 4**.** A summary of various results that were obtained from this scientific investigation.

Plot #	Description of those plots
29	Freq. response vs. pressure for cycling 15 inch. of CO_2 in the cavity with no substrate
30	Polynomial fit of the plot obtained in 30
31	Freq. response vs. pressure for cycling 15 in. of CO in the cavity with no substrate
32	Freq. response vs. pressure for cycling 15 in. of O_2 in the cavity with no substrate
33	Freq. response vs. pressure for cycling 15 in. of H_2 in the cavity with no substrate
34	Freq. response vs. pressure for cycling 15 in. of CO_2 in the cavity with ~20 mg of single-walled carbon nanotubes (SWCNT) in it (untreated)
35	Polynomial fit of the plot in 35
36	Freq. response vs. pressure for cycling 15 in. of CO in the cavity with ~20 mg of SWCNT in it (untreated)
37	Freq. response vs. pressure for cycling 15 in. of O_2 in the cavity with ~20 mg of SWCNT in it (untreated)
38	Freq. response vs. pressure for cycling 15 in. of H_2 in the cavity with ~20 mg of SWCNT in it (untreated)
39	Freq. response vs. pressure for cycling 15 in. of CO_2 in the cavity with ~20 mg of SWCNT heated in air (oxidized)
40	Freq. response vs. pressure for cycling 15 in. of O_2 in the cavity with ~20 mg of SWCNT heated in air (oxidized)
41	Freq. response vs. pressure for cycling 15 in. of CO_2 in the cavity with ~20 mg of charcoal granules
42	Freq. response vs. pressure for cycling 15 in. of CO in the cavity with ~20 mg of charcoal granules
43	Freq. response vs. pressure for cycling 15 in. of O_2 in the cavity with ~20 mg of charcoal granules
44	Freq. response vs. pressure for cycling 15 in. of H_2 in the cavity with ~20 mg of charcoal granules
45	Freq. response vs. pressure for cycling 15 in. of O_2 in the cavity with ~24 mg of Silica Gels.
46	Freq. response vs. pressure for cycling 15 in. of CO_2 in the cavity with ~10 mg of cotton
47	Freq. response vs. pressure for cycling 15 in. of CO in the cavity with ~10 mg of cotton
48	Freq. response vs. pressure for cycling 15 in. of O_2 in the cavity with ~10 mg of cotton
49	Quantitative hysteresis obtained for various gases compared with SWCNT and empty cavity

(table continues)

Table 4 *(continued).*

Plot #	Description of those plots
50	Quantitative hysteresis obtained for various gases compared with all substrates
51	Frequency shifts obtained from different gases for fixed pressure in an unloaded cavity
52	Frequency shifts obtained from different gases for fixed pressure in test cavity loaded with nanotubes
53	Comparing the frequency shifts obtained in two cavities for the same gases and fixed pressures
54	Frequency shifts in loaded cavity from different gases for fixed pressure compared for the frequency shift for the same gas in an unloaded cavity at that pressure
55	Real part of dielectric constant computed for various gases in unloaded cavity

The vacuum-tight resonant cavity was subjected to different gases cycled through at controlled pressure. Figs. 26 and 27 show the frequency response of the resonant cavity when 15 inches/50790Pa of CO_2 was admitted into the cavity in increments of one-inch pressure and then degassed at the same rate. Polynomial fits reveal the extent of hysteresis that was observed in the resonant cavity when no substrate was present in it.

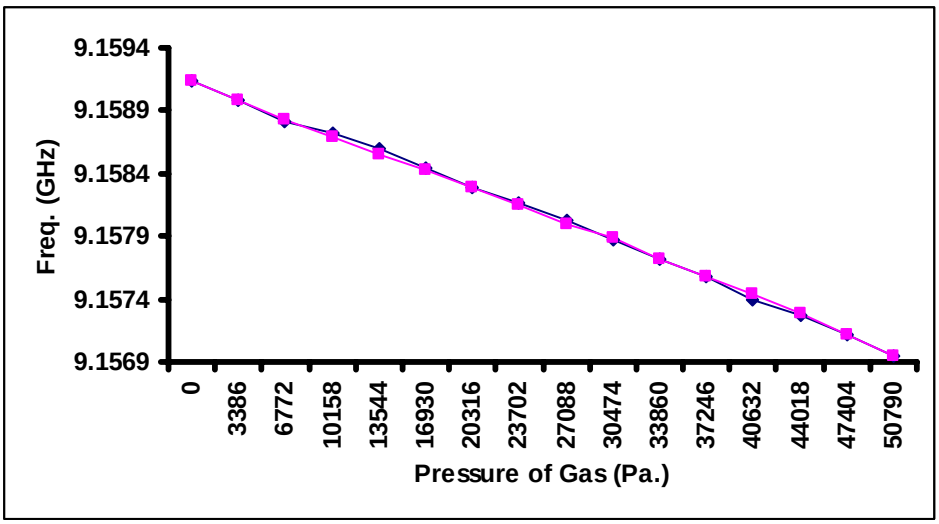

FIG. 26**.** Resonant frequency response of the reference cavity for cycling CO_2 through it. (pink: gassing; blue: degassing)

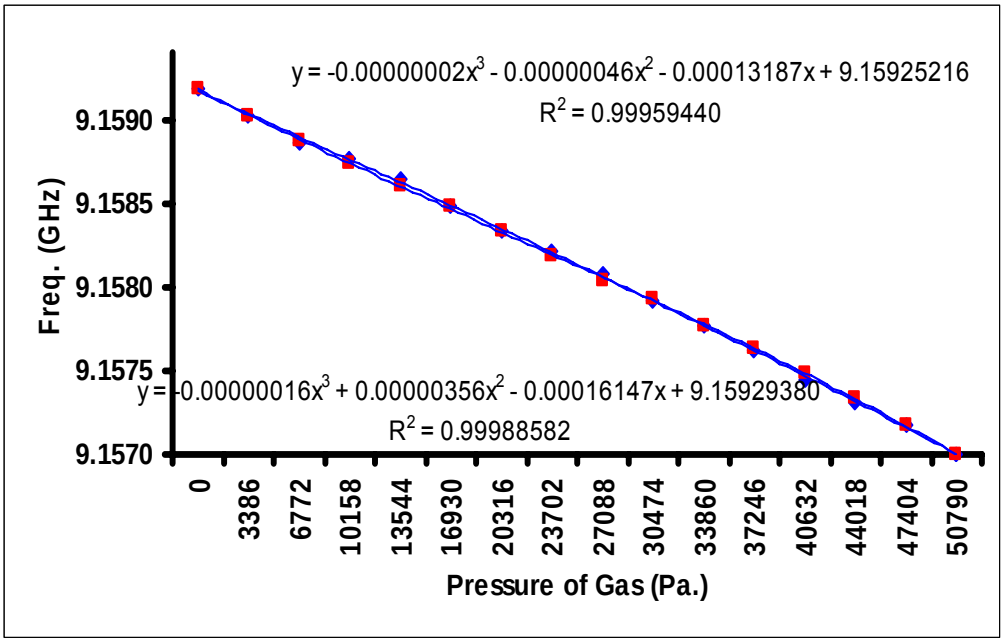

FIG. 27. Polynomial fit of the resonant frequency response of the reference cavity for cycling CO_2 through it.

Using a similar procedure and experimental protocols, several other runs were made with carbon monoxide, oxygen and hydrogen gas molecules. The resonant frequency response to the molecules has been plotted in Figs. 28-30.

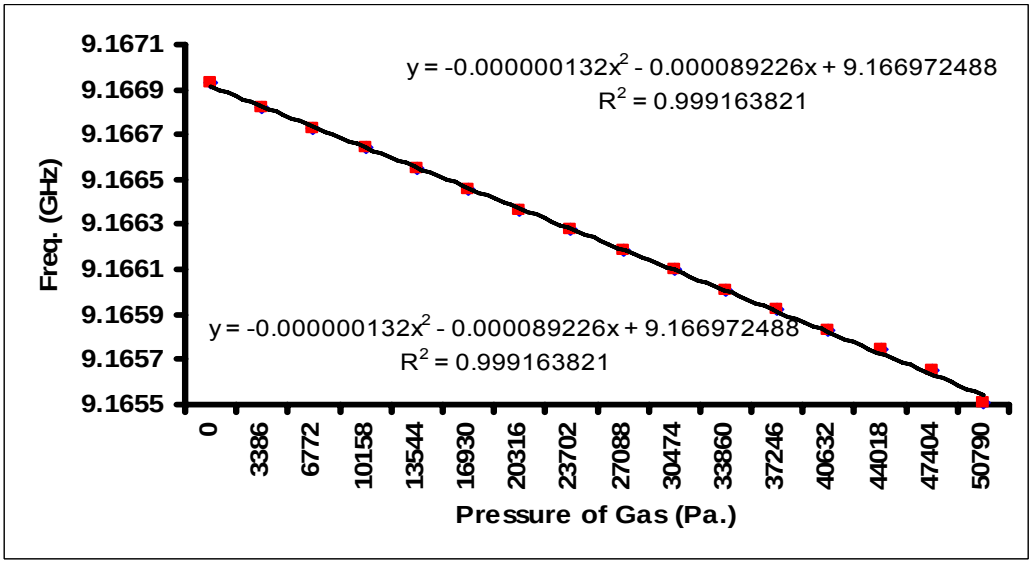

FIG. 28. Frequency response of the reference cavity upon cycling CO through it.

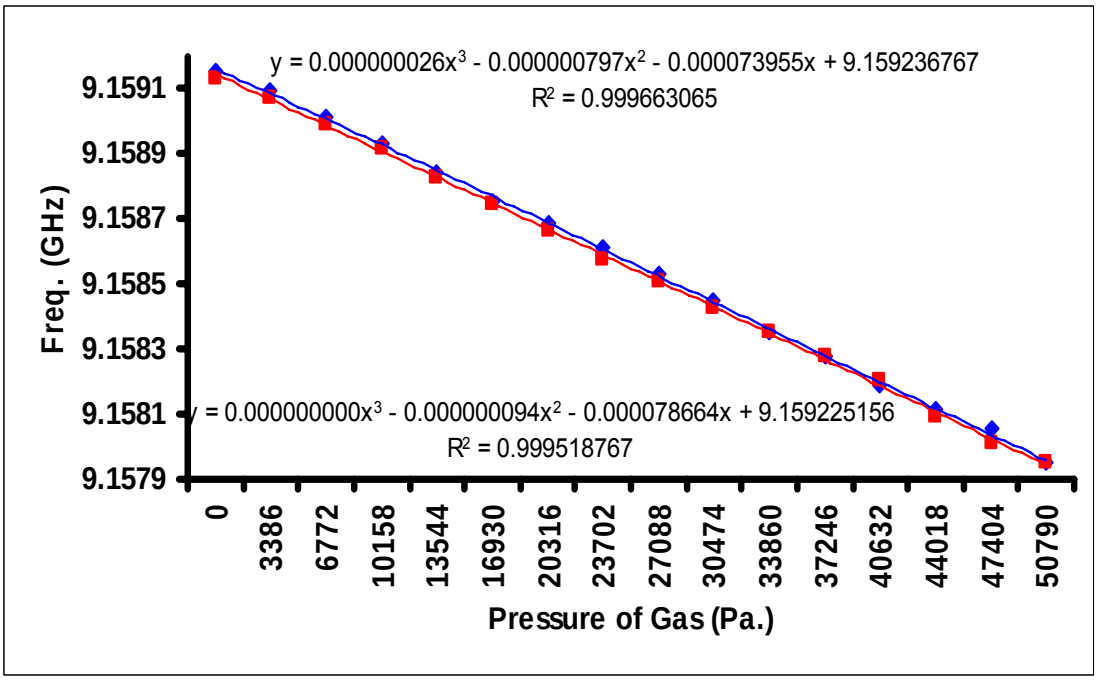

FIG. 29. Response of the reference cavity upon cycling O_2 through it.

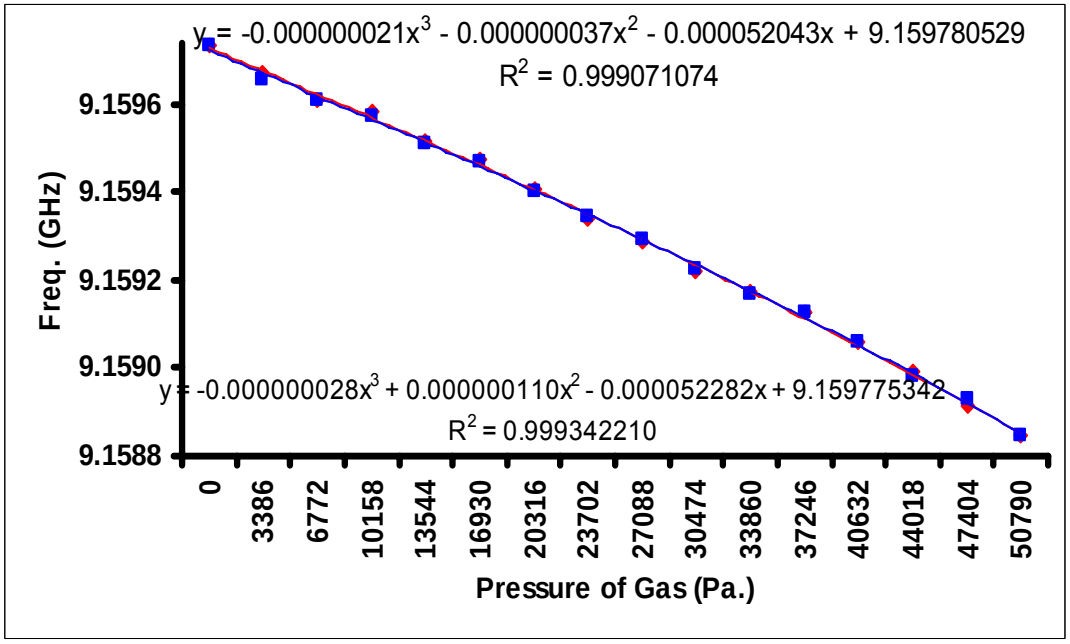

FIG.30. Frequency response of the resonant cavity for cycling (15 inch) of H_2 through it.

With these runs, I collectively obtained the resonance dispersion as well as the minimal adsorption response for all four primary gases under study. The next step of the experiment was to see how these gases might respond with various substrates. Using the protocols mentioned in the previous chapter, for each experimental investigation of the substrate I used clean samples and loaded them in a Teflon® cylinder inside the test cavity. The cavities were tested for leaks and, upon successful holding of vacuum, experiments were performed for various substrates. These plots are provided below in Figs. 31-45, where the corresponding substrates are identified in Table 4.

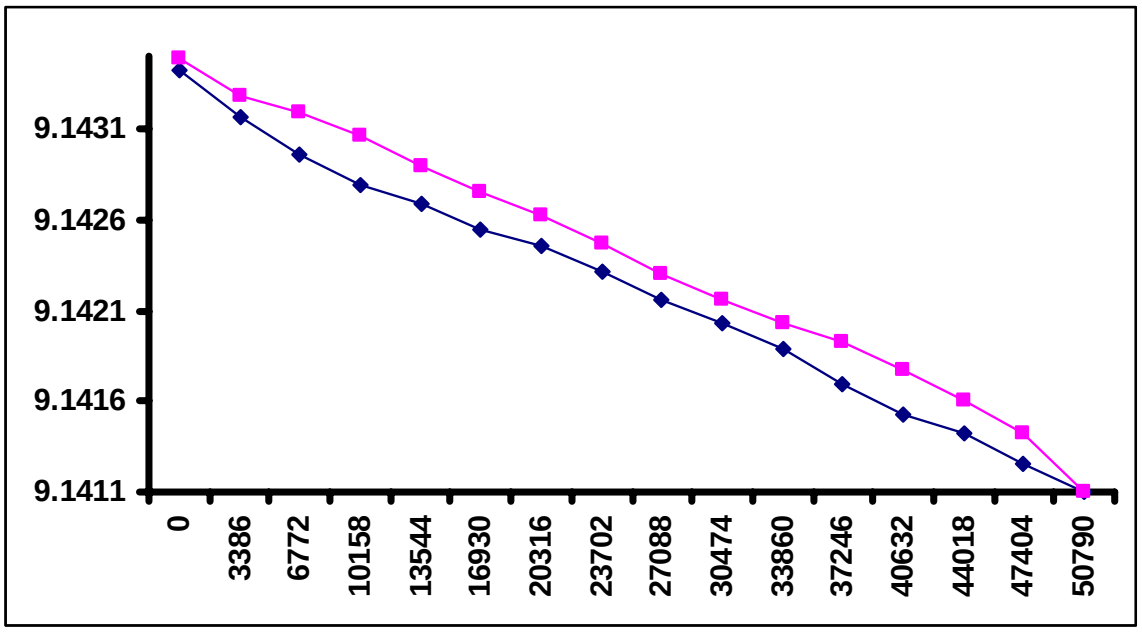

FIG. 31. Frequency response of cycling CO_2 through the test cavity loaded with ~20mg of SWCNT (blue: gassing; pink: degassing).

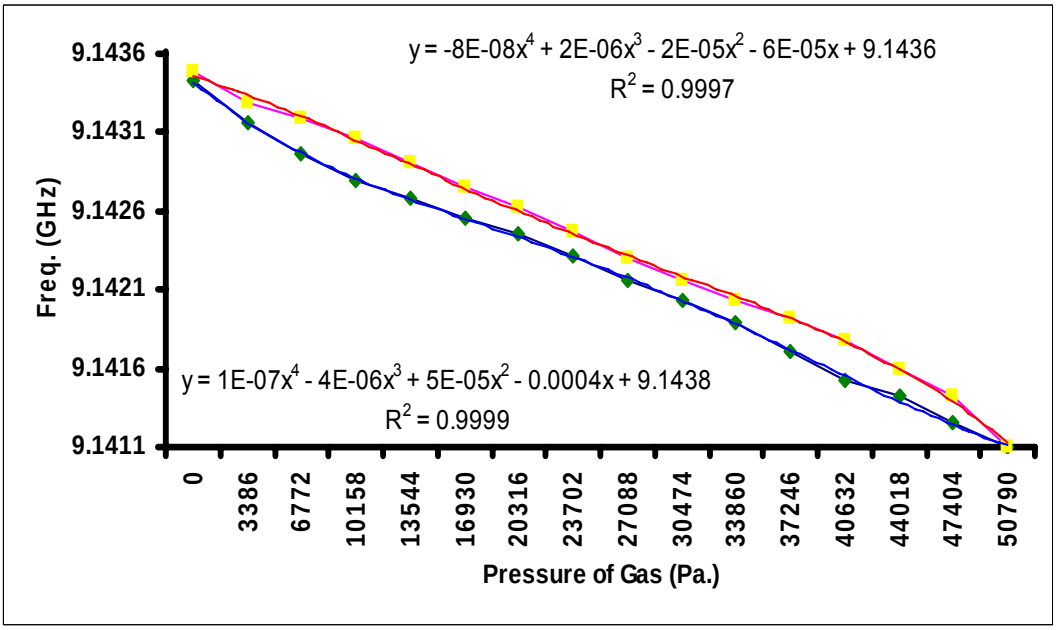

FIG. 32. Polynomial fitting to best R^2 to measure the hysteresis produced when cycling CO_2 through the test cavity loaded with ~20 mg of SWCNTs. (blue: gassing; pink: degassing).

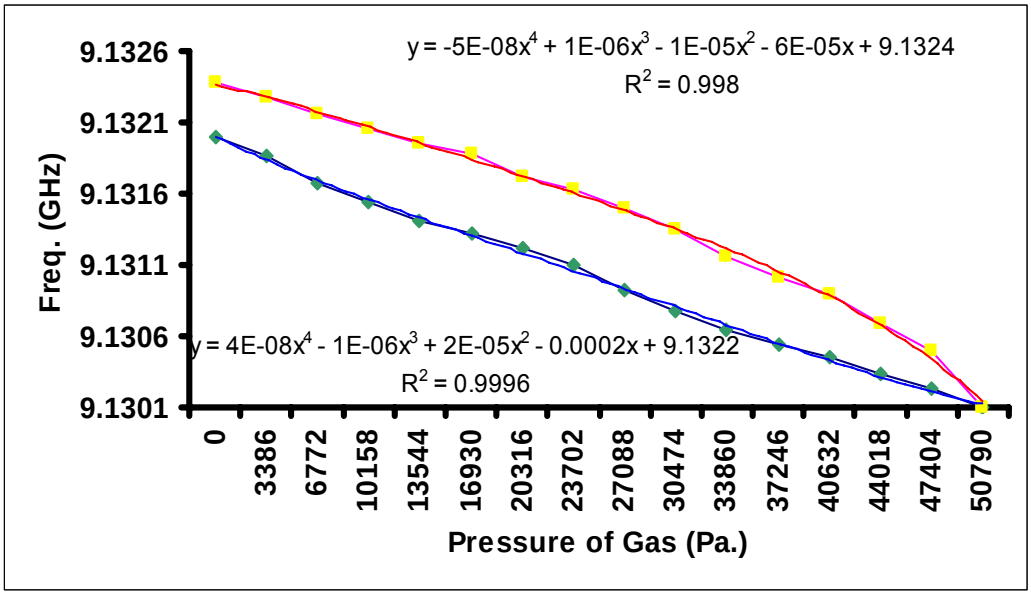

FIG. 33. Frequency response of cycling CO, through the test cavity loaded with ~20mg of SWCNT (blue: gassing; pink: degassing).

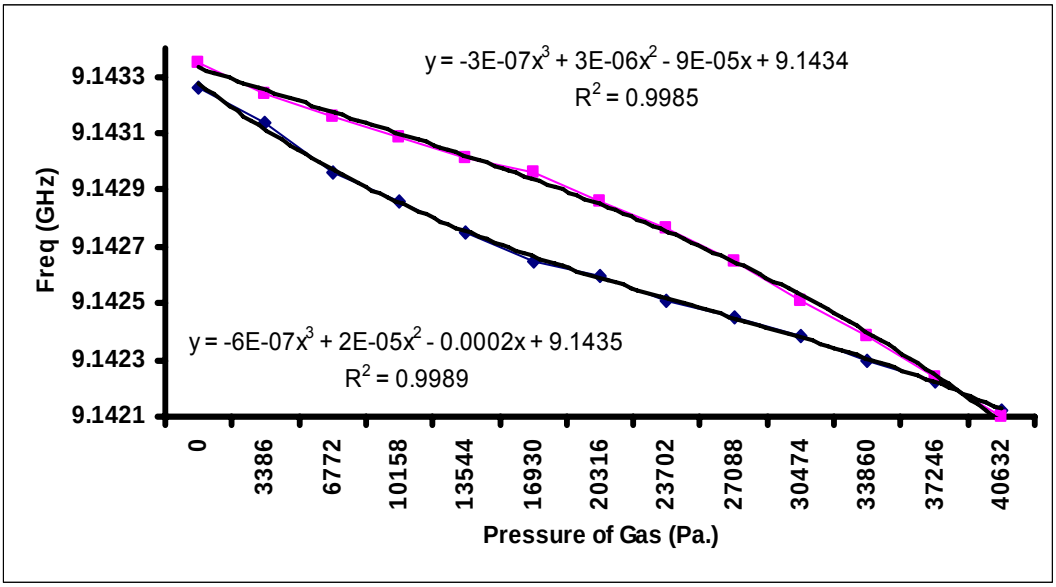

FIG. 34. Frequency response of cycling O_2, through the test cavity loaded with ~20mg of SWCNT.

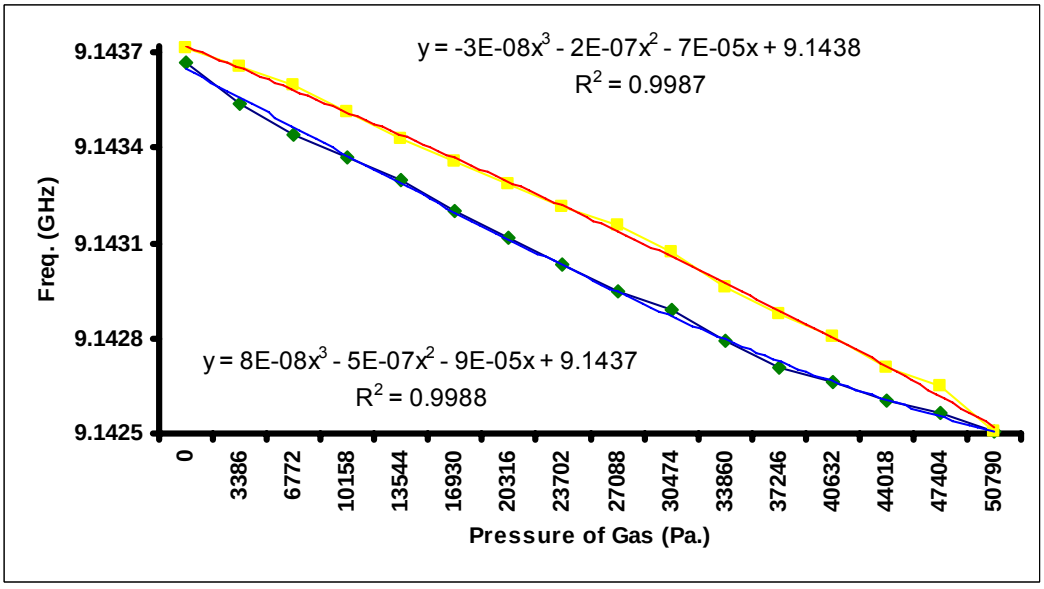

FIG. 35. Frequency response of cycling H_2, through the test cavity loaded with ~20mg of SWCNT (blue: gassing; pink: degassing).

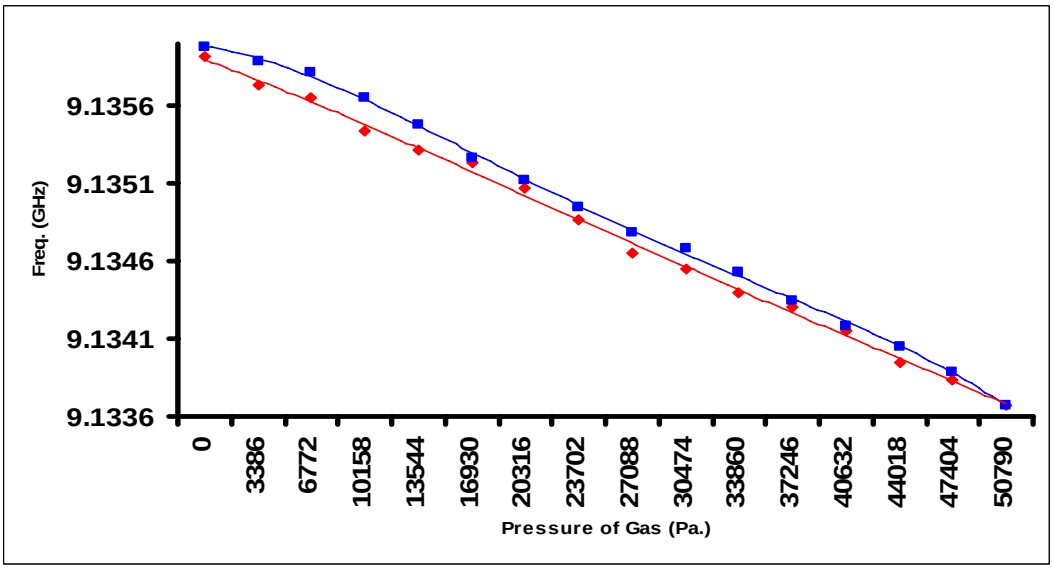

FIG. 36. Frequency response of cycling CO_2 through the test cavity loaded with ~20mg of atmospheric heated SWCNT (red: gassing; blue: degassing).

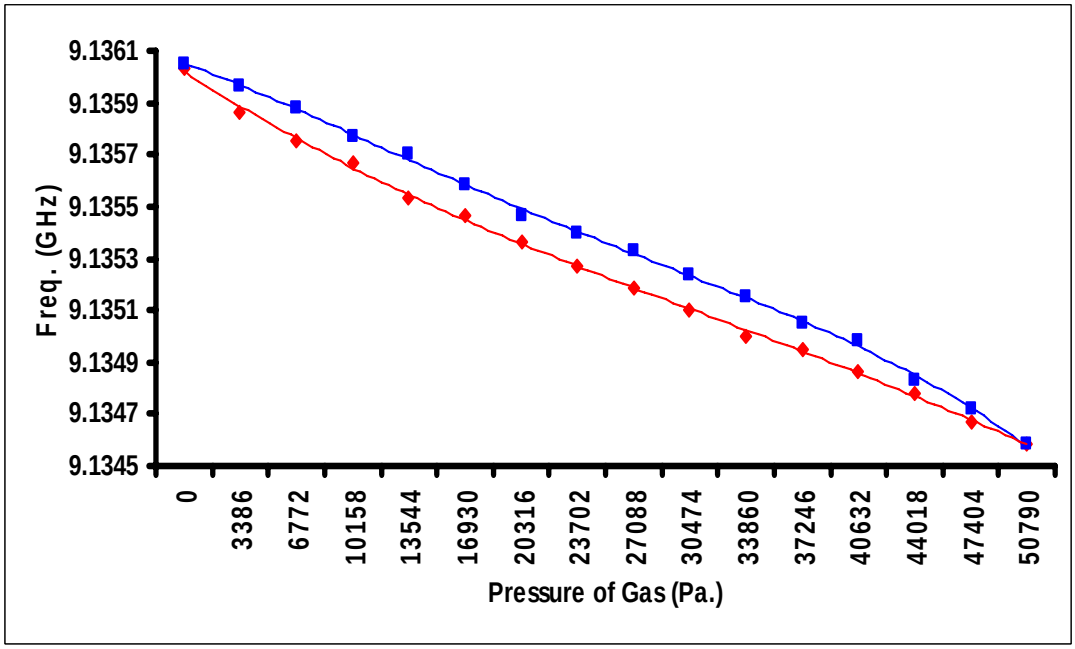

FIG. 37**.** Frequency response of cycling O_2 through the test cavity loaded with ~20mg of atmospheric heated SWCNT.

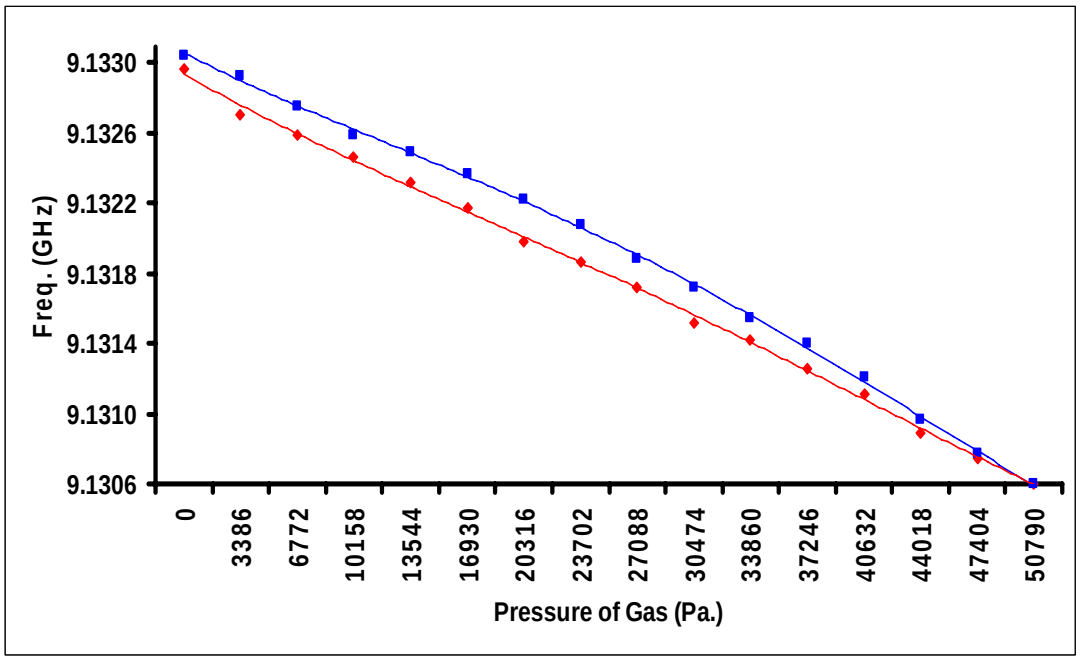

FIG. 38. Frequency response for cycling CO_2 in the test cavity with ~20 mg of charcoal granules (red: gassing; blue: degassing).

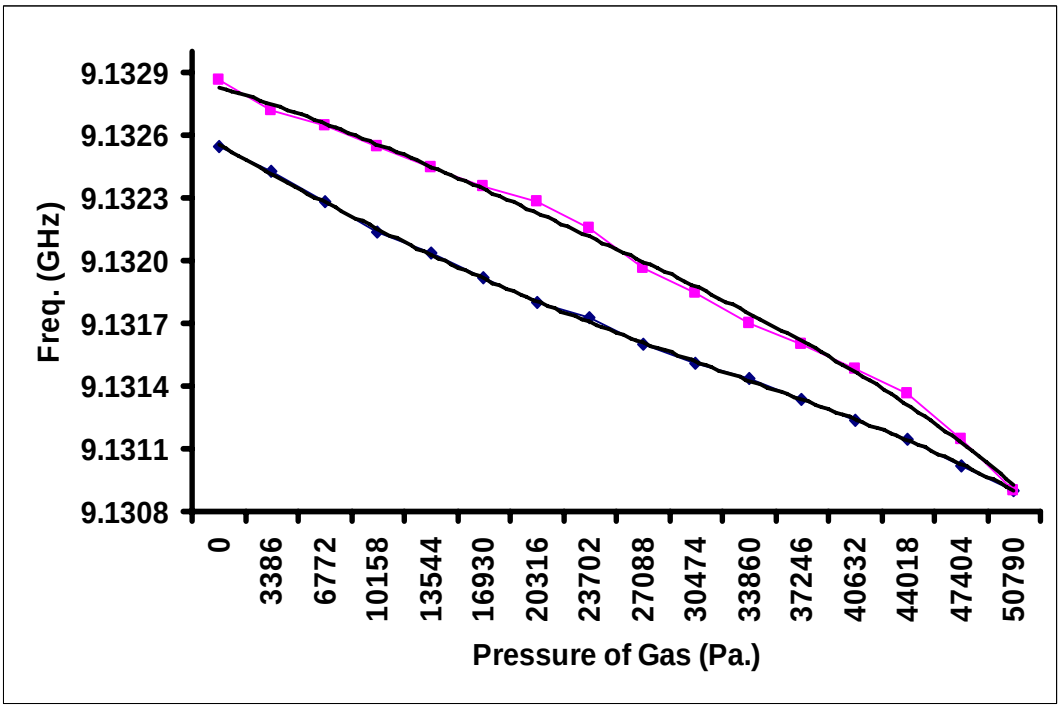

FIG. 39. Frequency response vs. pressure for cycling CO in the test cavity with ~20 mg of charcoal granules (blue: gassing; pink: degassing).

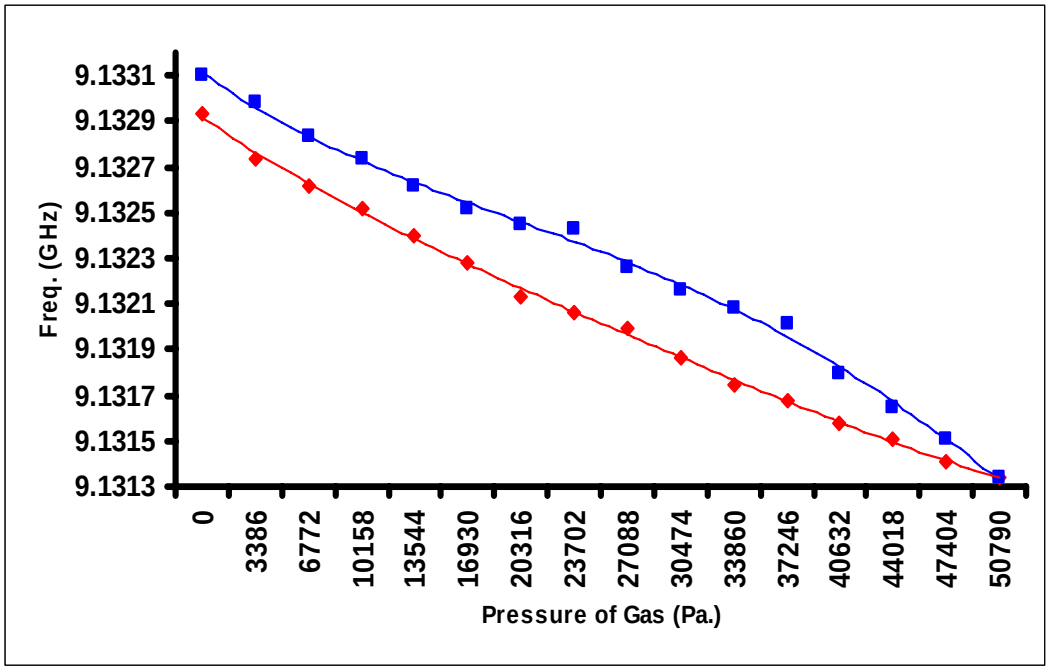

FIG. 40. Frequency response for cycling O_2 in the test cavity with ~20 mg of charcoal granules (red: gassing; blue: degassing).

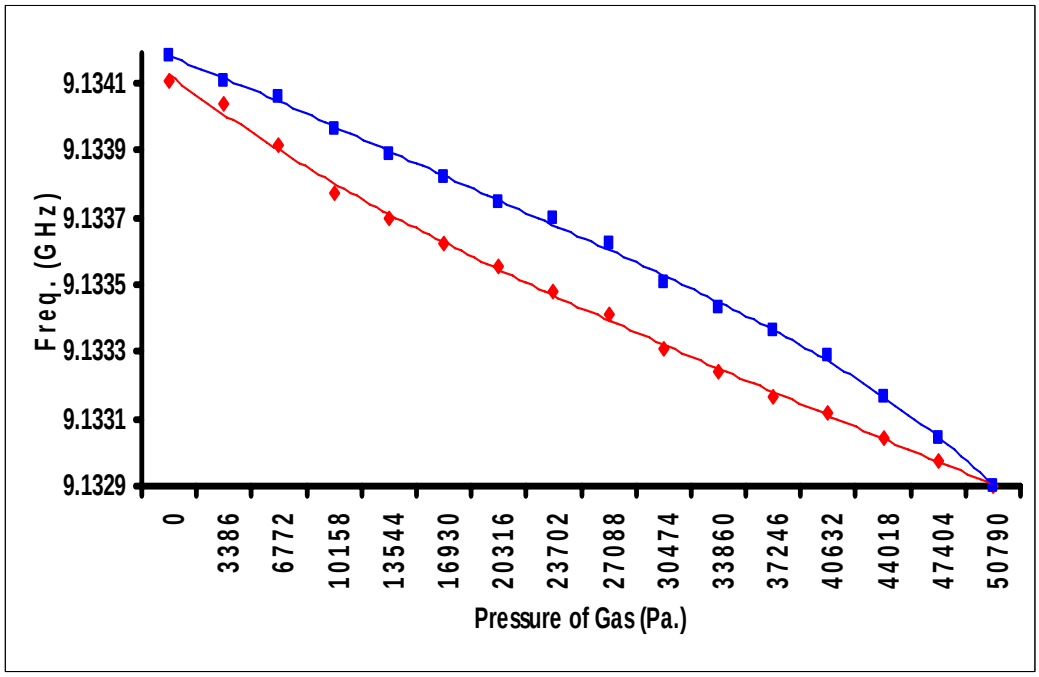

FIG. 41. Frequency response for cycling H_2 in the test cavity with ~20 mg of charcoal granules (red: gassing; blue: degassing).

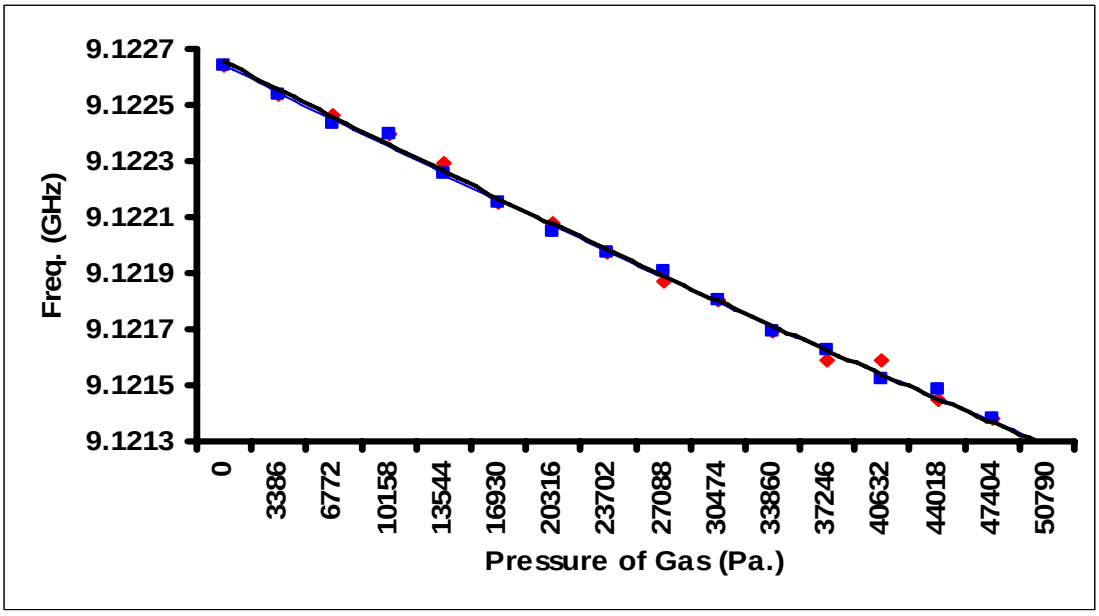

FIG. 42. Frequency response for cycling O_2 in the test cavity ~24 mg of Silica Gels. The gassing curve is indistinguishable from the degassing curve.

There is no significant adsorption of the gases studied for silica gel. Results on another substrate, cotton fibroins, are reported in the following graphs.

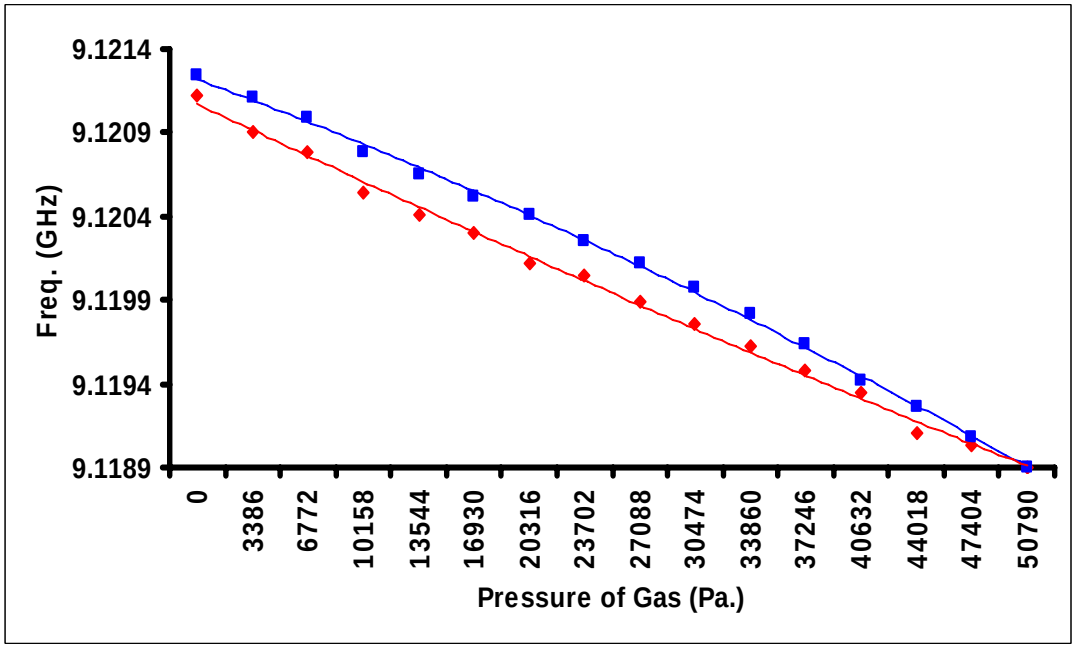

FIG. 43. Frequency response for cycling CO_2 in the test cavity with ~10 mg of cotton fibroins (red: gassing; blue: degassing).

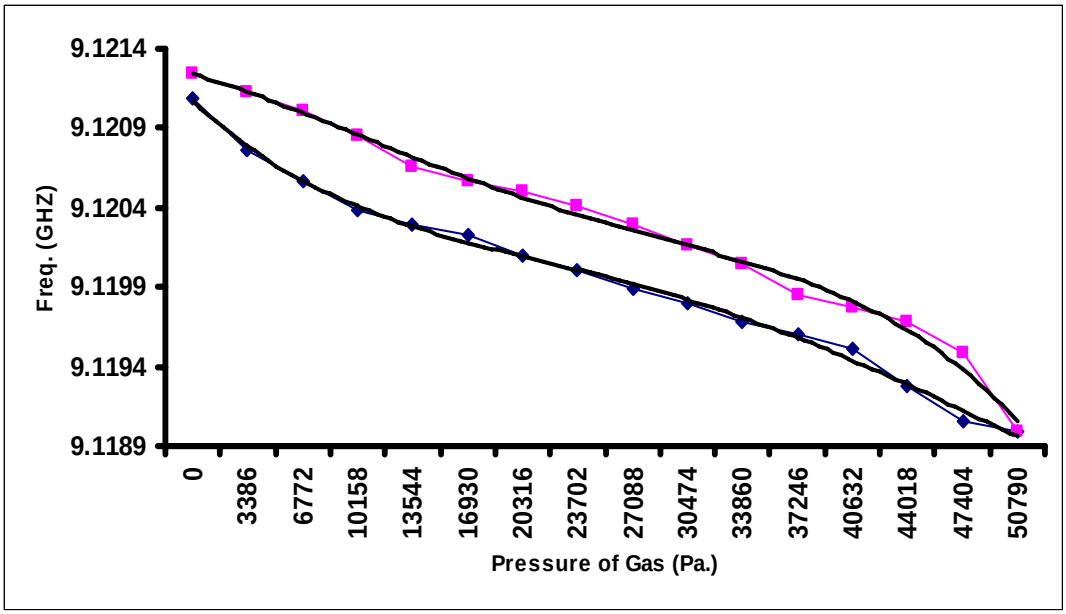

FIG. 44. Frequency response for cycling CO in the test cavity with ~10 mg of cotton fibroins (blue: gassing; pink: degassing).

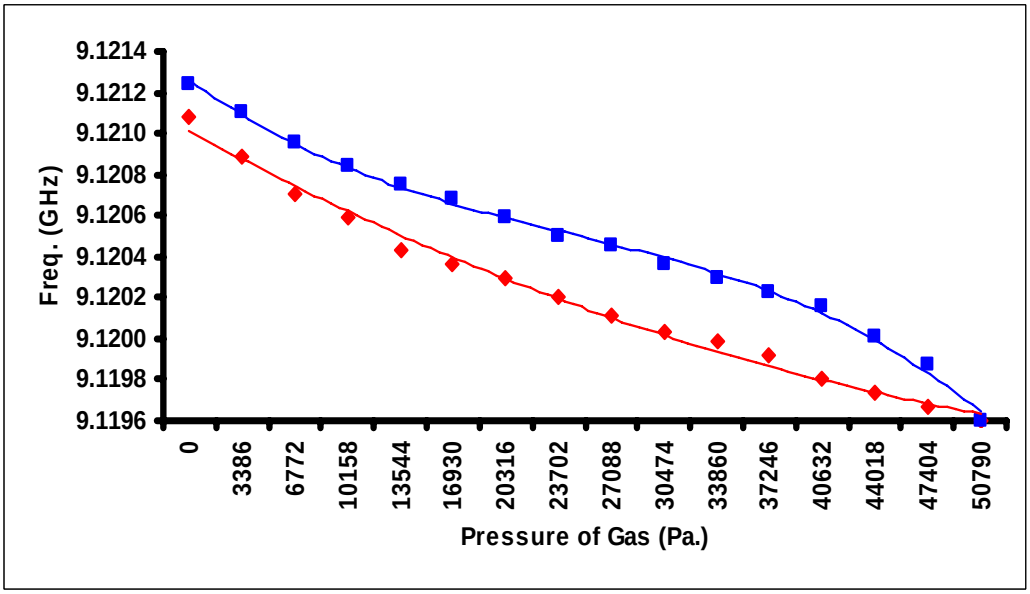

FIG. 45. Frequency response for cycling O_2 in the test cavity with ~10 mg of cotton.

So far it has been shown (Figs. 27-45) that there is a very selective as well as unique response of the resonant cavities to the gas exchange when loaded with different substrates. In order to obtain a conclusive picture from these results, it is necessary to answer the questions:

1) What type of frequency as well as dielectric response is obtained due to the presence of different media?

2) How does molecular adsorption affect the dielectric properties of nanomaterials loaded within the cavity?

3) Is the adsorption of the materials a physical property, or are there chemical changes happening that produce this specific response?

4) How different is the adsorption for these gases under different substrates in the resonant cavities?

5) What are potential applications of this scientific study?

Discussion and Interpretation of These Results

The results of the gas exchange experiments show that SWCNTs are ideal candidates for gas adsorption when compared with other substrates that were loaded into the resonant cavities. Shown in Fig. 46 and Table 5 is the quantitative comparison of the areas between the curves that appear when the cavities loaded with SWCNTs are cycled with different gases. A simple integration method was used to calculate the area between the curves obtained in Figs. 27-36. In this plot, a comparison was made between the unloaded cavity and the cavity loaded with SWCNTs to study the propensity of gas adsorption by these nanomaterials.

From the results shown in Fig.46 and Table 5, it can be seen that in loading the cavities with nanotubes and cycling various gases through them, there is still some residual gas present within the test cavity. On the other hand, the other cavity without substrate was completely degassed, and showed only a very negligible number of residual gas molecules that might be present on the walls of the cavity.

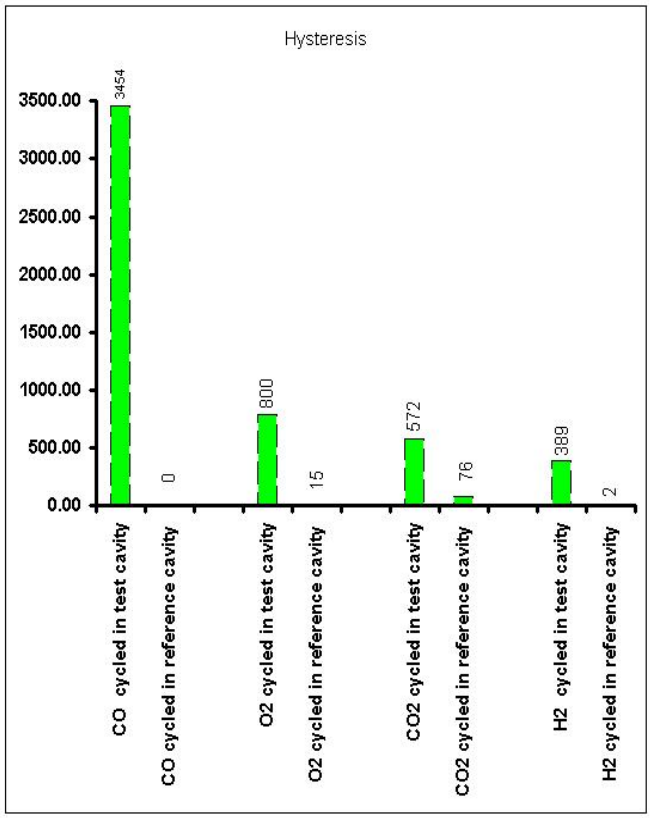

TABLE 5 (right, below). The quantitative values of the amount of hysteresis or the adsorption strengths for four different gases due to presence of nanotubes.

Environment	Hysteresis
CO cycled in test cavity	3454.49
CO cycled in reference cavity	0.00
O_2 cycled in test cavity	799.62
O_2 cycled in reference cavity	15.26
CO_2 cycled in test cavity	572.29
CO_2 cycled in reference cavity	76.32
H_2 cycled in test cavity	388.84
H_2 cycled in reference cavity	2.44

FIG. 46 (left, above). A comparative plot of quantitative Hysteresis of the adsorption of gases in the cavity loaded with SWCNT when compared to the cavity with no adsorbent material present.

So far, this analysis has summarized the response of carbon nanotubes (CNTs) to various gases and the CNT propensity for adsorption. Two significant questions need to be answered:

How do different gases shift the natural resonance of the cavity?

How does molecular adsorption on nanotubes scale the dielectric properties?

Figs. 47-51 show how the presence of various gas molecules inside the test cavity affects the dielectric response of pristine nanotubes.

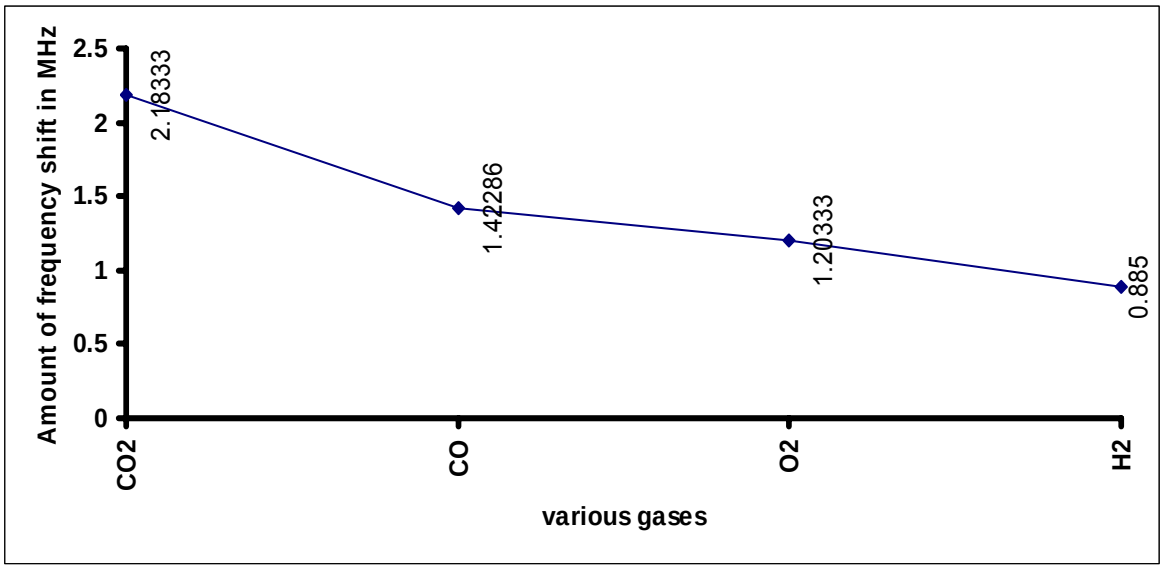

FIG. 47**.** Amount of frequency shift in the resonance frequency upon loading the cavity without substrate but just different gases with equal increments of pressure of CO_2, CO, O_2, and H_2.

The shifts in the resonance frequency of the reference cavity when subjected to gases have been plotted in Fig. 47. When ~20mg of SWCNT was introduced into the cavity there was a perturbation of the E vector which gave a significant shift in the resonant frequency of 15.6708333 MHz. Using the data shown in Table 6, shifts in the frequency were calculated for pressurizing the cavities with a total of 15 inches/50790Pa of various gas pressures. The shifts were calculated for these gases in both unloaded (no nanotubes) as well as loaded cavities. The results are summarized in Table 6, and the plots can be seen in Figs. 49-51.

TABLE 6. A summary of the shifts in the resonance frequency of the both reference and the test cavity observed when gases were loaded in them.

Pressure	*CO2*	*CO*	*O2*	*H2*	*CO2+ SWCNT*	*CO+ SWCNT*	*O2+ SWCNT*	*H2+ SWCNT*
0	9.159133	9.159133333	9.159133333	9.159133333	9.143462500	9.143462500	9.143462500	9.143462500
1	9.158983	9.159025833	9.159076667	9.159070833	9.143200000	9.143325833	9.143337500	9.143335000
2	9.158821	9.158928333	9.158993333	9.159013333	9.143000000	9.143129167	9.143187500	9.143235833
3	9.158721	9.158845833	9.158913333	9.158983333	9.142825000	9.142996667	9.143062500	9.143165000
4	9.1586	9.158755833	9.158823333	9.158915833	9.142725000	9.142874167	9.142887500	9.143094167
5	9.158438	9.158660833	9.158736667	9.158878333	9.142587500	9.142784167	9.142787500	9.142995000
6	9.158288	9.158568333	9.158670000	9.158810833	9.142487500	9.142680000	9.142675000	9.142910000
7	9.158167	9.158479405	9.158593333	9.158743333	9.142350000	9.142561667	9.142575000	9.142825000
8	9.158029	9.158390476	9.158513333	9.158688333	9.142200000	9.142383333	9.142525000	9.142740000
9	9.157867	9.158301548	9.158426667	9.158620833	9.142062500	9.142236667	9.142437500	9.142683333
10	9.157725	9.158212619	9.158336667	9.158573333	9.141925000	9.142100000	9.142375000	9.142584167
11	9.157575	9.158123690	9.158260000	9.158525833	9.141737500	9.142000000	9.142312500	9.142499167
12	9.157396	9.158034762	9.158173333	9.158458333	9.141562500	9.141914167	9.142225000	9.142456667
13	9.157267	9.157945833	9.158093333	9.158390833	9.141462500	9.141791667	9.142150000	9.142400000
14	9.157121	9.157856905	9.158033333	9.158315833	9.141287500	9.141691667	9.142050000	9.142357500
15	9.15695	9.157710476	9.157930000	9.158248333	9.141137500	9.141565000	9.141950000	9.142300833

Gas introduced in reference cavity	**Shift in Frequency observed (MHz)**
CO_2 cycled in cavity without any substrate	2.183333333
CO cycled in cavity without any substrate	1.422857143
O_2 cycled in cavity without any substrate	1.203333333
H_2 cycled in cavity without any substrate	0.885
Shift in Frequency due to loading of 20 mg. of SWCNTs	
"=($F_{unloaded}$ - F_{loaded})" (MHz)	
15.67083333	
Gas introduced in test cavity with 20mg SWCNT	**Shift in Frequency observed (MHz)**
CO_2 cycled in cavity loaded with nanotubes	2.325
CO cycled in cavity loaded with nanotubes	1.8975
O_2 cycled in cavity loaded with nanotubes	1.5125
H_2 cycled in cavity loaded with nanotubes	1.161666667

Fig. 48 shows the shifts in the resonance of the test cavity loaded with SWCNT and 50790 Pa pressure of different gases; these results are then compared in Fig. 49 with the shifts produced in the reference cavity with gases and no substrates.

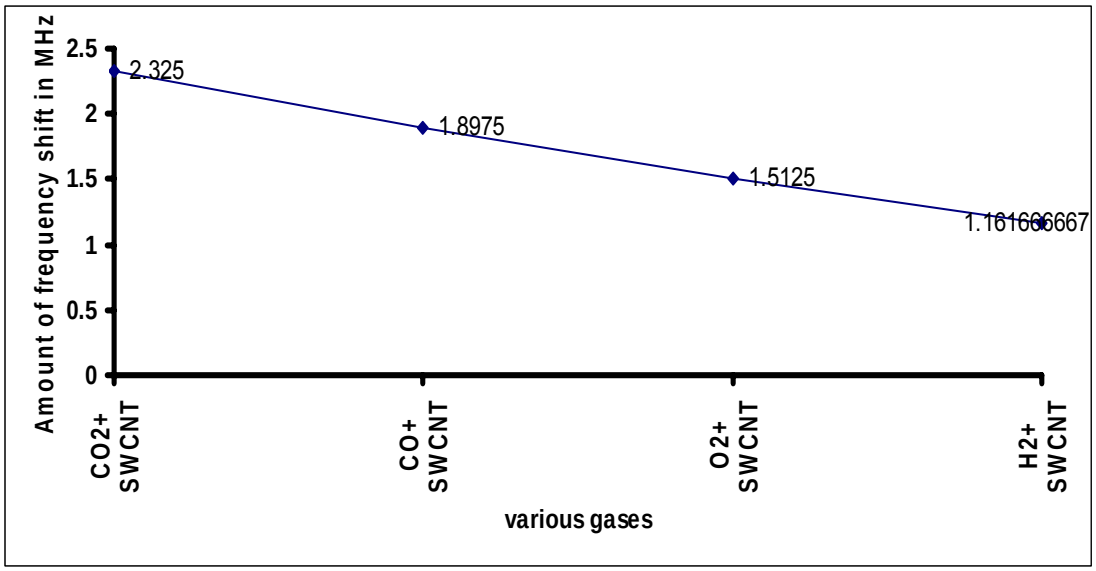

FIG. 48. Amount of resonance shift versus the type of gas when loaded in the test cavity with SWCNT present in them.

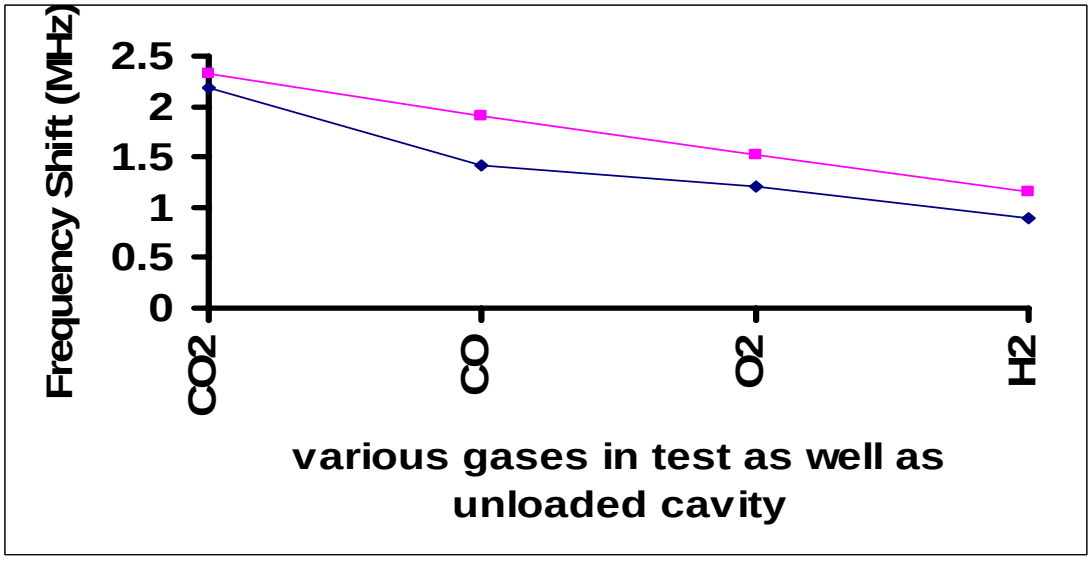

FIG. 49. Comparison of the shifts produced for a fixed pressure of a particular gas when introduced in both the reference as well as the test cavity is shown here (blue: the reference cavity; pink: the test cavity).

It can be seen from these plots that loading the cavity with nanotubes significantly increases the dielectric of the medium. In addition, there is a unique response to the effective

dielectric constant within the test cavity when loaded with gases and nanotubes. It has been possible to quantify the dielectric constant response of these cavities. Using Eq. (4.1) the real part of the dielectric constant has been calculated for the gases in both the unloaded and the loaded cavity. These responses, given by $(\varepsilon_u)_{gas}$ and $(\varepsilon_l)_{gas+swcnt}$, are listed in Tables 7 and 8, respectively. Fig. 50 shows the value for $(\varepsilon_u)_{gas}$ and Fig. 51 values for $(\varepsilon_l)_{gas+swcnt}$.

$$\frac{\varepsilon'-1}{2} \approx \frac{\Delta f}{f_o} \tag{4.1}$$

TABLE 7. Using Eq. (4.1), computed values of the real part of the dielectric constant for a fixed pressure of gas, keeping reference at 9.159 GHz.

	Δf MHz	ε'_{gas}
CO_2	2.183333	1.476755
CO	1.422857	1.310434
O_2	1.203333	1.262761
H_2	0.885	1.193237

Also, using Eq. (4.1) the real part of the dielectric constant for SWCNT was calculated with reference to the unloaded cavity and the results are included in Table 8.

TABLE 8. Using Eq. (4.1), computed values of the real part of the dielectric constant for a fixed pressure of gas introduced in the cavity loaded with SWCNTs, keeping reference at 9.159 GHz.

50790 Pa of gas in test cavity	$\varepsilon_{gas+SWCNT}$
CO_2	4.929593047
CO	4.836243604
O_2	4.752174514
H_2	4.675566102

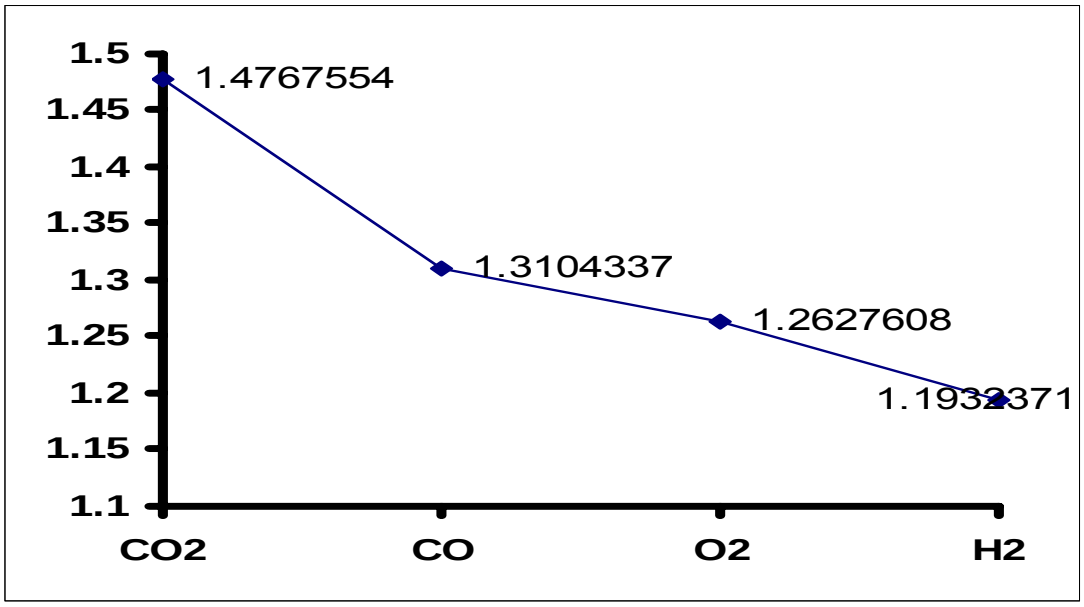

FIG. 50. A plot of the real part of the dielectric constant computed for 50790 Pa of various gases.

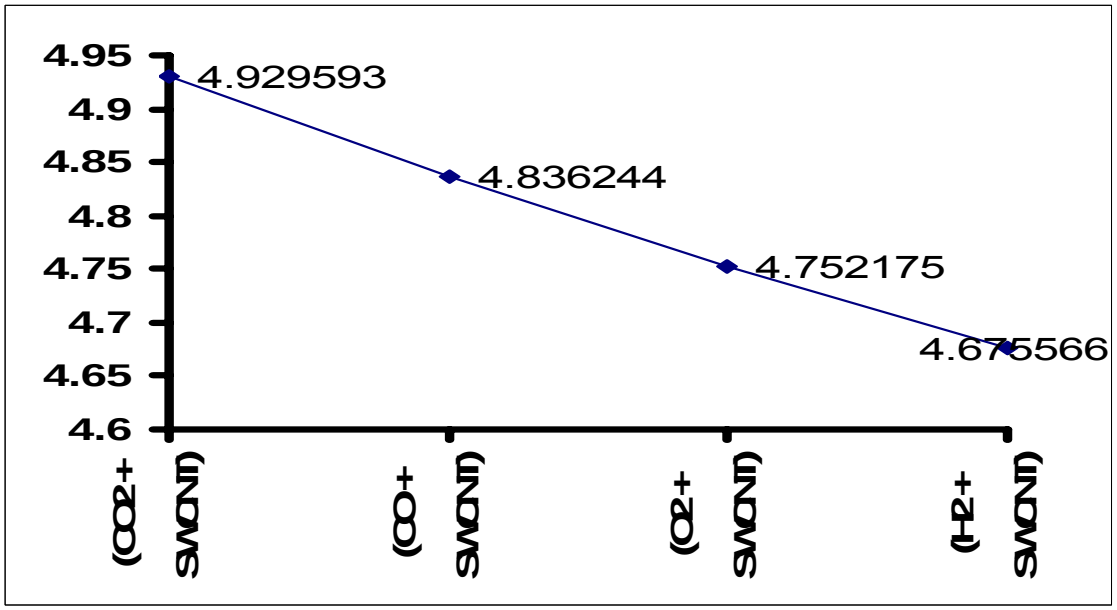

FIG. 51. Shown above is the real part of the dielectric constant for various gases adsorbed on SWCNT.

Figs. 46-51 show that there is a very selective adsorption response of the carbon nanotubes for various gases, and the molecular adsorption of the gases on the substrate has a

significant effect on the dielectric properties of carbon nanotubes. Shown in Table 9 is the ratio of the dielectric response ($\frac{(\varepsilon)_{gas+swcnt}}{(\varepsilon)_{SWCNT}}$), as well as the shift in the dielectric properties of pristine nanotubes $\left(\Delta\varepsilon_{nt} = \varepsilon_{gas+swcnt} - \varepsilon_{SWCNT}\right)$ when different gases are adsorbed on its surface.

TABLE 9. The relative effect of molecular adsorption on the dielectric response of SWCNTs.

Gas Type	$\varepsilon_{(gas + swcnt)}$	ε (nanotubes)	$\varepsilon_{gas+swcnt}/\varepsilon_{swcnt}$	$\Delta\varepsilon = \varepsilon_{gas+swcnt} - \varepsilon_{swcnt}$
CO_2	4.929593047	4.421903091	1.114812547	0.507689956
CO	4.836243604	4.421903091	1.093701853	0.414340513
O_2	4.752174514	4.421903091	1.074689883	0.330271423
H_2	4.675566102	4.421903091	1.057365122	0.25366301

Further Discussion of the Experimental Results

From these recent measurements of the frequency shifts of the resonant cavities with and without carbon nanotubes loaded in them, it is seen that the loaded resonant cavities with nanotubes have shown a characteristic response towards various gases cycled through them. These shifts are indicative of the dielectric permittivity of the sample being shifted due to the specific adsorption of different gas species on its surface. These results prompt the discussion of two important aspects of physics, in order to better understand the nature of polarization of nanomaterials when impregnated with different gases. The experimental results obtained so far will aid in answering two important questions related to the molecular interactions:

1) What happens to the dielectric permittivity of SWCNTs when different polar and non-polar gases come in contact with the sample?

2) What do we learn about the nature of interactions of gases with the nanomaterials loaded inside them from these unique shifts in the frequency of the resonant cavities as well as the unique Hysteresis observed in the loaded cavity?
3) In order to systematically answer these questions, some characteristic results are summarized below. From Figs. 47, 48, and 51-54 the following information can be concluded:
    a) The resonant cavity technique has been sensitive enough to detect a shift in the frequency response due to perturbation of an external load in them.
    b) The differential resonator response method has allowed us to quantify the selective interactions between SWCNTs and gases.
    c) The amount of shift in the frequencies of the resonator increases significantly as well as selectively when SWCNTs were loaded in the cavity. This response of SWCNTs has been unique as compared with the other substrates as well as with no substrates inside the resonant cavities.
    d) Correspondingly, using Eq. (4.1) the real part of the dielectric response of the resonant cavity was computed for both loaded and unloaded cavities.
    e) The effects of molecular adsorption on the dielectric properties of SWCNTs have also been shown, and it is clear that SWCNTs are ideal candidates for selectively adsorbing gas molecules compared to other substrates (S1-S5, Table 2.).

The results (Table 7) indicate that the amount of shift produced in the resonant frequencies of reference cavity follows the order given below:

$CO_2 > CO > O_2 > H_2$

with values being (1.4767554, 1.3104337, 1.2627606, 1.1932371) MHz respectively for the above molecules. These gases tend to follow the same pattern in terms of having a composite dielectric response on the bulk nanomaterials, except for the fact that the amount of gas adsorbed on the surface of the nanotubes during the entire cycle of gassing and degassing has changed its order as shown below:

$$CO > O_2 > CO_2 > H_2$$

The nature of these results indicates that the intermolecular forces and the coulombic forces play a dominant role in determining the nature of the binding of these molecules. Theoretical model predictions[51] on the nature of adsorption of molecules on the substrate have been worked out for different chirality of the nanotubes. The method proposed of theoretically modeling the results obtained in this scientific study is to computationally model theories developed in the work of Jorengsen *et al.*, Wallace and Sansom, and Zhao.[52] Necessary computations will have to be done for determining the potential due to bonding, bending and torsion of the molecules as described respectively below:

V_{bond}: $V(r) = \frac{K_r}{2}\left(r - b_{eq}\right)^2$ V_{bend}: $V_{bend}(\theta) = \frac{K_\theta}{2}\left(\theta - \theta_{eq}\right)^2$

V_{tors}: $V_{tors}(\varphi) = V_o + V_1(1 + Cos(\varphi)) + V_2(1 - Cos(\varphi)) + V_3(1 + Cos(3\varphi))$

This interaction energy between two dipoles can then be expanded as a function given below:

$$V_1 = \left[\mu_1 \bullet \mu_2 - \frac{3(\mu_1 \bullet \mathbf{r})(\mu_2 \bullet \mathbf{r})}{r^2}\right] r^{-3}$$

It is clear from these results that the amount of shift in the resonant cavities, the amount of gas adsorption, and the effective change in the real part of the dielectric response of SWCNTs are unique as well as distinguishable from one another and depend upon the nature of the perturbant in the system. This implies that, using a matrix of functionalized nanotubes, a loading wick can be

prepared inside the resonant cavity that will have chemical selective properties for the nature of a foreign agent[s] entering the system.

The intermolecular forces of gases and materials have been much studied, and very recently several researchers have tried to study the adsorption properties of nanotubes for different gases. Weber *et al*. have tried to determine the binding energy of methane on single-walled nanotube bundles using adsorption isotherm technique measurements at different temperatures.[53] It was pointed out that compared with methane, the binding energy values on SWCNTs were 76% larger than on planar graphite. Matranga *et al.*,[54] using grand canonical Monte Carlo simulations, reported finding the most suitable site for CO_2 adsorption in the nanotube bundles to be the interstitial channels compared with other locations like endohedral, grooves, and exterior surfaces in a bulk cluster of nanotubes. Our experimental results indicate that (7,5) and (6,5) nanotubes have more affinity towards CO than other gas molecules. Such results are yet to be theoretically modeled. It was shown in Cinke *et al.* that the adsorption of CO_2 is a physisorption process with heat of adsorption of 2303 J/mol (0.024 eV), which is far less than the heat of adsorption released in a chemisorption process (80,000 J/mol).[55] BET surface area of 1587 m^2/g suggests a cross-sectional flux for the gas molecules to reside on the Connolly surface of the nanotubes, thereby increasing their adsorption activity compared to charcoal and other substrates with their BET surface areas being 25-40% less than other substrates.[56] It is also indicative in our research at low microwave power that the adsorption of gases studied is also a physi-sorption process with no significant thermodynamic activity. The effective shift in the resonant frequencies as well as adsorption of gases on substrates like SWCNTs also indicate:

1) Polarization of gas molecules (nanotubes as well as the complex medium containing gas and nanotubes) significantly contributes towards the effective shift in the dielectric response of the cavity.
2) Binding energy of the gases on the ICs of SWCNTs is contributing to the effective areas between the curves during each cycle of gassing molecules through SWCNT loaded cavities.

Polarization or induced polarization response of gas molecules in an external electric field will require a separate study of dielectric relaxation time and their relationship with the orientation polarizability, which can be calculated using the Debye model.[57] Alternatively, a well- studied Claussius relationship model can also be used to relate the dielectric response of the gas molecules and the polarizability of those molecules between two adjacent atoms.[58] Static and frequency dependent polarizability tensors for nanotubes have been computed for different nanotubes by Jenson *et al.*[59] For numerical analysis of these results, the relationship shown by Eqs. (4.2 – 4.4)[60] can be used to compute the effective mean polarizability of SWCNTs in each direction.

$$\bar{\alpha} = \frac{1}{3}\left(\alpha_{xx} + \alpha_{yy} + \alpha_{zz}\right) \tag{4.2}$$

with anisotropy correction κ^2 defined as

$$\kappa^2 = \left[\left(\alpha_{xx} - \bar{\alpha}\right)^2 + \left(\alpha_{yy} - \bar{\alpha}\right)^2 + \left(\alpha_{zz} - \bar{\alpha}\right)^2 / 6\bar{\alpha}^2\right] . \tag{4.3}$$

Mean molecular polarizability can be related to the dielectric constant using the famous Claussius-Mossotti relationship given by Eq. (4.4)

$$\bar{\alpha} = \frac{3M}{4\pi N_a \rho}\frac{\varepsilon - 1}{\varepsilon + 2} \tag{4.4}$$

Several researchers[61] have tried to calculate computationally the static polarizabilities of SWCNTs for different types of SWCNTs. Using a tight binding model they have established the relationship between the band-gap energy and the polarizability of materials both parallel and perpendicular to the axis of these cylinders.[62] Sivasubramanian *et al.* have expressed the thermodynamic stability of these molecules to their polarizabilities by applying Landau-Lifshitz inequality[63] to the dielectric stability theorem

$$\eta = \frac{4\pi\alpha}{3\upsilon} < 1 \qquad (4.5)$$

where, η is the stability parameter and α is the polarizability of the material.

For our study, it will be interesting to computationally verify such claims as in Sivasubramanian *et al.* by placing the CO_2 molecules, as well as other gases, along the surface ridges and between interstitial channels and applying external fields. Another piece of work done by Torrens aids in understanding the parallel as well as perpendicular polarizability tensors.[64] We verify our calculations of dielectric constant values for the (7,5) nanotubes to be 4.142 using their mean polarizability values reported to be 1.237.[65]

Our underlying interest in these experimental results is to see how polarization affects the surface adsorption on these nanomaterials. The work of E.S. Snow *et. al*[66] finds that for the surface adsorbates, the polarization is proportional to the number of adsorbates, which is in turn proportional to the binding energy given by Eq. (4.6):

$$N = \frac{P}{P_o}\left(e^{(E_b - E_i)/kT}\right) \qquad (4.6)$$

where in the above equation N is the number of adsorbed molecules, P/P_o is the partial pressure of the gas molecules, and E_b-E_i is the effective binding energies of the molecules. For a fixed pressure of all gases the polarization simply relates to the binding energy using the above

equation, concluding that higher polarizability of the molecules on the surface of the adsorbent will lead to higher binding of the molecules on the substrate. Polarization *P* or γ can experimentally be calculated from the dielectric response of the material using the Claussius-Mossotti relationship given by Eq.s (4.7) and (4.8) below: [67]

$$\gamma = \gamma_{mol} + \frac{\mu^2}{3KT} \tag{4.7}$$

where γ is the total polarization, γ_{mol} is the polarizability of the free molecule and μ is the permanent dipole moment, and *K* and *T* are the Boltzmann constant and temperature, respectively. γ is related to the dielectric response of the material by Eq. (4.8) shown below:

$$\varepsilon = 1 + 4\pi \frac{N\gamma}{1 - \frac{4\pi}{3} N\gamma} \ . \tag{4.8}$$

And ε can be calculated directly by measuring the shift in the resonant frequency as defined by Eq. (4.1). Further theoretical modeling will increase understanding of the nature of the forces governing while the system is gassed, and allow observation of whether there is any change in the interaction forces upon cycling gases through the system under electromagnetic fields.

Conclusion

From the results obtained using the differential microwave resonant cavity techniques, it has been possible to selectively and sensitively discriminate between the adsorption phenomenon of both mildly polar as well as non-polar gases. Through this research it has been possible to study the propensity of SWCNTs for gas adsorption. The results are indicative of the fact that the resonator technique proves to be very sensitive for developing a chemical, biological sensor prototype. When loaded with specifically functionalized adsorbent, these sensors would be capable of producing a unique response toward the presence of that specific toxin. Such a

sensitive, specific device with a small response time (<1 sec) is supposed to demonstrate its competitiveness as compared with some other prototypes being developed.[68] In the following section an attempt has been made to demonstrate the prototype and design of such detectors that will be capable for both remote as well as hand-held detections. Also, the idea of selective loading of these gas molecules in the nanomaterials suggests the possible development of biomolecular pumps that can be used as respirocytes within the human body for artificial transportation of oxygen in human cells and blood plasmas.[69]

CHAPTER 5

APPLICATIONS OF THIS RESEARCH AND CONCLUSION

What Problem Is Solved by This Invention/Study?

Since the September 11 attacks on the United States, the problem of terrorism has petrified the entire world. Since then, there have been new standards established to inhibit terrorist activities. Military and intelligence agencies, the NSA, the FBI, and many other law enforcement agencies have been involved in executing plans that will enhance the security of the United States, as well as several other international bodies. In the past decade or so there have been many incidents of terrorist attacks, both inside and outside the United States, which have concerned governments worldwide.[70] Quoting directly from *A Military Guide to Terrorism in the Twenty First Century*: "Despite the consistent menace, terrorism is a threat that is poorly understood, and frequently confused due to widely divergent views over exactly what defines terrorism."[71]

The focus of this application is toward the threat posed by terrorism involving chemical and biological attacks. Combating terrorism is not only a priority for the FBI, the NSA, the DOD, and other security agencies, but is also a challenge to industries and academic researchers, as well as scientists worldwide. Our invention is a step toward the detection of chemical and biological agents capable of mass destruction of human lives and civilization itself. There have been several industrial toxins, as well as other toxins, known to many terrorist organizations worldwide that have been used as weapons of mass destruction. Detection of their precursors prior to use, as well as upon their usage, poses a great challenge to combat teams around the world. Many kinds of technologies are being developed across the globe in order to counteract these terrorist threats.

The microwave resonant cavity apparatus, when phase-locked to an electronic circuit capable of oscillating in a broad GHz frequency range, is highly sensitive and can be used to detect the deadly toxin gases in microseconds, thus enabling law enforcement agencies to carry out emergency rescue activities with safer and faster techniques. Due to the operational state of the system functioning in a GHz frequency range, the sensitivity of the equipment is in the order of the parts per billion (ppb) level for a toxin in the environment.

Possible Solutions to These Problems

A resonant cavity as shown in Fig. 52 operating in TE_{011} mode was used to sense the adsorption response of single-walled carbon nanotubes (SWCNTs) and other nanomaterials for different types of gas molecules. The range of the frequency signal as a probe for sniffing was chosen arbitrarily between 9.1 and 9.8 GHz. Other highly specific ranges of frequencies can be used to tune the circuitry to "sniff" particular types of toxins, depending upon the nature of their molarities as well as polarities. It was found that for different pressures of different gases and different types of nanomaterials, there were different responses in the shifts of the probe signal for each cycle of gassing and degassing of the cavity. The preliminary work done so far suggests that microwave spectroscopy of the complex medium of gases and carbon nanotubes can be used as a highly sensitive technique in studying the complex dielectric response of different polar as well as non-polar gases when subjected to intense electromagnetic fields within the cavity.

Carbon nanotubes have been shown to exhibit a number of unusual properties in their electrical conductivity and their complex dielectric response. Due to their unusual properties, researchers have found numerous applications for them.[72] Since Ijima discovered carbon nanotubes, many researchers worldwide have shown interest in them. Various studies are underway on these materials to characterize their electrical, optical, and mechanical as well as

thermal properties. In this study I have explored the adsorption response of these nanomaterials when loaded in a microwave resonant cavity and perturbed with a loading gas to be used as a probe for detection. Resonant cavities are well-known, highly sensitive devices that have been used to make measurements of fundamental properties of matter in all its phases.[73] A resonant cavity can be considered to be multiple LCR circuits connected in parallel. Because of their high quality factor (around 5000) these resonant cavities have been widely studied in determining the shifts in the resonant profiles. The frequency range of 9.1 – 9.8 GHz was used in our experiment to scan the cavity with the load placed in the most intense electric field vector of the cavity. Upon perturbing the cavity with a small load (20 mg of SWCNT) there was a shift in the center frequency of the apparatus as shown in Fig. 52. Also in this figure can be seen the broadening of the width at half-power maxima of the typical Lorentzian line shape. Using these fundamental properties of shift in the resonance, broadening of the spectral lines, and change in the amplitudes of the peaks, it was found that the resonant cavities respond very sensitively toward a gas. From these observations I also determined that a resonant cavity sensor of miniature sizes (Fig. 53), loaded with functionalized SWCNTs, can be engineered to selectively and sensitively detect toxins. The determination of which functionality group to be attached to the end-chains of the nanotubes depends upon the chemical to be detected. This method of actively sensing foreign toxins proves to be a unique, sensitive method that can assist emergency first responder teams.

The entire concept of developing a working sensor has been summarized in Fig. 53.

FIG. 52. A sample miniaturized resonant cavity to selectively detect toxins.

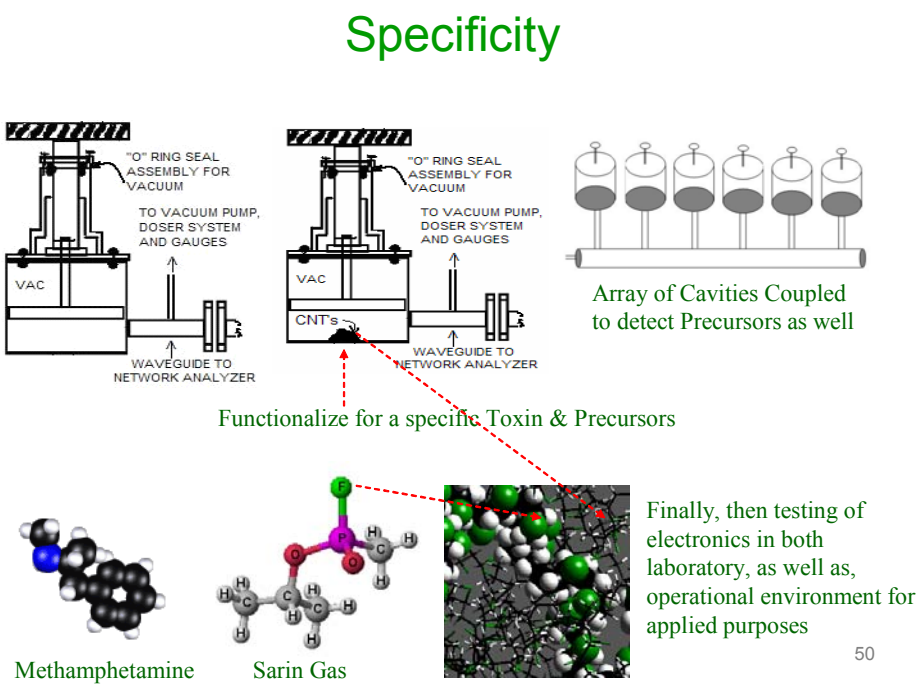

FIG. 53. The entire concept of developing arrays of cavities phase-locked with electronics and loaded with chemi-selective material for specific detection.

What Can Be Done to Further Accomplish Prototyping?

The work done in this research project is a proof-of-concept that demonstrates the possibility of prototyping this research into a commercial sensor for operational use. Further experimental testing and chemical research has to be done in secured locations in order to build a device with minimum false-positives and a larger database of toxins to be detected. Wet and dry chemistry work in conjunction with computer modeling has to be done in a secured installation to choose a better chemo-selective material for adding specificity to this device. Some of the tasks as mentioned in this section are believed to be critical, and by setting milestones for this project, it is believed that a highly sensitive, as well as specific, operational prototype can be developed in two phases of one year each.

Theoretical Modeling and Molecular Dynamics

MS Accelrys® based software can be used in pre-laboratory work to calculate the binding energies of specific chemo-selective materials that will be used to functionalize the nanotube samples acting as a wick for the resonant cavities. Shown in Figs. 54-57 on the following pages are some of the activities that need to be done in the future in order to test the functionalized materials.

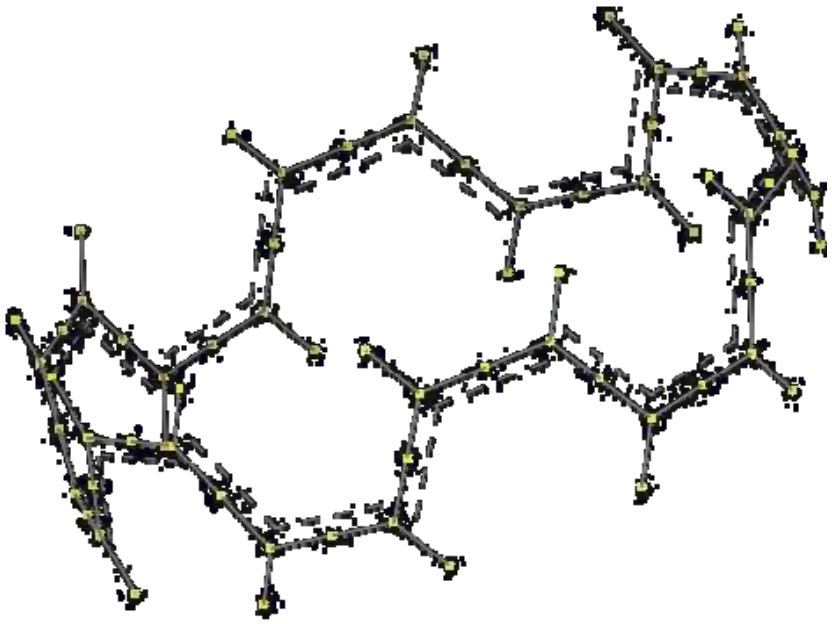

FIG. 54**.** Using the above-mentioned software, an armchair type (10,10) single walled nanotube was created. The dots in yellow on end units depict the possible sites for attaching the dangling bonds of any functionalizing material.

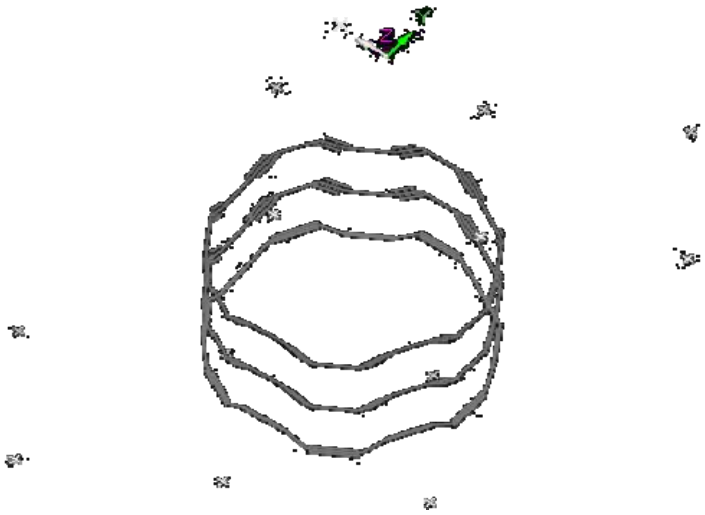

FIG. 55. This figure tries to depict the intended study of modeling the nanotubes and studying their response to any external electromagnetic field. Forcite based calculations can be performed to study the dielectric response of the functionalized material.

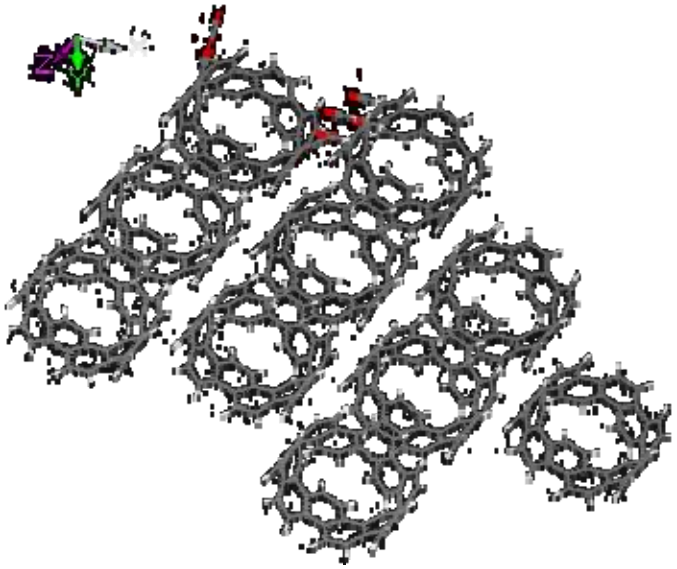

FIG. 56. Dynamic analysis on bundled nanotubes with armchair symmetry and 5 carbon monoxide molecules.

Miniaturization of Electronics

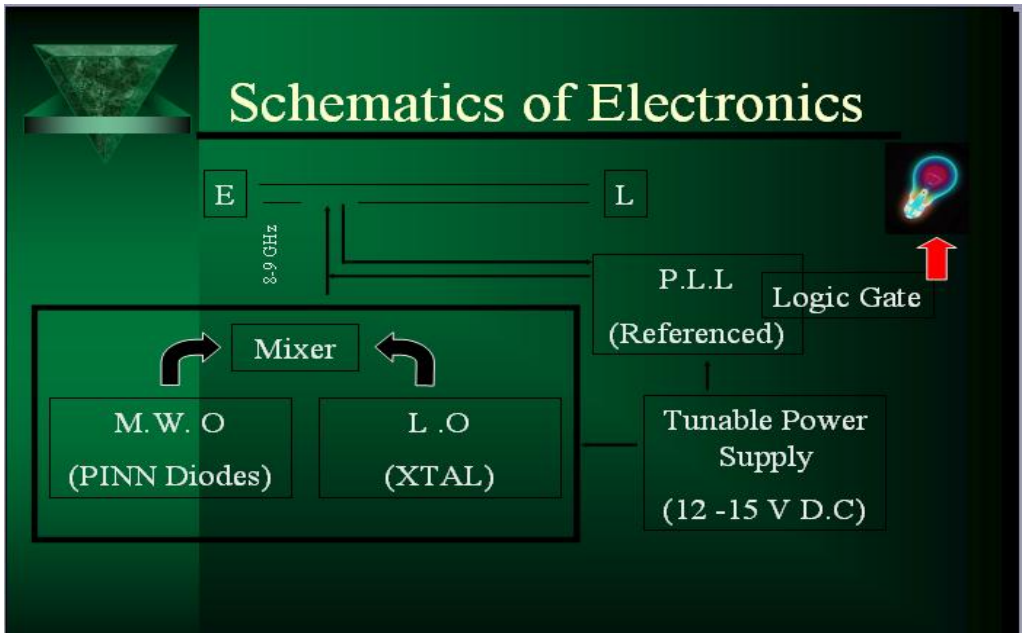

FIG. 57. Schematics of the electronics that will replace our microwave network analyzer to energize the cavity shown in Fig. 52. This size of the electronics will significantly reduce the size of our prototype.

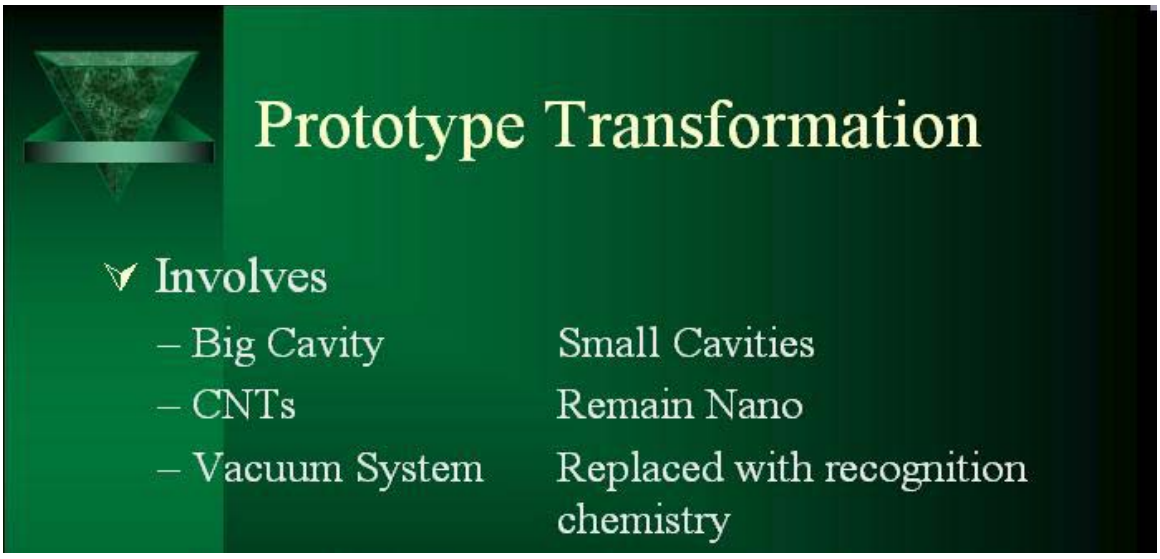

FIG. 58. A simple approach showing how the laboratory research equipment can be engineered into a working portable prototype for the detection of toxins.

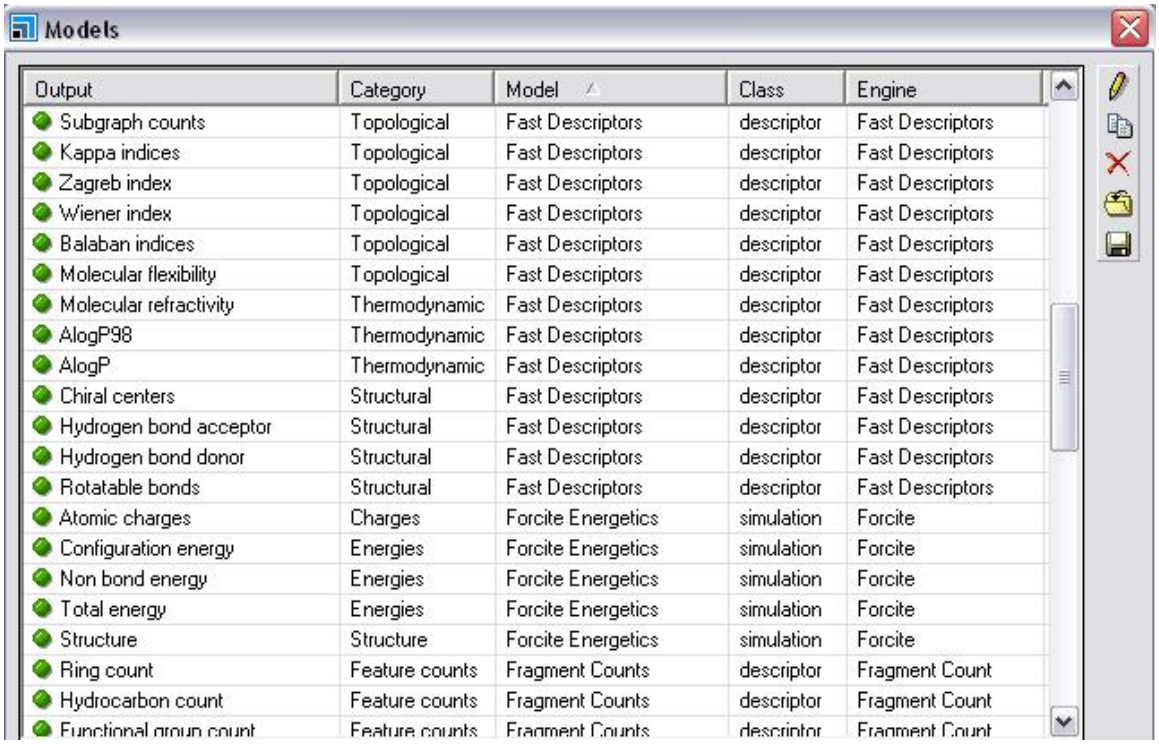

Output	Category	Model	Class	Engine
Subgraph counts	Topological	Fast Descriptors	descriptor	Fast Descriptors
Kappa indices	Topological	Fast Descriptors	descriptor	Fast Descriptors
Zagreb index	Topological	Fast Descriptors	descriptor	Fast Descriptors
Wiener index	Topological	Fast Descriptors	descriptor	Fast Descriptors
Balaban indices	Topological	Fast Descriptors	descriptor	Fast Descriptors
Molecular flexibility	Topological	Fast Descriptors	descriptor	Fast Descriptors
Molecular refractivity	Thermodynamic	Fast Descriptors	descriptor	Fast Descriptors
AlogP98	Thermodynamic	Fast Descriptors	descriptor	Fast Descriptors
AlogP	Thermodynamic	Fast Descriptors	descriptor	Fast Descriptors
Chiral centers	Structural	Fast Descriptors	descriptor	Fast Descriptors
Hydrogen bond acceptor	Structural	Fast Descriptors	descriptor	Fast Descriptors
Hydrogen bond donor	Structural	Fast Descriptors	descriptor	Fast Descriptors
Rotatable bonds	Structural	Fast Descriptors	descriptor	Fast Descriptors
Atomic charges	Charges	Forcite Energetics	simulation	Forcite
Configuration energy	Energies	Forcite Energetics	simulation	Forcite
Non bond energy	Energies	Forcite Energetics	simulation	Forcite
Total energy	Energies	Forcite Energetics	simulation	Forcite
Structure	Structure	Forcite Energetics	simulation	Forcite
Ring count	Feature counts	Fragment Counts	descriptor	Fragment Count
Hydrocarbon count	Feature counts	Fragment Counts	descriptor	Fragment Count
Functional group count	Feature counts	Fragment Counts	descriptor	Fragment Count

FIG. 59. A snapshot of the screen taken from the software that informs us of all the possible calculations that can be performed on a particular ensemble of the system.

Other Possible Applications: Potential Biomolecular Nanopumps as Artificial Oxygen Delivery Vessels *"Nanorobots"* (Freitas)

Work at Foresight Institute of Technology indicates the possibility of preparing biomolecular pumps that can act as artificial oxygen delivery machineries. It is seen through my experimental investigation that carbon-based nanomaterials have shown a selective response towards adsorption of gases and which can be used as reverse-osmotic tanks to collect the carbon dioxide released from metabolic activities. Equipped with robotic machinery valves, these cylindrical pathways can even be used to deliver oxygen into the bloodstream.[74] An interesting article published by Insepov *et al*.[75] illustrates the concept of developing nanopumps that can store as well as release gas molecules through a controlled and precisely mounted nanopump by producing Rayleigh waves. It is believed that with the advancements in technology as well as the concept as discussed by Insepov *et al.*, the applications pursued by many molecular institutes and other energy research laboratories[76] might become reality.

Conclusion

Publications by a number of researchers[77] demonstrate the ongoing work in developing state-of-the-art sensing technologies. As mentioned by Insepov *et al.*,[78] the most prominent technologies listed in the reference are based upon the following detection principles: ion mobility spectrometry, gas chromatography with ion mobility spectrometry, flame photometry, electrochemistry, color change chemistry, surface acoustic wave, photoionization, gas chromatography with flame photometry, gas chromatography, thermal and electrical conductivity, infrared spectroscopy, mass spectrometry, Fourier transform infrared spectroscopy, forward looking infrared with spectral filtering, light detection and ranging, gas chromatography with mass spectrometry, gas chromatography with infrared spectroscopy, gas chromatography

with surface acoustic wave detection, photoacoustic infrared spectroscopy, flame ionization, liquid chromatography, ion chromatography, capillary zone electrophoresis, ultraviolet spectroscopy, and metal oxide sensor. Technical details on these techniques can be found in the literature cited, but it is essential to point that not one such technology exists that has the qualities of producing a reasonable-cost sensor equipment with full-proof operational positives available on the market. Either the method of detection in such technologies is too complicated for commercial application, adding to their procurement as well as operational costs on an annual basis, or else they suffer from benign failures, such as producing too many false positives. Considering the issues around unit cost, mean time between failures, manpower costs, operational costs, number of false positives per year, size, weight, and operational environment to be scanned, it appears that the microwave resonant cavities could offer a viable solution to most of these problems. With an opportunity to advance and develop an integration of such a technology, this concept prototype could be developed for operational testing at a national research laboratory.

The experimental results provided in the previous chapter show evidence of the first tangible form of this device. The experimental results in the previous chapter also put forward the concept design of a sensor. Besides preparing beds of these nanomaterials to be used as gas masks and filters, there is also a very likely possibility of manufacturing nano-based robotic type devices that will have a significant application toward the biomolecular industry.[79]

In conclusion, the work done for this doctoral dissertation has met its experimental requirements in full, and the results obtained from such a study point to new directions for in-depth investigations of the gas-surface interactions with nano-sized materials. The microwave spectroscopy techniques used in this study proved to be very sensitive as well as less erroneous

in determining the microscopic properties of materials using macroscopic techniques. A detailed synopsis related to the extensive microwave spectroscopy and instrumentation that has been developed and progressed since the last decade is appended (Appendix B).

APPENDIX A

DATA TABLES

TABLE A1. Data on the reference cavity response to cycling Carbon Monoxide through it.

Pressure (Pa.)	Frequency (GHz.) While Gassing	Frequency (GHz.) While Degassing
0	9.166899167	9.166899167
3386	9.166791667	9.166791667
6772	9.166694167	9.166694167
10158	9.166611667	9.166611667
13544	9.166521667	9.166521667
16930	9.166426667	9.166426667
20316	9.166334167	9.166334167
23702	9.166245238	9.166245238
27088	9.166156310	9.166156310
30474	9.166067381	9.166067381
33860	9.165978452	9.165978452
37246	9.165889524	9.165889524
40632	9.165800595	9.165800595
44018	9.165711667	9.165711667
47404	9.165622738	9.165622738
50790	9.165476310	9.165476310

TABLE A2**.** Data on the reference cavity response to cycling oxygen through it.

Pressure (Pa)	Frequency (GHz) While Gassing	Frequency (GHz) While Degassing
0	9.159153333	9.159136667
3386	9.159096667	9.159073333
6772	9.159013333	9.158993333
10158	9.158933333	9.158920000
13544	9.158843333	9.158830000
16930	9.158756667	9.158746667
20316	9.158690000	9.158663333
23702	9.158613333	9.158576667
27088	9.158533333	9.158510000
30474	9.158446667	9.158426667
33860	9.158356667	9.158353333
37246	9.158280000	9.158276667
40632	9.158193333	9.158206667
44018	9.158113333	9.158093333
47404	9.158053333	9.158013333
50790	9.157950000	9.157950000

TABLE A3. Data on the reference cavity response to cycling carbon dioxide through it.

Pressure (Pa.)	Frequency (GHz.) While Gassing	Frequency (GHz.) While Degassing
0	9.159133333	9.159141667
3386	9.158983333	9.158979167
6772	9.158820833	9.158833333
10158	9.158720833	9.158687500
13544	9.158600000	9.158554167
16930	9.158437500	9.158433333
20316	9.158287500	9.158283333
23702	9.158166667	9.158145833
27088	9.158029167	9.157995833
30474	9.157866667	9.157887500
33860	9.157725000	9.157720833
37246	9.157575000	9.157583333
40632	9.157395833	9.157437500
44018	9.157266667	9.157283333
47404	9.157120833	9.157120833
50790	9.156950000	9.156950000

TABLE A4**.** Data on the reference cavity response to cycling hydrogen through it.

Pressure (Pa)	Frequency (GHz) While Gassing	Frequency (GHz) While Degassing
0	9.159732500	9.159732233
3386	9.159670000	9.159658333
6772	9.159612500	9.159610000
10158	9.159582500	9.159575000
13544	9.159515000	9.159512500
16930	9.159477500	9.159472500
20316	9.159410000	9.159405000
23702	9.159342500	9.159347500
27088	9.159287500	9.159292500
30474	9.159220000	9.159225000
33860	9.159172500	9.159170000
37246	9.159125000	9.159125000
40632	9.159057500	9.159057500
44018	9.158990000	9.158982500
47404	9.158915000	9.158930000
50790	9.158847500	9.158847500

TABLE A5**.** Data on the response of test cavity loaded with 20mg of SWCNTs and cycled with carbon monoxide.

Pressure (Pa)	Frequency (GHz) While Gassing	Frequency (GHz) While Degassing
0	9.131990833	9.132369167
3386	9.131854167	9.132265000
6772	9.131657500	9.132146667
10158	9.131525000	9.132042500
13544	9.131402500	9.131938333
16930	9.131312500	9.131866667
20316	9.131208333	9.131713333
23702	9.131090000	9.131613333
27088	9.130911667	9.131488333
30474	9.130765000	9.131345000
33860	9.130628333	9.131155000
37246	9.130528333	9.131004167
40632	9.130442500	9.130881667
44018	9.130320000	9.130685000
47404	9.130220000	9.130487500
50790	9.130093333	9.130093333

TABLE A6. Data on the response of test cavity loaded with 20mg of SWCNTs and cycled with oxygen.

Pressure (Pa)	Frequency (GHz) While Gassing	Frequency (GHz) While Degassing
0	9.143537500	9.143500000
3386	9.143412500	9.143425000
6772	9.143262500	9.143350000
10158	9.143137500	9.143237500
13544	9.142962500	9.143162500
16930	9.142862500	9.143087500
20316	9.142750000	9.143012500
23702	9.142650000	9.142962500
27088	9.142600000	9.142862500
30474	9.142512500	9.142762500
33860	9.142450000	9.142650000
37246	9.142387500	9.142512500
40632	9.142300000	9.142387500
44018	9.142225000	9.142237500
47404	9.142125000	9.142100000
50790	9.142025000	9.142025000

TABLE A7**.** Data on the response of test cavity loaded with 20mg of SWCNTs and cycled with carbon dioxide.

Pressure (Pa)	Frequency (GHz) While Gassing	Frequency (GHz) While Degassing
0	9.143462500	9.143525000
3386	9.143200000	9.143325000
6772	9.143000000	9.143225000
10158	9.142825000	9.143100000
13544	9.142725000	9.142937500
16930	9.142587500	9.142787500
20316	9.142487500	9.142662500
23702	9.142350000	9.142512500
27088	9.142200000	9.142337500
30474	9.142062500	9.142200000
33860	9.141925000	9.142062500
37246	9.141737500	9.141962500
40632	9.141562500	9.141812500
44018	9.141462500	9.141637500
47404	9.141287500	9.141462500
50790	9.141137500	9.141137500

TABLE A8**.** Data on the response of test cavity loaded with 20mg of SWCNTs and cycled with hydrogen.

Pressure (Pa)	Frequency (GHz) While Gassing	Frequency (GHz) While Degassing
0	9.143678333	9.143720833
3386	9.143550833	9.143664167
6772	9.143451667	9.143607500
10158	9.143380833	9.143522500
13544	9.143310000	9.143437500
16930	9.143210833	9.143366667
20316	9.143125833	9.143295833
23702	9.143040833	9.143225000
27088	9.142955833	9.143168333
30474	9.142899167	9.143083333
33860	9.142800000	9.142970000
37246	9.142715000	9.142885000
40632	9.142672500	9.142814167
44018	9.142615833	9.142715000
47404	9.142573333	9.142658333
50790	9.142516667	9.142516667

TABLE A9**.** Data on the response of test cavity loaded with 20mg of oxidized SWCNTs and cycled with carbon dioxide.

Pressure (Pa)	Frequency (GHz) While Gassing	Frequency (GHz) While Degassing
0	9.135916667	9.135983333
3386	9.135733333	9.135883333
6772	9.135650000	9.135816667
10158	9.135433333	9.135650000
13544	9.135316667	9.135483333
16930	9.135233333	9.135266667
20316	9.135066667	9.135116667
23702	9.134866667	9.134950000
27088	9.134650000	9.134783333
30474	9.134550000	9.134683333
33860	9.134400000	9.134533333
37246	9.134300000	9.134350000
40632	9.134150000	9.134183333
44018	9.133950000	9.134050000
47404	9.133833333	9.133883333
50790	9.133675000	9.133675000

TABLE A10**.** Data on the response of test cavity loaded with 20mg of oxidized SWCNTs and cycled with oxygen.

Pressure (Pa)	Frequency (GHz) While Gassing	Frequency (GHz) While Degassing
0	9.136033333	9.136050000
3386	9.135866667	9.135966667
6772	9.135750000	9.135883333
10158	9.135666667	9.135766667
13544	9.135533333	9.135700000
16930	9.135466667	9.135583333
20316	9.135366667	9.135466667
23702	9.135266667	9.135400000
27088	9.135183333	9.135333333
30474	9.135100000	9.135233333
33860	9.135000000	9.135150000
37246	9.134950000	9.135050000
40632	9.134866667	9.134983333
44018	9.134783333	9.134833333
47404	9.134666667	9.134716667
50790	9.134583333	9.134583333

TABLE A11**.** Data on the response of test cavity loaded with 20mg of activated charcoal and cycled with carbon monoxide.

Pressure (Pa)	Frequency (GHz) While Gassing	Frequency (GHz) While Degassing
0	9.132545000	9.132859167
3386	9.132424167	9.132714167
6772	9.132279167	9.132641667
10158	9.132134167	9.132545000
13544	9.132037500	9.132448333
16930	9.131916667	9.132351667
20316	9.131795833	9.132279167
23702	9.131723333	9.132158333
27088	9.131602500	9.131965000
30474	9.131505833	9.131844167
33860	9.131433333	9.131699167
37246	9.131336667	9.131602500
40632	9.131240000	9.131481667
44018	9.131143333	9.131359833
47404	9.131022500	9.131143333
50790	9.130901667	9.130901667

TABLE A12**.** Data on the response of test cavity loaded with 20mg of activated charcoal and cycled with oxygen.

Pressure (Pa)	Frequency (GHz) While Gassing	Frequency (GHz) While Degassing
0	9.132931667	9.133100833
3386	9.132738333	9.132980000
6772	9.132617500	9.132835000
10158	9.132520833	9.132738333
13544	9.132400000	9.132617500
16930	9.132279167	9.132520833
20316	9.132134167	9.132448333
23702	9.132061667	9.132425833
27088	9.131989167	9.132255000
30474	9.131868333	9.132158333
33860	9.131747333	9.132085833
37246	9.131675000	9.132013333
40632	9.131578333	9.131795833
44018	9.131505833	9.131650833
47404	9.131409167	9.131505833
50790	9.131336667	9.131336667

TABLE A13**.** Data on the response of test cavity loaded with 20mg of activated charcoal and cycled with carbon dioxide.

Pressure (Pa)	Frequency (GHz) While Gassing	Frequency (GHz) While Degassing
0	9.132925000	9.133004167
3386	9.132665833	9.132883333
6772	9.132545000	9.132714167
10158	9.132424167	9.132545000
13544	9.132279167	9.132448333
16930	9.132134167	9.132327500
20316	9.131942500	9.132182500
23702	9.131820000	9.132037500
27088	9.131675000	9.131844167
30474	9.131481667	9.131675000
33860	9.131385000	9.131505833
37246	9.131215833	9.131360833
40632	9.131070833	9.131167500
44018	9.130853333	9.130925833
47404	9.130708333	9.130732500
50790	9.130563333	9.130563333

TABLE A14**.** Data on the response of test cavity loaded with 20mg of activated charcoal and cycled with hydrogen.

Pressure (Pa)	Frequency (GHz) While Gassing	Frequency (GHz) While Degassing
0	9.13414000	9.13421250
3386	9.13406750	9.13414000
6772	9.13394667	9.13409167
10158	9.13380167	9.13399500
13544	9.13372917	9.13392250
16930	9.13365667	9.13385000
20316	9.13358417	9.13377750
23702	9.13351167	9.13372917
27088	9.13343917	9.13365667
30474	9.13334250	9.13353583
33860	9.13327000	9.13346333
37246	9.13319750	9.13339083
40632	9.13314917	9.13331833
44018	9.13307667	9.13319750
47404	9.13300417	9.13307667
50790	9.13293167	9.13293167

TABLE A15**.** Data on the response of test cavity loaded with 24mg.of silica gels and cycled with oxygen.

Pressure (Pa)	Frequency (GHz) While Gassing	Frequency (GHz) While Degassing
0	9.122640000	9.122640000
3386	9.122535000	9.122535000
6772	9.122465000	9.122430000
10158	9.122395000	9.122395000
13544	9.122290000	9.122255000
16930	9.122150000	9.122150000
20316	9.122080000	9.122045000
23702	9.121975000	9.121975000
27088	9.121870000	9.121905000
30474	9.121800000	9.121800000
33860	9.121695000	9.121695000
37246	9.121590000	9.121625000
40632	9.121590000	9.121520000
44018	9.121450000	9.121485000
47404	9.121380000	9.121380000
50790	9.121275000	9.121275000

TABLE A16. Data on the response of test cavity loaded with 10mg. of cotton and cycled with carbon monoxide.

Pressure (Pa)	Frequency (GHz) While Gassing	Frequency (GHz) While Degassing
0	9.121082500	9.121240000
3386	9.120767500	9.121127500
6772	9.120565000	9.121015000
10158	9.120385000	9.120857500
13544	9.120295000	9.120655000
16930	9.120227500	9.120565000
20316	9.120092500	9.120497500
23702	9.120002500	9.120407500
27088	9.119889250	9.120295000
30474	9.119800000	9.120160000
33860	9.119687500	9.120047500
37246	9.119597500	9.119845000
40632	9.119507500	9.119777500
44018	9.119282500	9.119687500
47404	9.119057500	9.119485000
50790	9.118990000	9.118990000

TABLE A17. Data on the response of test cavity loaded with 10mg. of cotton and cycled with oxygen.

Pressure (Pa)	Frequency (GHz) While Gassing	Frequency (GHz) While Degassing
0	9.121060000	9.121217500
3386	9.120857500	9.121082500
6772	9.120677500	9.120925000
10158	9.120565000	9.120812500
13544	9.120407500	9.120721833
16930	9.120340000	9.120655000
20316	9.120272500	9.120565000
23702	9.120182500	9.120475000
27088	9.120092500	9.120430000
30474	9.120002500	9.120340000
33860	9.119957500	9.120272500
37246	9.119890000	9.120205000
40632	9.119777500	9.120137500
44018	9.119710000	9.119980000
47404	9.119642500	9.119845000
50790	9.119575000	9.119575000

TABLE A18. Data on the response of test cavity loaded with 10mg. of cotton and cycled with carbon dioxide.

Pressure (Pa)	Frequency (GHz) While Gassing	Frequency (GHz) While Degassing
0	9.121127500	9.121240000
3386	9.120902500	9.121105000
6772	9.120790000	9.120992500
10158	9.120542500	9.120790000
13544	9.120407500	9.120655000
16930	9.120295000	9.120520000
20316	9.120115000	9.120407500
23702	9.120047500	9.120250000
27088	9.119890000	9.120115000
30474	9.119755000	9.119980000
33860	9.119620000	9.119822500
37246	9.119485000	9.119642500
40632	9.119350000	9.119417500
44018	9.119102500	9.119260000
47404	9.119035000	9.119080000
50790	9.118900833	9.118900833

APPENDIX B

SUMMARY OF USEFUL LITERATURE RELEVANT TO MICROWAVE INSTRUMENTATION AND RESEARCH DONE IN THE PAST

This appendix contains synopses of useful works studied for this dissertation, which provided rich resources and a better understanding of the application and instrumentation techniques related to microwave spectroscopy.

1. Paper by E. Bourdel *et al.* on measurement of moisture content using resonant cavities:
E. Bourdel and Daniel Pasquet, "Measurement of the moisture content with a cylindrical resonating cavity in TM_{010} mode," IEEE Trans. Instrum. Meas. **49** (5), (2000).

Summary of the paper:

The authors have introduced a concept of using a cylindrical resonant cavity in new resonant mode TM_{010} to measure the moisture content and specific mass of cigarettes. Theoretical calculations were done to derive the relationships between the complex permittivity of the sample and the characteristics of the cavity. The authors have researched this new mode in which a large part of the electromagnetic energy is in the center of the cavity and the electric field vector lies along the axis of the cavity. This paper lacks critical information concerning the dimensions of the waveguide, sample in place as well as the cavity on the whole. The only information provided is that the cavity is oscillating at 5GHz. For this mode the propagation constant is zero and the authors have derived the relation for the real as well as the imaginary part of the dielectric response of the sample with small diameters as given below:

$$\varepsilon' = 1 - \frac{\delta\omega}{\omega_o}\frac{2}{u_{01}-1}\frac{J_1(u_{01})}{Y_0(u_{01})}\frac{1}{\pi}\left(\frac{4a^2}{{u_{01}}^2 b^2}+\frac{3}{2}\right) \tag{A1}$$

$$\varepsilon'' = \frac{1}{Q_o}\frac{{u_{01}}^2}{(u_{01}-1)}\frac{J_1(u_{01})}{Y_0(u_{01})}\frac{1}{\pi}\left(\frac{4a^2}{{u_{01}}^2 b^2}+\frac{3}{2}\right) \tag{A2}$$

where $\delta\omega$ is the small shift in the frequency of the cavity near its natural resonance, u_{01} is the first root of the equation $J_o(x) = 0$, J_1 and Y_o are modified Bessel functions and Q_o is the characteristic response of the quality factor of the resonant cavity. a and b are the radii of the cavity and the sample respectively. The Q response is generally calculated by measuring the changes in the resonant response of the cavity. From the calculations and experimental studies, the researchers deduced important relationships between the specific mass of the sample and its complex permittivity. In this work the researchers have measured Q_o values for various samples and have plotted several graphs, i.e.

$\frac{\delta\omega}{\omega_0}$ and $\frac{1}{Q}$ were plotted against various moisture contents, slopes and the intercept of ε'' *vs.* ε' was calculated from the plots and it was deduced that the specific mass of the sample was related to the complex permittivity of the sample by Eq. (A3):

$$\varpi = \frac{\varepsilon' - 1 - \frac{\varepsilon''}{2}}{a} \qquad \text{(A3)}$$

where a in this equation has an inverse dimensions of density (g^{-1}. cm^3)

Using the best-fit methods and plotting the polynomial of the variation of ε' vs. the moisture contents the authors were able to determine the amount of moisture for the other samples, too. This is an interesting analytical treatment of their data to quantify the contaminants in the cavity and the approach can be introduced in analyzing our experimental results.

2. Paper by C. K. Jen on method for measuring the constant dielectric constant of gases using microwave spectroscopy techniques: C.K. Jen, "A Method for measuring the constant dielectric constant of gases at microwave frequencies by using a resonant cavity," J. App. Phys. **19**, 649 (1948).

Summary of the paper:

Researchers in this paper have demonstrated a sensitive technique to measure the dielectric response of the gases contained in a microwave resonant cavity operating in their X bands (8-12.5 GHz generally used for communications satellite and radar). Using standard microwave resonant cavity techniques, the researchers measured the change in the resonant frequencies to compute the real part of the dielectric response and observed the change in amplitude and the change in the breadth of the resonant response curve, which also is the observed quality response of the cavity. From the Q factor response of the cavity the researchers were able to calculate the imaginary part of the dielectric response of the signal. The resonant cavities behave like a low frequency resonant circuit and the circuit's properties are characterized by a loss factor and the resonant frequencies. In this paper the authors have used the analogies of any traditional resonant circuits, and their experimental apparatus was set up as a magic tee junction. The details of their apparatus set up and the concepts governing magic tees can be found in the reference section of this paper. It is found that the authors have used the following relationships to calculate the real as well as the imaginary part of the dielectric response of the gases introduced into the cavity.

$$\varepsilon' = 1 - \frac{2}{(f_o)_{empty}}[(f_o)_{gas} - (f_o)_{empty}] \qquad \text{(A4)}$$

$$\varepsilon'' = (\delta_o)_{gas} - (\delta_o)_{empty} \qquad \text{(A5)}$$

where in Eq.s (A4) and (A5) above f_o is the frequency response of the analyzer when either filled with gas or when empty and δ_o is the lossy tangent of the cavity when either empty or filled with the gases. The lossy part can be calculated from the inverse of the quality factor of the cavity observed by measuring the width at half power maxima. The authors though have failed to

quantify in their work the amount or pressure of the gas being introduced into the cavity. The authors in their work studied the response for methyl chloride as well as a certain fraction of ratios for deuterated ammonia. In my work I have studied the complex response of various gases with amorphous in-homogeneous materials like carbon nanotubes at different gas pressures for each cycle of gassing as well as degassing.

3. Paper by Paul G. Steffes on measuring the millimeter wave properties of atmospheric constituents: Paul G. Steffes, "Laboratory measurement of microwave and millimeter-wave properties of planetary atmospheric constituents," Procedings of International Conference on Laboratory Research for Planetary Atmospheres, **1** (1989).

Summary of the paper:

This paper discusses the importance of measuring the microwave and mm wave properties of atmospheric constituents that can be critical for the interpretation of radio occultation measurements. The paper discusses the apparatus and techniques involved in measuring the refractivity and absorptivity of atmospheric constituents at wavelengths between mm and cm range. Both spacecraft radio occultation experiments as well as earth-based radio emission measurements were made to study the opacity of atmospheric gases to wavelengths greater than 1 cm. Whenever there is opacity in the constituents, the techniques of using cylindrical resonant cavities can come in handy. The authors observed the response on the Q factor of the cavity upon introducing low-loss gas mixtures in their apparatus and deduced

$$\alpha = (Q_L^{-1} - Q_C^{-1})\,\pi/\lambda \qquad \text{(A6)}$$

where α is the absorptivity of the gas mixture measured in nepers km^{-1}, where 1 neper is 8.686 db km^{-1}, Q_l is the quality factor response of the cavity when the gas is present inside and the Q_C value is when the cavity is under vacuum. This equation can be used for the apparatus and measurements used in my experiment as my system operated in the X band range and had a low

gas mixture. The change in the attenuation coefficient of the results vs. the gas pressure can also be plotted. The authors in this paper have even studied the mixture response of sulfuric acid vapors and carbon monoxide and have systematically compared the response of the apparatus with different vapor mixtures. This result or study can be used in our experimental application of developing customized sensors. The authors have even studied different apparatuses like the semi-confocal Fabry-Perot cavity, avoiding the difficulties of using the cavities at shorter wavelengths than 1 cm. A cautionary note from the author in this paper is that as the quality factor of the cavity is defined as the ratio of the resonant center frequency to the resonance half-power bandwidth, the ratio of the energy stored in the resonator to the energy lost per cycle is proportional. Therefore, stronger coupling between the resonator and the spectrum analyzer or sweep oscillator causes mode energy loss per cycle and hence reduces the Q value of the cavity. To avoid such losses I had used gold-plated electrodes in a coaxial wire to connect the crystal detectors to the resonant cavity coupled to the X band waveguides. The author also mentions the important detail of investigating the possibility of errors and measuring the percentage errors. In their above paper, the uncertainties were classified into two categories:

a) due to instrumental error and

b) due to noise.

Reducing the sources for these uncertainties, especially the noise, increases the sensitivities of the measurement significantly.

In the second part of the paper the authors have calculated the refractive index of gases which is defined as the velocity of the electromagnetic waves in a vacuum which is c and the velocity of the waves in gases given by V_g. Using the proportionality of frequency with velocity it can be expressed as

$$n = \frac{c}{v_g} = \frac{f_v}{f_g} \tag{A7}$$

where f_v is the frequency observed in vacuum and f_g is the frequency observed in the presence of the gas. From here the refractivity is expressed as *(n-1)* 10^6*. So by simply measuring the change in the resonance frequency, the refractivity of the gas can be calculated. The author in this paper even expressed the refractivity in terms of molar concentration of the gases. Since the refractivity of the gas is directly proportional to the molecular density of the gas ρ, the refractivity is often expressed in a form which is normalized by molecular density in terms of the temperature and pressure of the gas, i.e.

ρ = P/RT where ρ is the density in molecules per cm^3 and *P* is the pressure in atmospheres, *R* is the ideal gas constant (1.362344 x 10-22 cm^3 atm/molecule/kelvin), and *T* is the temperature in degrees Kelvin. Thus, the density-normalized refractivity N/ρ can now be expressed as *NRT/P*.

The author in this paper has also addressed other issues, like measuring the complex permittivity of liquids and solids using other experimental setups like the coaxial line, which is not being discussed in this paper as it is beyond the scope of this thesis.

4. J. F. Rouleau's paper on the use of a differential resonant cavity to measure humidity in gases: J. F. Rouleau, J. Goyette, T. K. Bose, and M. F. Frechette, "Investigation of a microwave differential cavity resonator device for the measurement of humidity in gases," Rev. Sci. Instrum., **70** (9), (1999).

Summary of the paper:

In this paper the authors have investigated a microwave differential device based upon the resonant cavity technique to measure small quantities of water vapor present in the gases. Recording the induced variations in the relative permittivity due to a shift in the resonant

frequency of the resonator did all this. Two resonators were coupled, one of which was a reference device. The output signal was related to the difference in reflection coefficients of the reference as well as the test cavities. A simple model was also prepared where the authors studied the proportionality between the difference of the reflection coefficients and the variation in the dielectric constants of the gases. The model was developed on the famous Claussius-Mossotti (CM) equation for the binary gas mixture at a given concentration and pressure.

In this modeling approach the CM equation for polar gases was studied for gases with low pressure. But this approach required prior knowledge of the $A_{\epsilon,}$ which is the first dielectric virial coefficient of the CM function and is related to the total polarizability of a polar molecule. Their experimental setup was similar to ours, in which the two resonant cavities were connected to a 180^{o} hybrid junction. More details on their apparatus setup can be found in the reference provided for this paper.

In order to calculate the reflection coefficient differences between the resonators, the authors used the standard electrical and electromagnetic theories of admittance and reflections at the boundaries.

Admittance, which is the inverse of the impedance for an LCR circuit is given by

$$Y = \frac{\omega LG - j\,(1-\omega^2 LC)}{\omega L}. \qquad \text{(A8)}$$

Where L is the inductance of the circuit, G is the conductance, C is the capacitance from the relation provided in the above equation, the complex reflection coefficient is related to the admittance by:

$$\Gamma^{*} = \frac{Y_o - Y}{Y_o + Y} \qquad \text{(A9)}$$

where Y_o is the characteristic admittance of the system connected to the cavity. From the Taylor series expansion of Eq. (A9) and rearranging of the terms, the authors have been able to calculate the detection threshold of the molecules which is given by

$$\frac{\varepsilon - 1}{\varepsilon + 2} = A_{\varepsilon}\rho + B_{\varepsilon}\rho^2 + C_{\varepsilon}\rho^3 + \ldots \qquad \text{(A10)}$$

Where $A_{\varepsilon}, B_{\varepsilon}, C_{\varepsilon}$ are respectively the first, second and third dielectric virial coefficients representing contributions from individual molecules, pairs and triplets. From the first order approximation, when the pressure of the system is low the density of the gas molecules starts following the ideal gas behavior. Then only the first term can be considered in the above equation, and hence we get

$$\varepsilon = \frac{1 + 2A_{\varepsilon}\rho}{1 - A_{\varepsilon}\rho} \approx 1 + 3A_{\varepsilon}\rho \qquad \text{(A11)}$$

For any polar molecules the first dielectric coefficients can be derived from the molecular properties as mentioned in the reference.

5. H. E. Bussey's survey paper on microwave properties of materials: H. E. Bussey, "Measurement of RF properties of materials: A survey," Proceedings of the IEEE, **55** (6), (1967).

Summary of the paper:

This paper published by the author is a short survey where the author reports on various measurement techniques to measure RF properties of materials. In this report the author discusses dielectric constant measurements methods:

a) Capacitor measurements of ε^* where the author has referred to the National Bureau of Standards (NBS) technique of measuring ε by measuring the change in the capacitance and of conductance as the two are related by :

$$\varepsilon' = 1 + \Delta C / C_o$$

$$\varepsilon'' = \Delta G / \omega C_o$$

Where $C_o = \varepsilon_o S / s$ is the vacuum capacitance of the sample (A12)

b) Certain immersion techniques used then to measure the loss tangents of the sample, but which were not that popular.

c) Cavity and transmission line methods in which:

- short circuited lines
- resonators
- perturbation methods
- re-entrant cavities

were some of the techniques studied as a part of the cavity and line methods whose details can be found in several works published to date.

d) Voltage ratio to measure *Q* changes.

e) Material resonators and many other specialized measurements referred to in this paper.

Also the author mentions several other techniques in which magnetic measurements were made in those days. The survey also lists an extensive list of good references that offer details on specific measurement methods.

6. S. B. Cohn's paper on microwave measurement of high-dielectric constant materials: S. B. Cohn and K. C. Kelly, "Microwave measurement of high-dielectric constant materials," IEEE Trans. Microwave Theory Tech. **MTT-14** (9), (1966).

Summary of the paper:

The authors of this paper made a very valid point in mentioning one serious source of

error in measuring the microwave properties of high dielectric materials, which according to this paper is the presence of air gaps between the sample and the cavity's boundary walls. In my experimental study I have made a considerable effort to eliminate such error margins by performing experiments under low and ultra-high vacuum conditions. In this paper, the authors measured the properties either by closely fitting the sample in a circular waveguide or by placing the load in the center of the radial waveguide. The apparatus was resonating in the circular electric mode in which the electric fields were parallel to the metal walls. From a theoretical standpoint, at microwave frequencies the dielectric constants are basically quantified by measuring the enhanced capacitance effect produced by the dielectric sample. These effects produce a change in many macroscopic properties of the system, including change in velocity propagation, change in the resonant frequencies, change in the index of refraction of the material, and change in the quality factor of the resonator. However, the author states that the accuracy of the measurement can be seriously affected if the configuration of the system permits electric field lines to pass from the dielectric sample to the conducting boundaries by way of irregular medium or air gaps. In our experiment, the essence of the setup was not just simply to measure the dielectric response of single-walled carbon nanotubes, but instead to measure the complex permittivity of the medium when the sample was loaded with different gas molecules.

The authors understood the effective capacitance of their setup in the presence of air gaps to be analogous, and have related the real part of the relative permittivity of the medium by:

$$\varepsilon_r^{'} = \frac{\varepsilon_r}{1 + \frac{2 t_a \varepsilon_r}{t_d}} \tag{A13}$$

where t_a is the length of the air gap and t_d is the sample thickness.

The authors performed their experiments using the circular waveguide dielectrometer resonating in TE_{011} mode, whose setup can be studied in the reference. By measuring the characteristic impedance of the setup, and by measuring the free space wavelength and the diameter of the waveguide, the authors measured the susceptance of the cavity in the TE_{011} mode, given by

$$B_a = \frac{Y_{oa}}{j} = -\frac{1}{\eta}\left(\left(\frac{\lambda}{.820D}\right)^2 - 1\right)^{1/2} \tag{A14}$$

where λ is the free space wavelength within the waveguide, D is is the diameter, B_a is the susceptance of the waveguide setup. Susceptance is basically the imaginary part of the admittance and can be expressed as:

$$Y = G + jB \tag{A15}$$

where Y is the admittance, measured in siemens, G is the conductance, measured in siemens, $j = \sqrt{-1}$, B is the susceptance, measured in siemens.

The authors found a similar relationship in the susceptance of the sample and then according to the conditions of resonance where the two susceptances were equated to obtain the relationship for ε_r response of the sample to the cutoff wavelength of the waveguide.

The technique of measuring the dielectric response using the method described by the author above is an interesting technique. But it can suffer from severe drawbacks, such as when the impedance response of the system is measured with variation in temperatures, and it does not provide us with much necessary information concerning the refractivity of the sample or the loading limit of the system, especially in situations like ours where both polar as well as non-polar gas molecules were loaded into the cavity that already has an inhomogeneous load in it.

The authors even tried the radial waveguide methods to achieve the same result in which the radius of the sample does not play an important role. This can be studied in the reference mentioned in the paper.

7. Yoshio Kobayashi 's paper on microwave measurement of dielectric properties of materials: Y. Kobayashi and M. Katoh, "Microwave measurement of dielectric properties of low-loss materials by the dielectric rod resonator method," IEEE Trans. Microwave Theory Tech. **MTT-33 (**7), (1985).

Summary of the paper:

The authors in this paper have tried to measure the dielectric response of a material in the shape of a rod by placing it between two conducting plates. They have used a form of cylindrical cavity resonator, the difference being in the absence of conducting walls and in the measurement of the system properties in terms of surface resistance. It is a design involving short-circuiting the two conducting plates with a dielectric in between. Two dielectric rod resonators were prepared with two different lengths and they were resonating in $TE0_{11}$ and $TE0_{1l}$ modes for $l \geq 2$ resonant modes. The authors have used the resonators' resonant frequency without the dielectric placed between them to compute the ε_r values given by:

$$\varepsilon_r = \left(\frac{\lambda_o}{\pi D}\right)^2 \left(u^2 + v^2\right) + 1 \qquad \text{(A16)}$$

where $v^2 = \left(\frac{\pi D}{\lambda_o}\right)^2 \left[\left(\frac{\lambda_o}{\lambda_g}\right)^2 - 1\right]$ (A17)

and λ_g is $= \frac{2L}{l}$.

In any case this is a different geometry problem and is being mentioned for reference purposes only. It appears that due to lack of insulation in such a setup there will be more energy

loss to the vicinity of the rods. In other words, the energy stored in the dielectric will be less, and hence the quality factor of the resonator will be low.

8. A. W. Kraszewski 's paper discussing techniques to measure moisture content in soybean seeds: A. W. Kraszewski, T. S. You, and S. O. Nelson, "Microwave resonator technique for moisture content determination in single soybean seeds," IEEE Trans. Instrum. Meas. **38** (1), (1989).

Summary of the paper:

This paper introduces a new simple statistical model to describe using the curve fitting the amount of moisture content in soy bean seed. The data of frequency shifts and the changes in the Q values of their rectangular waveguide resonator (in H_{105} and H_{107} resonating modes) was statistically plotted to the mass of water (m_w) , the mass of a dry sample (m_d) and the mass of moist sample (m_m). The observed experimental parameters were the change in the resonance shift and the change in the transmission coefficient of the cavity due to the introduction of dry as well as moist seed.

A linear equation was derived from the fitting plots of Δf vs. m_w in a single soybean seed and ΔT vs. m_w in a single soybean seed and was compared to the values of dry seeds' perturbation into the cavity. The authors have used a nice empirical technique to study their results statistically and it may in some way prove useful in doing our experimental analysis of loading the nanotubes with different gases. An example of such an analysis would be a study of the shift due only to the nanotubes compared with the shifts with the gas being loaded into the sample. It will be necessary to study though Van Bladel (Ch. 10) as well as R.F. Harrington *Time Harmonic Electromagnetic Fields* (p. 317) to understand the importance of the fact that a dielectric object of given volume and relative permittivity will produce different resonant frequency shifts and different changes in the cavity Q factor depending upon its shape, location

in the cavity, and orientation with respect to the electric field vector. In my study I took this fact into account by containing our load in a Teflon® sample holder of fixed dimensions as described in the experimental setup section of this dissertation.

9. F. I. Shimabukuro's paper on attenuation measurements: Fred I. Shimabukuro and C.Yeh, "Attenuation measurement of very low loss dielectric waveguides by the cavity resonator methods applicable in the millimeter/submillimeter wavelength range," IEEE Trans. Microwave Theory Tech. **36** (7), (1988).

Summary of the paper:

This is again a paper that refers to a study of the dielectric response of a setup comprised of a dielectric rod resonating between two conducting plates. The concept in such techniques is employing the dielectric rods as waveguides themselves. My setup is quite different and unique from this, as I had loaded dielectrics inside the waveguides to measure the attenuation coefficients or, for that matter, the change in the resonant profile of the cavity due to the presence of dielectric materials. In this paper the authors state that their dielectric resonators behave like cylindrical cavities oscillating in TE_{11} mode, which was the dominant guided mode for this resonator.

They established the relationship between the longitudinal fields both inside and outside the core region of the oscillator. This is an interesting technique as they refer to the same transcendental equations as those within the cylindrical cavities and other waveguide configurations.

In this ultrahigh Q dielectric rod based resonant cavity, the Q of a resonator is given by

$$Q = \omega \frac{\overline{W}}{\overline{P}} \tag{A18}$$

where $\overline{P}$ is the average power loss, $\overline{W}$ is the total time averaged energy stored, and ω is the resonant frequency of the oscillations.

$\overline{P}$ can be expressed as a sum of $\overline{P}_{\text{dielectric}} + \overline{P}_{\text{wall}}$

where $\overline{P}_{\text{dielectric}} = \frac{1}{2}\sigma_d \int_0^d \int_{Ad} E_1 \bullet E_1^* dA dz$, (A19)

σ_d is the conductivity of the dielectric material, E_1 is the electric field within the dielectric rod,

and $\overline{P}_{\text{wall}} = 2\left(\frac{R_s}{2}\right)\int_{Aw} (H_t \bullet H_t^*)\, dA$ (A20)

In Eq. (A20), R_s is the surface resistance of the walls of the resonator, H_t is the tangential component of the magnetic field along the metal wall and Aw is the area of each surface wall. The total time averaged electrical and magnetic energies stored inside the conductor is given by

$\overline{W}$ where

$$\overline{W} = 2\ \overline{W}_{\text{m}} = 2\ \overline{W}_{\text{e}} = \mu \int_V (H \bullet H^*) DV = \varepsilon \int_V (E \bullet E^*) DV\ . \qquad \text{(A21)}$$

Hence the Q value of the resonator then can easily be computed from the above equations and expressing them in the expression for Q given above.

In my experimental approach I have used a resonator in the form of a cylindrical resonant cavity in which the ohmic losses have been reduced and the energy stored is very high per cycle, thereby giving a very high quality factor for the resonant circuit. In previous sections of my thesis, I have mentioned the cavity perturbation techniques, along with the theory of perturbation due to inhomogeneous materials loaded inside the cavity.

10. M. W. Pospieszalski 's paper on TEM line microwave circuits: Marian W. Pospieszalski, "Cylindrical dielectric resonators and their application in TEM line microwave circuits," IEEE Trans. Microwave Theory Tech. **MTT-27** (3), (1979).

Summary of the paper:

The paper cited here has a similar concept as discussed before, in which the authors tried placing a low-loss high dielectric between two conducting plates and using it as a resonator. These types of materials do not readily lose their charges to the vicinity and possess high permittivity implying the charges are not that free to move. In simpler words, the fields are much contained inside a high *k* dielectric with low ohmic losses in their walls. A dielectric resonator composed of an isotropic cylindrical sample placed in between conducting walls was resonating in a TE mode. The conducting plates were perpendicular to the cylindrical axis of the resonator. Even though this paper does talk about the resonant modes and resonating frequency inside a dielectric resonator, it is a different geometrical concept from ours. In my work I have used a cylindrical waveguide with a perturbing dielectric load inside the resonator instead of having a cylindrical dielectric resonator placed in a rectangular waveguide.

11. C. N. Works' paper on resonant cavities for dielectric measurements: C. N. Works, "Resonant cavities for dielectric measurements," J. App. Phys. **18,** 605-612 (July 1947).

Summary of the paper:

This paper features a discussion over a method that was used in 1947, where the researchers used re-entrant cavities, which can be considered as a cylinder within a cylinder of two different diameters. These cavities were tunable as they had a tuning rod, and the sample, which was in the shape of a disk, was placed at the bottom floor of the inner cavities. The *Q* factor calculated for such cavities is given as:

$$Q = 4\pi\left(G/10\right)^{1/2} b \frac{\log_e(b/a)}{b/a+1}(f)^{1/2} \times 10^{-4} \qquad \text{(A22)}$$

where b is the inside radius of the outer conductor and a is the outer radius of the inner conductor. In order to calculate the dielectric response of their samples, the authors used an approach of measuring the capacitance between the two end posts of the cavities in resonance with a dielectric placed in between them. These techniques were very common in those days, but in the paper the authors fail to derive the expressions for both the real as well as the imaginary parts of the dielectric response. Hence it becomes difficult to understand the effect of the dielectric on the resonant frequencies as well as the Q value of the apparatus. As we know, the real part of the dielectric response tells us about the perturbation effects on the cavity resonance and the imaginary part tells us about the loss tangents of the cavity. Even though the authors tried to express the dissipation factor of the material by employing the change of voltages method, but the expression lacks the appreciation towards the change in the quality factors of the cavity.

12. S. Roberts' paper on measuring dielectric constant of materials in centimeter wavelength region: S. Roberts and A. Von Hippel, "A new method for measuring dielectric constant and loss in the range of centimeter waves," J. App. Phys. **17**, 610-616 (July 1946).

Summary of the paper:

This is an interesting paper as it discusses the limitations in the 1940's to the determination of the complex dielectric response of the materials under ultrahigh frequency. The authors in this paper demonstrate a new method of a hollow pipe, which required only a weak oscillator and small amounts of the dielectric material.

In this hollow-pipe method, the standing wave ratios (SWRs) technique was used to determine the complex dielectric response of the material. This technique uses the theory of the

capacitance of a condenser being proportional to the dielectric constant or the so-called permittivity of the material. The capacitance is defined by the relationship

$$C = \left(\varepsilon^* C_o\right) / \varepsilon_o \tag{A23}$$

where C_o is the capacitance of free space or the vacuum capacitance and ε_o is the vacuum permittivity, based on the standard electrical theories of building capacitance in a capacitor when subjected to a sinusoidal voltage where the current phase leads the voltage by (90^o- δ), It can be defined by

$$\mathrm{I} = j\omega CV = j\omega \frac{\left(C_o \varepsilon^* V\right)}{\varepsilon_o} \tag{A24}$$

where ε^* is a complex response of the dielectric and has a real and imaginary part in it where the real part is involved in the charging current density and the imaginary part (which is also a lossy part) is responsible for the loss in the charge current density when the medium is subjected to the periodic electromagnetic field. Hence the dielectric response is then given by

$$\varepsilon^* = \varepsilon' - j\varepsilon'' \ . \tag{A25}$$

The loss tangent, which is the ratio of the loss current to the charging current, is given by taking the ratio of the imaginary part to the real part of the dielectric constant:

$$\tan\delta = \frac{\varepsilon''}{\varepsilon'} . \tag{A26}$$

The measurement approach used was such that the electromagnetic fields were enclosed in a rectangular shaped hollow pipe which is closed on its two ends by a reflecting conductor and a transmitter of the electromagnetic radiations. This waveguide geometry sets up a standing wave pattern and the dielectric is inserted in the closed end of the pipe, thereby filling a certain fraction of the volume due to its height *d*. The dielectric material is responsible for reflecting/transmitting

the electromagnetic radiations back to the detector and the electric field strengths are measures by measuring the intensity of the nodes as well as the antinodes. As an example, by taking the ratio of E_{min}/E_{max} and by calculating the terminal impedance of the line from the voltage ratios V_{min}/V_{max}, the authors tried to calculate ε' & ε''. It is an interesting technique, but this technique is not going to work for the anisotropic material which will have different response in different loadings and will produce a lot of noise in the SWRs.

13. Walter Gordy' s paper on microwave spectroscopy: Walter Gordy, "Microwave Spectroscopy," Rev. Mod. Phys. **20 (**4), (1948).

Summary of the paper:

This paper is useful for those who wish to understand the developmental stages in microwave spectroscopy during World War II. It focuses more on the electronics and their properties at the time of their development. The author in this survey manuscript starts with asserting the superiority of microwave spectroscopy in comparison to optical spectroscopy. In those days, microwave spectroscopy became favored over optical spectroscopy because its resolution was far higher than that of infra-red resolution spectroscopy. In this survey the author has summarized the instruments and the experimental methods that were developed during those days. The paper discusses the development of waveguides and the associated components with their attenuation coefficients. The author even mentions the absorption cells that were developed out of the waveguides to study the millimeter-wave region.

In the later section of the paper the author has listed various sources of microwaves including magnetrons and klystrons, as well as their associated power supplies. There is a detailed electronics bibliography in this section of the manuscript listing references dealing with the operations of microwave sources and the associated noise and power attenuation.

In the third section of the paper the author has detailed the working principles of detection systems such as the superheterodyne receivers, crystal video receivers and the associated modulation methods to avoid the excessive low frequency noise which is generated when crystals are used to detect the powers above the microwatt range. These methods were superior to other methods like infra-red or optical dispersions to measure the intensity of the absorption lines in molecules. In order to read the theoretical analysis of the effects of different forms and frequencies of modulation on the line shape, the reader can refer to Townes and Schalow's *Microwave Spectroscopy* or R. Karplus [Phys. Rev. *73*, 1027 (1948)] where the terms like weak and strong modulation of the spectroscopy lines have been well defined. For those interested in understanding the electronics of various microwave devices, it will be interesting to note how different types of other modulations of the signals are produced, like the sinusoidal and the square wave modulations and their respective applications. Microwave spectroscopy is an interesting technique for understanding the quantum mechanical structures of various types of light as well as heavy molecules. It is beyond the scope of this thesis to discuss into details of microwave electronics at large. It is simply necessary to mention that in our experimental studies, I have used a crystal source for microwave generation and even used crystal diodes to detect the reflection or transmission response of the system.

14. B. Bleaney's paper on cavity resonators and measurements with centimeter electromagnetic waves: B. Bleaney, J. H. N. Loubser and R. P. Penrose, "Cavity Resonators for Measurements with Centimeter Electromagnetic Waves," Proc. Phys. Soc., **59,** 185-199 (1946).

Summary of the paper:

An indirect effect due to simultaneous resonance in two different modes is discussed in relation to the measurement of absorption by resonant cavities. The author in this paper discusses

several schemes of waveguide coupling with the resonators, either through probes, loops or holes. Emphasis has been made over the coupling in H_o mode of the waveguides to the resonant cavities. The author(s) have studied in this work the effect due to simultaneous resonance in two different modes in relation to the measurement of absorption by resonant cavities. The authors have also measured the temperature coefficient of the dielectric constant of six non-polar liquids by introducing these liquids inside the resonators. In hollow resonators loss of energy by radiation is negligible, and the dissipation in resistive loss is very small, since these resonators are typically well-polished and have uniform surfaces inside the resonators. The resonators are quite different from the lump circuits, as in these designs the concepts of current and voltage are replaced by those of magnetic and electric field, and the concept of impedance is therefore only of subsidiary importance. Instead, properties like the dielectric response as well as magnetic susceptibility play an important role.

The hollow resonators can be divided into two broad categories: coaxial lines and wave-guide (cavity) resonators. The only difference between the two is that in coaxial resonators the waves of normal types (i.e. those that oscillate normal to the surface) travel with the same velocity as those in the free space, and the two successive points of resonance on those particular waves are a half-wavelength apart. So in order to ensure that only normal waves propagate through these transmission lines, the diameter of the outer cylinder should be smaller than the half-wavelengths. Transmission lines exhibit low quality factors. Waveguides and cavity resonators offer a possible solution to the sensitive resonances of electromagnetic radiations. Even though in a waveguide there can be an unlimited number of modes inside, by adjusting the geometries of the iris hole couplers, the input, the output feeder holes on the coupling

waveguides and the effective volume of the cylindrical cavities, the number of fundamental modes that can be energized inside a resonant cavity can be limited.

15. J. H. Van Vleck's paper on absorption of EM radiation by oxygen molecules: J. H. Van Vleck, "The absorption of microwaves by oxygen," Phys. Rev. **71** (7), (December 1946).

Summary of the paper:

Even though oxygen is electrically non-polar, oxygen gas absorbs microwaves because the magnetic moment of oxygen interacts with the electromagnetic fields. Van Vleck and Weiskopf did a very nice fundamental study on the collision broadening of the molecules and their detection by the spectral line shapes whose width at half power maxima (WHPM) also gives us information over the absorption of microwaves by these molecules. Oxygen molecules are paramagnetic, implying that they possess permanent magnetic dipole moment which consequently absorbs microwaves, since transitions for magnetic dipole radiations are permitted and they resonate in the microwave region.

The general quantum-mechanical expression for the absorption co-efficient is given by

$$\gamma = 10^6 \left(Log_{10} e\right)\left(\frac{8\pi^3 \nu N}{3hc}\right)\frac{\sum_{i,j}\left\{\left|\mu_{i,j}\right|^2 f(\nu_{i,j},\nu)\right\} e^{-E_j/kT}}{\sum_j e^{-E_j/kT}} \qquad \text{(A27)}$$

in which *f* is the structure factor which determines the typical shape of the resonant profile and near resonance can be simply expressed as

$$f(\nu_{i,j},\nu) = \frac{1}{\pi}\left[\frac{\Delta\nu}{(\nu_{i,j}-\nu)^2 + \Delta\nu^2}\right] \quad . \qquad \text{(A28)}$$

In the above equation, $\nu_{i,j}$ is the frequency of the corresponding spectral line and ν is the frequency of the incident radiation. In other words, $\nu_{i,j}$ can be obtained from the WHPM. In case

of a non-resonant or diagonal part of the absorption, even the Debye model can be used, in which the expression for absorption coefficient is given by

$$\gamma = 10^6 \left(Log_{10} e\right)\left(\frac{8\pi^2 \nu^2 N\mu^2}{3kTc}\right)\frac{\Delta\nu}{\nu^2 + \Delta\nu^2} \quad . \tag{A29}$$

So from Eq. (A29) the numerical value can be calculated keeping in mind that one-third of the mean average total moment is of diagonal variety and two-thirds is consumed by the non-diagonal part. And then at 293°K and 76 cm of mercury pressure, the numerical value of the absorption coefficient for the oxygen molecules becomes

$$\gamma = 0.34\left(\frac{\nu}{c}\right)^2 \left[\left[\frac{\Delta\nu/c}{(\nu/c)^2 + (\Delta\nu/c)^2}\right]\right] db/km. \tag{A30}$$

The equation above gives the principal part of the oxygen absorption if the wavelength is greater than about 1.5 cm. The theory gets complicated if we need to calculate the dependency of the absorption coefficient on the pressure of the molecules as well as the wavelength and hence keep the numerical analysis simple. This relation is approximately the same as the one provided by R. G. Steefes in his experimental observation of the absorption of atmospheric constituents of gases at centimeter wavelength and can be expressed in terms of Q values of the cavity as shown below:

$$\alpha = (Q_L^{-1} - Q_C^{-1})\,\pi/\lambda \tag{A31}$$

16. W. D. Hershberger's paper on absorption of microwaves by gases: W. D. Hershberger, "The absorption of microwaves by gases," J. App. Phys, **17** (June 1946).

Summary of the paper:

The author reflects the experimental as well as the theoretical calculations that had been performed to date with ammonia. In those days, the researchers had extensively researched

complex molecule ammonia and studied the absorption characteristics of microwaves of 1 cm (~ 24GHz) wavelength. The author investigated whether any other gas molecules exhibited similar characteristics of absorption of microwaves in that comparable wavelength, and found that approximately 14 gas molecules exhibited almost similar characteristics whose references have been provided in this reference of the paper. In addition, the dielectric response of these gas molecules at room temperature and pressure of 1 atm was measured using a rectangular waveguide system set up with a wave meter. Using the absorption coefficient vs. pressure curve, the authors calculated the maximum value attained by the absorption coefficient. They found that the plane waves (non-polarized) having a wavelength of 1.25 cm will be attenuated to *1/e* of initial power after traversing a layer of ammonia 1.2 cm thick. This experimental approach might not be directly related to our setup of a cylindrical cavity resonator. But the concept of attenuation as well as the absorption coefficient can be applied in a similar way by considering the loaded and unloaded *Q* factor response of the cavity. Cleeton and Williams found in 1934 that for ammonia the absorption coefficient of the power in ammonia is expressed by:

$$\alpha_p = -\left(\left[1 - (\lambda/2b)^2 \right]^{1/2} \log P / P_o \right) / L \qquad \text{(A32)}$$

In this expression λ is the wavelength inside the gas and can be measured using the wave meter techniques. P/P_o is the ratio of the power attenuated and can be measured using the standard oscilloscope signal and its attenuation or even by measuring the V_{min}/V_{max} ratios. And L is the length of the waveguide, with *b* being the width of the waveguide.

17. H. R. L. Lamont, "Atmospheric Absorption of Millimeter Waves," Proc. Phys. Soc. (London) **61**, 562-569 (July 1948).

Summary of the paper:

During the days of World War II, all sorts of measurements were being made to

determine the attenuation of electromagnetic waves in the region of 5 mm wavelengths. The authors have measured the absorption coefficient of high frequency microwaves in atmospheric oxygen over the path length of about 2 Km and have related the field strength of electromagnetic radiations in a dry environment through oxygen over a sea level of about 2Km. They found their results in agreement with those of Van Vleck, Weiskopf, and others like Penrose and Townes and Schalow's theoretical developments done in those days. The researchers used the superheterodyne receivers and transmitters with good sensitivity selectively to particular wavelengths between 6.34 mm and 4.48 mm. To understand the details of superheterodyne receivers and transmitters, the reader can refer to any advanced engineering textbook [26]. The basic principle rests in tuning to an intermediate frequency to match the impedance of receivers. Depending upon the bandwidth to be used for propagation of the electromagnetic radiations, selective filters and mixers were used to mix all the signals of the local oscillator within the receiver with the entire incoming signal from the RF source.
From their experimental results the authors established a relationship between the electrical field strengths of the propagating EM radiations through the atmosphere over a distance *d,* which can be summarized by Eq. (A33) as well as by the illustration shown below.

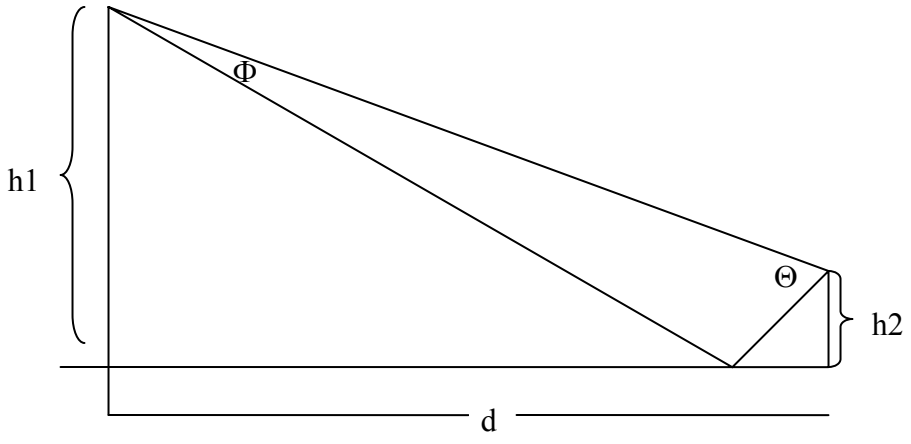

FIG. 60. Field Strength mapped to trigonometric relationships.

The illustration above simplifies using standard trigonometric procedures to explain the effective relationships between the electric field strength varying with distance as well as height. The authors used the following equation

$$If \;\; d >> h_1 \quad then \;\; \Theta = 2h_1/d \,; \Phi = 2h_2/d \tag{A33}$$

to determine that the field strength varies as

$$E = \left(E_o/d\right)e^{-\alpha d} \tag{A34}$$

The electric field strength is measured in decibels relative to an arbitrary level for known values of *d* by putting the above form in logarithmic form. The authors have measured these values under different atmospheric conditions and have even tried to calculate the percentage errors caused by both impurities due to relative humidity and by the equipment noise.

ENDNOTES

[1] J. A. Roberts *et al.*, "Electromagnetic wave properties of polymer blends of single wall carbon nanotubes using a resonant microwave cavity as a probe," J. Appl. Phys. **95** (8), 4352, (2004)

[2] S. Ijima, Nature **354,** 56 (1991).

[3] K. Tanaka, T. Yamabe, and K. Fukui, *The Science and Technology of Carbon Nanotubes* (Elsevier Publications, Amsterdam, 1999), pp. 2-3.

[4] Ibid., pp. 42-43.

[5] Ibid., p. 46.

[6] MS Visualizer 4.0, A molecular dynamic software, (Accelrys Systems Inc.,) used for simulation.

[7] K. H. Hong, "Microwave Properties of Liquids and Solids Using a Resonant Microwave Cavity as a Probe," Ph. D. dissertation, University of North Texas, 1974; "Microwave Properties of Liquids and Solids Using a Microwave Cavity as a Probe" (with K. H. Hong), J. Appl. Phys. **45**, 2452-2456 (1974).

[8] Mildred S. Dresselhaus *et al*., "Introduction to Carbon Materials," in Thomas W. Ebbesson, *Carbon Nanotubes Preparation and Properties* (CRC Press inc., Cleveland Ohio, 1997), pp.1-29.

[9] Ibid.

[10] Ibid.

[11] David Tomanek, "Carbon Nanotubes - A Time Line," < http://www.pa.msu.edu/cmp/csc/nttimeline.html>, accessed Sept. 23, 2006, University of North Texas.

[12] R. Saito, G. Dresselhaus, and M. S. Dresselhaus, *Physical Properties of Carbon Nanotubes* (Imperial College Press, London, 1999), Ch 3. pp. 35-53; P.M. Ajayan, *Carbon Nanotubes: Preparation and Properties* (CRC Press Inc., Cleveland Ohio, 1997), Ch. 3, pp. 111-126; S. Amelinckx, A. Lucas, and P. Lambin, *The Science and Technology of Carbon Nanotubes* (Elsevier Science Ltd., Amsterdam, 1999), Ch 3. pp. 14-28.

[13] Saito, Dresselhaus, and Dresselhaus, pp. 35-53.

[14] Ijima, 56.

[15] Motoo Yumura, "Synthesis and Purification of Multiwalled and Single Walled Carbon Nanotubes," in K. Tanaka, T. Yamabe, K. Fukui, *The Science and Technology of Carbon Nanotubes* (Elsevier Science Ltd., Kindlington, Oxford OX5 1GB, UK, 1999), pp. 2-11; R. Saito, G. Dresselhaus, and M. S. Dresselhaus, "Synthesis of Carbon Nanotubes," in R. Saito, G.

Dresselhaus, M S Dresselhaus, *Physical Properties of Carbon Nanotubes*, (Imperial College Press, London, 1999), pp. 73-82; Thomas W. Ebbesson, "Production and Purification of Carbon Nanotubes," in Thomas W. Ebbesson, *Carbon Nanotubes Preparation and Properties* (CRC Press Inc., USA, 1997), pp. 139-153; Eugene G. Gamaly, "Growth Mechanism of Carbon Nanotubes," in Thomas W. Ebbesson, *Carbon Nanotubes Preparation and Properties* (CRC Press Inc., USA, 1997), pp. 163-185; Peter J. F. Harris, "Synthesis: Preparation methods, growth mechanisms and processing techniques," in Peter J.F. Harris, *Carbon Nanotubes and Related Structures: New Materials for the Twenty First Century* (The Press Syndicate of The University of Cambridge, Cambridge, UK, 1999), pp. 16-52.

[16] S. Amelinckx, A. Lucas, and P. Lambini, "Electron Diffraction and Microscopy of Nanotubes," Rep. Prog. Phys. **62**, 1471-1524, (1999).

[17] Saito, Dresselhaus, and Dresselhaus, pp. 35-53

[18] Ibid.

[19] Ibid.

[20] Ibid.

[21] A. Anand *et al.*, "Select Gas Absorption in Carbon Nanotubes, Loading a resonant cavity to sense airborne toxin gases," Nucl. Instrum. Meth. in Physics Research B **241**, 511-516 (2005).

[22] Ibid.

[23] Y. Ye *et al.*, "Hydrogen adsorption and cohesive energy of single walled carbon nanotubes," Appl. Phys. Lett. **74,** 16 (1999).

[24] Saito, Dresselhaus, and Dresselhaus, pp. 35-53; J. E. Schindall *et al.*, "Researchers fired up over new battery," MIT News Office, Correspondent: Deborah Halber, Website: < http://web.mit.edu/newsoffice/2006/batteries-0208.html>, published Feb. 8, 2006, accessed Feb. 26, 2007.

[25] *Radar Circuit Analysis*, Air Force radar manual (Washington, 1950), pp. 2-65.

[26] Ibid.; Wikipedia under GNU License, http://en.wikipedia.org/wiki/Bandwidth, accessed Jan 20, 2007 at University of North Texas.

[27] F. Manolache and D. D. Sandu, "Quantum effects modeled by electric fields" Phys Rev. A **49** (4), 2318 (1994).

[28] J.C. Slater, "Microwave Electronics," Rev. Mod. Phys. **18,** 441-512, (1946)

[29] Wikipedia under GNU License, http://en.wikipedia.org/wiki/Bandwidth, accessed Jan 20, 2007 at University of North Texas.

[30] A. F. Harvey, *Microwave Engineeering* (Academic Press, 1963).

[31] *Radar Circuit Analysis*, U.S. Air Force radar manual (Washington, 1950), Ch. 10.

[32] C. G. Montgomery, *Technique of Microwave Measurement* (McGraw Hill, NY-London, 1947), p. 294.

[33] D.J. Griffiths, "Guided Waves," in *Introduction to Electrodynamics* (Prentice Hall, upper saddle river NJ, 1999) Ch.9.5 p.406.

[34] A. F. Harvey, pp.196-199

[35] C. G. Montgomery, p. 294.

[36] Radar Circuit Analysis, Ch. 10.

[37] C. G. Montgomery,.p. 294.

[38] J. N. Dahiya, Ph. D. dissertation, University of North Texas Library, 1980, pp. 13-15

[39] V. Prakash and J. A. Roberts, "Perturbation of a Resonant Cavity by select Alcohol Vapors," J. Microwave Power and Electromag. Energy **21 (1)**, 45-50 (1986).

[40] C.G. Montgomery, Technique of Microwave Measurements (McGraw-Hill Book company, Inc., NY-London, 1947), Ch. 5, p. 298

[41] A. F. Harvey, *Microwave Engineering* (Acad. Press, 1963), Ch.5, p. 196.

[42] J. C. Slater, 441-512

[43] G. L. Ragan, *Microwave Transmission Circuits*, *Vol. 9* (M.I.T. Radiation Laboratory, Cambridge, MA, 1948) p. 655.

[44] D. P. Pritzkan, G. Bowden, A. Menegat, and R. H. Siemann, *Experimental Design to Study RF Pulsed Heating*, SLAC-PUB-8070 (1999).

[45] A. Anand *et al.*, 511-516.

[46] E. Bourdel and D. Pasquet, "Measurement of the moisture content with a cylindrical resonant cavity," IEEE Trans. Instrum. Meas. **49** (5), (2000).

[47] C. K. Jen, "A method for measuring the constant dielectric constant of gases at microwave frequencies by using a resonant cavity," J. App. Phys.**19**, 649 (1948); J.F. Rouleau *et al*., "Investigation of a microwave differential cavity resonator device for the measurement of humidity in gases," Rev. Sci. Instrum **70** (9)**,** (1999).

[48] CRC Handbook for Chemistry and Physics, (1992).

[49] Microwave network analyzer purchased through Naval Grant number – ONR-N00013-03-0880

[50] J. N. Dahiya, pp. 13-15; V. Prakash and J. A. Roberts, 45-50; K. H. Hong, Ph. D. dissertation; J. Appl. Phys.

[51] Pine *et al.*, *Oranic Chemistry* 2nd ed. (McGraw Hill, Cleveland, 1964); V. Ploeg *et al.*, J. Chem. Phys. **94**, 5650 (1991).

[52] Jorengsen *et al.*, J. Am. Chem. Phys. **106**, 6638 (1984); E. Jayne Wallace and Mark S. P. Sansom, "Carbon nanotube/detergent interactions via coarse-grained molecular dynamics," Nanoletters (in press); Jijun Zhao, "Gas molecules adsorption on carbon nanotubes," Mat. Res. Soc. Symp. Proc. **633**, A13.48.1 (2001).

[53] S. E. Weber, S. Talapatra, C. Journet, A. Zambano, and A. D. Migone, "Determination of the binding energy of methane on single-walled carbon nanotube bundles," Phys. Rev. B. **61**, (19) (2000).

[54] Christopher Matranga, L. Chen, Bradley Bockrath, and J. K. Johnson, "Displacement of CO2, by Xe in single walled carbon nanotube bundles," Phys. Rev. B **70** (165416), (2004).

[55] M. Cinke, Jing Li, Charles W. Bauschlicher Jr., Alessandra Ricca, and M. Meyyappan, "CO2 adsorption in single-walled carbon nanotubes," Chem. Phys. Lett. **376**, 761 (2003).

[56] Ibid.

[57] J. N. Dahiya, S. K. Jani, and J. A. Roberts, "Phase transition studies in polar and nonpolar liquids at microwave frequencies," J. Chem. Phys. **74** (6), (1991).

[58] J. Huot and T. K. Bose, "Experimental determination of the dielectric virial coefficients of atomic gases as a function of temperature," J. Chem. Phys. **95** (4), (1991); Lesse Jensen, Per-Olof Astrand, Anders Osted, J. Kongsted, and K. V. Mikkelsen, "Polarizability of molecular clusters as calculated by a dipole interaction model," J. Chem. Phys. **116** (10) (2002).

[59] Lesse Jensen, O. H. Schmidt, K. V. Mikkelsen , and Per-Olof Astrand, "Static and frequency-dependent polarizability tensors for carbon nanotubes," J. Chem. Phys. **104**, 10462 (2000).

[60] Ibid.

[61] Lesse Jensen, O. H. Schmidt, K. V. Mikkelsen , and Per-Olof Astrand, "Static and frequency-dependent polarizability tensors for carbon nanotubes," J.Chem. Phys. **104**, 10462 (2000); Lorin X. Benedict, S. G. Louie, and M. L. Cohen, "Static polarizabilities of single walled carbon nanotubes," Phys. Rev. B. **52** (11), (1994); S. Sivasubramanian, A. Widom, and Y. N. Srivastava, "The Claussius-Mossotti Phase Transition in Polar Liquids," arXiv:cond-mat/0301613v1, (2003)

[62] Lorin X. Benedict, S. G. Louie, and M. L. Cohen.

[63] S. Sivasubramanian, A. Widom, and Y. N. Srivastava.

[64] Francisco Torrens, "Effect of type, size, and deformation on the polarizability of carbon nanotubes from atomic increments," Nanotechnology **15**, S259-264, (2004).

[65] Ibid.

[66] E. S. Snow, F. K. Perkins, E. J.Houser, S. C. Badescu, and T. L. Reinecke, "Chemical detection with a nanotube capacitor," Science **307** (2005).

[67] Ibid.

[68] M. Arab, F. Picaud, M. Devel, C. Ramseyer, and C. Girardet, "Molecular Selectivity due to adsorption properties in nanotubes," Phys. Rev. B. **69**, 165401 (2004); R. Langlet, M. Arab, F. Picaud, M. Devel, and C. Girardet, "Influence of molecular adsorption on the dielectric properties of a single walled nanotube: A model sensor," J. Chem. Phys. **121** (19), (2004); M.Grujicic, G. Cao, and W. N. Roy, "A computational analysis of the carbon nanotube based resonant circuit sensors," Applied Surface Science **229**, 316-323 (2004).

[69] Robert A Freitas Jr. Nanomedicine http://www.foresight.org/Nanomedicine/ accessed : December 12th 2006.

[70] Congressional testimony, "Threat of Terrorism to the United States," May 2001, http://www.fbi.gov/congress/congress01/freeh051001.htm accessed January 2006.

[71] "A Military Guide to Terrorism in the Twenty-First Century," Aug. 15, 2005 <http://www.fas.org/irp/threat/terrorism/index.html>, accessed January 2006.

[72] J. A. Roberts *et al.*

[73] K. H. Hong, Ph. D. dissertation; J. Appl. Phys.

[74] Robert A Freitas Jr.

[75] Zeke Insepov, Dieter Wolf, and Ahmed Hassanein, "Nanopumping using carbon nanotubes," Nanoletters, **6** (9), 1893 (2006).

[76] Robert A Freitas Jr.

[77] [65] Zeke Insepov, Dieter Wolf, and Ahmed Hassanein, "Nanopumping using carbon nanotubes," Nanoletters, **6** (9), 1893 (2006); J. Van Bladel, *Electromagnetic Fields* (McGraw Hill Company, NY-London, 1964), Ch.10; C. H.Townes and A. L. Schalow, *Microwave Spectroscopy* (Dover Publications, NY, 1975) Ch. 14, p. 378; *Guide for the Selection of Chemical Agent and Toxic Industrial Material Detection Equipment for Emergency First Responders*, U.S. Department of Justice and Department of Defense Technical Information Center Report (Washington, 2000); Jason D. Sternhagen *et al.*, "A Novel Acoustic Gas and Temperature Sensor," IEEE Sensors Journal, **2** (4), (2002); M. Binhack *et al*., "Modeling of

Double Saw Resonator Remote Sensor," IEEE 1416-2003 Ultrasonic Symposium, (2003); Ivan D. Avramov, "The RF-powered surface wave sensor oscillator – a successful alternative to passive wireless sensing," IEEE Transactions on Ultrasonic, Ferroelectrics, and Frequency Control, **51** (9), (2004); Edward J. Staples, "Detection of Volatile Organic Compounds in Gasoline and Diesel Using the zNose, http://www.estcal.com/TechPapers/Industrial/GasolineEvaluation.doc accessed Jan 23, 2005.

[78] Insepov, Wolf, and Hassanein.

[79] Robert A Freitas Jr.

REFERENCE LIST

Ajayan, P.M. *Carbon Nanotubes: Preparation and Properties* (CRC Press Inc., Cleveland, 1997), Ch. 3, pp. 111-126.

Amelinckx, S., Lucas, A. and Lambini, P. *The Science and Technology of Carbon Nanotubes* (Elsevier Science Ltd., Amsterdam, 1999), Ch 3. pp. 14-28.

Amelinckx, S., Lucas, A. and Lambini, P. "Electron Diffraction and Microscopy of Nanotubes," *Rep. Prog. Phys.* **62**, 1471-1524, (1999).

Anand *et al.* "Select Gas Absoprtion in Carbon Nanotubes, Loading a Resonant Cavity to Sense Airborne Toxin Gases," *Nucl. Instrum. Meth. in Physics Research B* **241**, 511-516 (2005).

Arab, M., Picaud, F., Devel, M., Ramseyer, C. and Girardet, C. "Molecular Selectivity Due to Adsorption Properties in Nanotubes," *Phys. Rev. B* **69**, 165401 (2004).

Avramov, I.D. "The RF-powered Surface Wave Sensor Oscillator – A Successful Alternative to Passive Wireless Sensing," *IEEE Transactions on Ultrasonic, Ferroelectrics, and Frequency Control*, **51** (9), (2004).

Bandwidth. Wikipedia, http://en.wikipedia.org/wiki/Bandwidth accessed 20 January 2007.

Benedict, L.X., Louie, S.G. and Cohen, M.L. "Static Polarizabilities of Single Walled Carbon Nanotubes," *Phys. Rev. B.* **52** (11), (1994).

Binhack *et al*. "Modeling of Double Saw Resonator Remote Sensor," IEEE 1416-2003 Ultrasonic Symposium, (2003).

Bleaney, B., Loubser, J.H.N. and Penrose, R.P. "Cavity Resonators for Measurements with Centimeter Electromagnetic Waves," *Proc. Phys. Soc.* **59** 185-199 (1946).

Bourdel, E. and Pasquet, D. "Measurement of the Moisture Content with a Cylindrical Resonant Cavity," *IEEE Trans. Instrum. Meas*. **49** (5), (2000).

Bussey, H.E. "Measurement of RF Properties of Materials: A Survey," *Proceedings of the IEEE*, **55** (6), (1967).

Cinke, M., Li, J., Bauschlicher Jr., C.W., Ricca, A. and Meyyappan, M. "CO_2 Adsorption in Single-Walled Carbon Nanotubes," *Chem. Phys. Lett*. **376**, 761 (2003).

Cohn S.B. and Kelly, K.C. "Microwave Measurement of High-Dielectric Constant Materials," *IEEE Trans. Microwave Theory Tech*. **MTT-14** (9), (1966).

CRC Handbook for Chemistry and Physics, Ed 72, (Amsterdam, 1993).

Dahiya, J.N., dissertation, University of North Texas Library, 1980, pp. 13-15.

Dahiya, J.N., Jani, S.K. and Roberts, J.A. "Phase Transition Studies in Polar and Nonpolar Liquids at Microwave Rrequencies," *J. Chem. Phys*. **74** (6), (1981).

Dresselhaus *et al*. "Introduction to Carbon Materials," in Thomas W. Ebbesson, *Carbon Nanotubes Preparation and Properties* (CRC Press Inc., USA, 1997), pp.1-29.

Ebbesson, T.W. "Production and Purification of Carbon Nanotubes," in Thomas W. Ebbesson, *Carbon Nanotubes Preparation and Properties* (CRC Press Inc., USA, 1997), pp. 139-153.

Edwards, D.H., Hooper, G. and Collyer, A.A. "Ionization Measurement in Reactive Shock and Detonation Waves Using Microwave Techniques," *J. Phys. D* **4**, 854 (1971).

Freitas Jr., R.A. Nanomedicine. http://www.foresight.org/Nanomedicine/ accessed 12 December 2006.

Gamaly, E.G. "Growth Mechanism of Carbon Nanotubes," in Thomas W. Ebbesson, *Carbon Nanotubes Preparation and Properties* (CRC Press Inc., USA, 1997), pp. 163-185.

Gordy, W. "Microwave Spectroscopy," *Rev. Mod. Phys*. **20 (**4), (1948).

Griffiths, D.J. "Guided Waves," in *Introduction to Electrodynamics* (Prentice Halls, Upper Saddle River , NJ, 1999) Ch.9.5, p. 406.

Grujicic, M., Cao, G. and Roy, W.N. "A Computational Analysis of the Carbon Nanotube Based Resonant Circuit Sensors," *Applied Surface Science* **229**, 316-323 (2004).

Guide for the Selection of Chemical Agent and Toxic Industrial Material Detection Equipment for Emergency First Responders, U.S. Department of Justice and Department of Defense Technical Information Center Report (Washington, 2000).

Harris, P.J.F. "Synthesis: Preparation Methods, Growth Mechanisms and Processing Techniques," in Peter J. F. Harris, *Carbon Nanotubes and Related Structures: New Materials for the Twenty First Century* (Press Syndicate of the University of Cambridge, Cambridge, UK, 1999), pp. 16-52.

Harvey, A.F. *Microwave Engineeering* (Academic Press, 1963)), Ch.5, p. 196.

Hershberger, W.D. "The Absorption of Microwaves by Gases," *J. App. Phys*, **17** (June 1946).

Hong, K.H. *Microwave Properties of Liquids and Solids Using a Resonant Microwave Cavity as a Probe*, dissertation, University of North Texas, 1974.

Hong *et al* ."Microwave Properties of Liquids and Solids Using a Microwave Cavity as a Probe" *J. Appl. Phys*. **45**, 2452-2456 (1974).

Huot J. and Bose, T.K. "Experimental Determination of the Dielectric Virial Coefficients of Atomic Gases as a Function of Temperature," *J. Chem. Phys*. **95** (4), (1991).

Ijima, S. *Nature* **354,** 56 (1991).

Insepov, Z., Wolf, D. and Hassanein, A. "Nanopumping using Carbon Nanotubes," *Nanoletters* **6** (9), 1893 (2006).

Jen, C.K. "A Method for Measuring the Constant Dielectric Constant of Gases at Microwave Frequencies by Using a Resonant Cavity," *J. App. Phys*. **19**, 649 (1948).

Jensen, L., Astrand, P., Osted, A., Kongsted, J. and Mikkelsen, K.V. "Polarizability of Molecular Clusters as Calculated by a Dipole Interaction Model," *J. Chem. Phys*. **116** (10) (2002).

Jensen, L., Schmidt, O.H., Mikkelsen, K.V. and Astrand, P. "Static and Frequency-Dependent Polarizability Tensors for Carbon Nanotubes," *J. Chem. Phys*. **104**, 10462 (2000).

Jorengsen *et al.*, *J. Am. Chem. Phys*. **106**, 6638 (1984).

Kobayashi Y. and Katoh, M. "Microwave Measurement of Dielectric Properties of Low-loss Materials by the Dielectric Rod Resonator Method," *IEEE Trans. Microwave Theory Tech*. **MTT-33** (7), (1985).

Kraszewski, A.W. You, T.S. and Nelson, S.O. "Microwave Resonator Technique for Moisture Content Determination in Single Soybean Seeds," *IEEE Trans. Instrum. Meas.* **38** (1), (1989).

Lamont, H.R.L. "Atmospheric Absorption of Millimeter Waves," *Proc. Phys. Soc*. (London), **61**, 562-569 (July 1948).

Langlet, M., Arab, F., Picaud, M. and Girardet, C. "Influence of Molecular Adsorption on the Dielectric Properties of a Single Walled Nanotube: A Model Sensor," *J. Chem. Phys*. **121** (19), (2004).

Manolache, F. and Sandu, D.D. "Quantum Effects Modeled by Electric Fields" *Phys. Rev. A* **49** (4), 2318 (1994).

Matranga, C., Chen, L., Bockrath, B. and Johnson, J.K. "Displacement of CO_2, by Xe in Single Walled Carbon Nanotube Bundles," *Phys. Rev. B* **70,** 165416, (2004).

"A Military Guide to Terrorism in the Twenty-First Century," Aug. 15, 2005, http://www.fas.org/irp/threat/terrorism/index.html accessed 5 January 2006.

Montgomery, C.G. *Technique of Microwave Measurement* (McGraw Hill, Cleveland, 1947), p. 294.

Pine *et al.*, *Organic Chemistry* 2nd ed. (McGraw Hill, Cleveland, 1964).

Ploeg *et al.*, *J. Chem. Phys*. **94**, 5650 (1991).

Pospieszalski, M.W. "Cylindrical Dielectric Resonators and Their Application in TEM Line Microwave Circuits," *IEEE Trans. Microwave Theory Tech*. **MTT-27** (3), (1979).

Prakash, V. and Roberts, J.A. "Perturbation of a Resonant Cavity by Select Alcohol Vapors," *J. Microwave Power and Electromag. Energy* **21 (1)**, 45-50 (1986).

Pritzkan, D.P., Bowden, G., Menegat, A. and Siemann, R.H. *Experimental Design to Study RF Pulsed Heating*, SLAC-PUB-8070 (1999).

Radar Circuit Analysis, U.S. Air Force Radar Manual (Washington, 1950).

Ragan, G.L. *Microwave Transmission Circuits*, Vol. 9 (M.I.T. Radiation Laboratory, Cambridge, MA, 1948), p. 655.

Roberts *et al.*, "Electromagnetic Wave Properties of Polymer Blends of Single Wall Carbon Nanotubes Using a Resonant Microwave Cavity as a Probe," *J. App. Phys*. **95** (8), 4352 (2004).

Roberts, S. and Von Hippel, A. "A New Method for Measuring Dielectric Constant and Loss in the Range of Centimeter Waves," *J. App. Phys*. **17**, 610-616 (July 1946).

Rouleau, J.F., Goyette, J., Bose, T.K. and Frechette, M.F. "Investigation of a Microwave Differential Cavity Resonator Device for the Measurement of Humidity in Gases," *Rev. Sci. Instrum*. **70** (9), (1999).

Saito, R., Dresselhaus, G. and Dresselhaus, M.S. "Synthesis of Carbon Nanotubes," in R. Saito, G. Dresselhaus, M. S. Dresselhaus, *Physical Properties of Carbon Nanotubes*, (Imperial College Press, London, 1999), pp. 73-82.

Saito, R., Dresselhaus, G. and Dresselhaus, M.S. *Physical Properties of Carbon Nanotubes* (Imperial College Press, London, 1999), Ch 3. pp. 35-53.

Schindall *et al.*, "Researchers Fired Up over New Battery," MIT News Office, Correspondent: Deborah Halber, Feb. 8, 2006, http://web.mit.edu/newsoffice/2006/batteries-0208.html accessed 26 February 2007.

Shimabukuro, F.I. and Yeh, C. "Attenuation Measurement of Very Low Loss Dielectric Waveguides by the Cavity Resonator Methods Applicable in the Millimeter/Submillimeter Wavelength Range," *IEEE Trans. Microwave Theory Tech*. **36** (7), (1988).

Slater, J.C. "Microwave Electronics," *Rev. Mod. Phys*. **441** (1941).

Snow, E.S., Perkins, F.K., Houser, E.J., Badescu, S.C. and Reinecke, T.L. "Chemical Detection with a Nanotube Capacitor," *Science* **307** (2005).

Staples, E.J. "Detection of Volatile Organic Compounds in Gasoline and Diesel Using the zNose," http://www.estcal.com/TechPapers/Industrial/GasolineEvaluation.doc accessed 23 January 2005.

Steffes, P.G. "Laboratory Measurement of Microwave and Millimeter-Wave Properties of Planetary Atmospheric Constituents," *Proceedings of International Conference on Laboratory Research for Planetary Atmospheres*, **1** (1989).

Sternhagen *et al.*, "A Novel Acoustic Gas and Temperature Sensor," *IEEE Sensors Journal*, **2** (4), (2002).

Tanaka, K., Yamabe, T. and Fukui, K. *The Science and Technology of Carbon Nanotubes* (Elsevier Publications, Amsterdam, 1999).

"Threat of Terrorism to the United States," U.S. Congressional testimony, May 2001, http://www.fbi.gov/congress/congress01/freeh051001.htm accessed January 2006.

Tomanek, D. "Carbon Nanotubes - A Time Line." http://www.pa.msu.edu/cmp/csc/nttimeline.html accessed 23 September 2006.

Torrens, F. "Effect of Type, Size, and Deformation on the Polarizability of Carbon Nanotubes from Atomic Increments," *Nanotechnology* **15**, S259-264, (2004).

Townes, C.H. and Schalow, A.L. *Microwave Spectroscopy* (Dover Publications, NY, 1975) Ch. 14, p. 378.

Van Bladel, J. *Electromagnetic Fields* (McGraw Hill Company, Cleveland, 1964), Ch.10.

Van Vleck, J.H. "The Absorption of Microwaves by Oxygen," *Phys. Rev.* **71**, (7), (December 1946).

Wallace, E.J. and Sansom, M.S.P. "Carbon Nanotube/Detergent Interactions via Coarse-grained Molecular Dynamics," *Nanoletters* (in press).

Weber, S.E., Talapatra, S., Journet, C., Zambano, A. and Migone, A.D. "Determination of the Binding Energy of Methane on Single-walled Carbon Nanotube Bundles," *Phys. Rev. B.* **61**, (19) (2000).

Works, C.N. "Resonant Cavities for Dielectric Measurements," *J. App. Phys*. **18,** 605-612 (July 1947).

Ye *et al.*, "Hydrogen Adsorption and Cohesive Energy of Single Walled Carbon Nanotubes," *Appl. Phys. Lett*. **74,** 16 (1999).

Yumura, M. "Synthesis and Purification of Multiwalled and Single Walled Carbon Nanotubes," in K. Tanaka, T. Yamabe, K. Fukui, *The Science and Technology of Carbon Nanotubes* (Elsevier Science Ltd., Kindlington, Oxford OX5 1GB, UK, 1999), pp. 2-11.

Zhao, J. "Gas Molecules Adsorption on Carbon Nanotubes," *Mat. Res. Soc. Symp. Proc*. **633**, A13.48.1 (2001).